EDGE CAPS FOR REINFORCING COMPOSITE LAMINATES

by

William Edward Howard

Thesis submitted to the Faculty of the
Virginia Polytechnic Institute and State University
in partial fulfillment of the requirements for the degree of

MASTER OF SCIENCE

in

Engineering Mechanics

APPROVED:

R. M. Jones, Chairman

M. W. Hyer

J. N. Reddy

July 1985

Blacksburg, Virginia

EDGE CAPS FOR REINFORCING COMPOSITE LAMINATES

by

William Edward Howard

Committee Chairman: Robert M. Jones
Engineering Science and Mechanics

(ABSTRACT)

A method for reinforcing the free edges of a symmetric 11-ply graphite-epoxy laminate by adding a one-layer Kevlar-epoxy edge cap is studied. Generalized plane strain finite element analysis is used to predict that interlaminar stresses are reduced when an edge cap is added to the laminate. Different edge cap designs are evaluated. A three-dimensional composite failure criterion and finite element analysis are used in a progressive laminate failure analysis to predict the failure load of the reinforced laminate.

The results of an experimental program are presented. Capped laminates are shown to be on average 130% to 140% stronger than uncapped laminates when subjected to static tensile or tension-tension fatigue loading. In addition, the coefficient of variation of the static tensile failure load decreases from 24% to 8% with the addition of edge caps.

The predicted failure load which is calculated with the finite element results is 10% lower than the actual failure load. For both the capped and the uncapped laminates, actual failure loads are much lower than those predicted using classical lamination theory stresses and a 2-D failure criterion.

Possible applications of the free edge reinforcement concept are given. Suggestions for future research are made.

AKNOWLEDGEMENTS

The work described herein was performed under a grant from NASA-Langley Research Center (NASA grant number NAG-1-389). Mr. Mark Shuart was the project monitor.

The author would like to express deep appreciation to Dr. Robert M. Jones for his patience and helpfulness during this project. Also, thanks to Mr. Terry Gossard Jr. for his work during the experimental part of the project.

TABLE OF CONTENTS

CHAPTER 1

INTRODUCTION

Because of their high strength- and stiffness-to-weight ratios, fiber-reinforced laminated composite materials are being used in an increasing number of weight-critical structures. In order for these materials to be used to the limits of their potential, however, the behavior of laminated composites when subjected to various loading conditions must be better understood. One problem which is unique to laminated materials is delamination under loading in the plane of the laminate. For example, a laminate with a hole cut through its thickness can delaminate near the hole even though no through-the-thickness loading is present. This three-dimensional problem is very difficult to analyze; however, a similar two-dimensional problem exists. Some flat laminates with free edges will delaminate near the edges when subjected to a uniform axial load, as shown in Figure 1-1.

The laminate free edge problem was studied by Pipes and Pagano [1] in 1970. They concluded that edge delaminations are caused by Z-direction (the coordinate system is defined in Figure 1-1) normal stresses which peak near the free edge. Pipes and Pagano noted that this Z-direction stress increases very rapidly near the free edge, and they theorized that a mathematical singularity exists. They were unable to

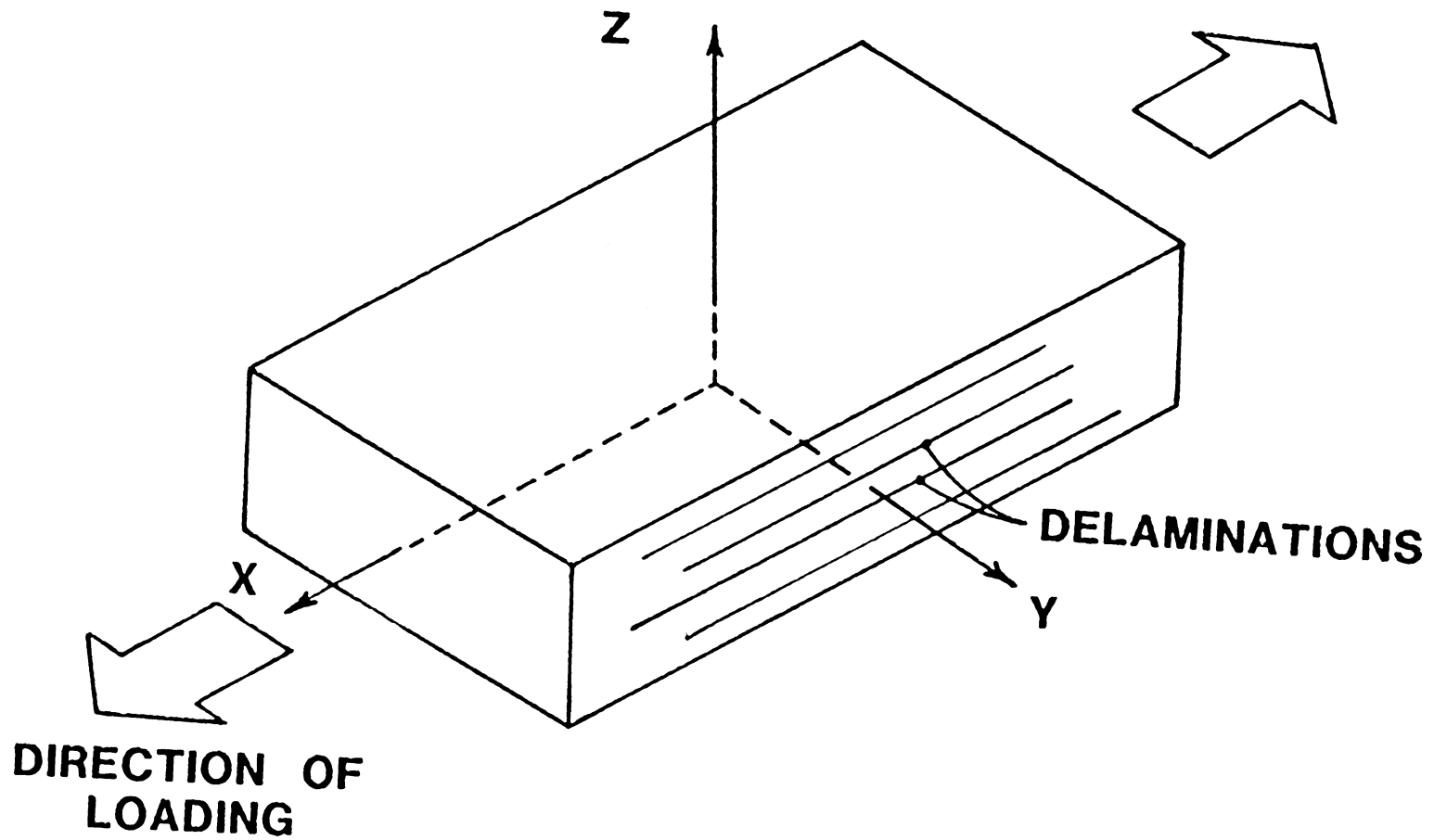

FIGURE 1-1 Free Edge Problem

prove the existence of a singularity because the stresses under consideration were not calculated from an exact solution but rather from an approximate finite-difference solution. Pipes and Pagano noted, however, that the free edge problem is similar to a problem examined by Bogy [2] in 1968. Bogy considered two wedges of different isotropic elastic materials which were bonded to each other along one face. The wedges were subjected to normal and shearing tractions on the faces not bonded (see Figure 1-2). Bogy's exact solutions for plane strain and generalized plane stress problems contain mathematical singularities at the point of intersection of the bonded and loaded faces.

Several authors have presented approximate numerical results for the free edge problem. In particular, Wang and Crossman [3] used finite element analysis to examine interlaminar stresses near the edge. Wang and Crossman concluded that although the existence or nonexistence of a singularity cannot be proven using FE analysis, the solution which is obtained is insensitive to the grid size which is used. This conclusion is significant because it indicates that a "stable" solution exists for the free edge problem. Pagano and Pipes [4], in followup work to their original paper, used a refined finite difference grid to show that the solution obtained is relatively insensitive to grid size and concluded that further attempts to refine approximate solutions would

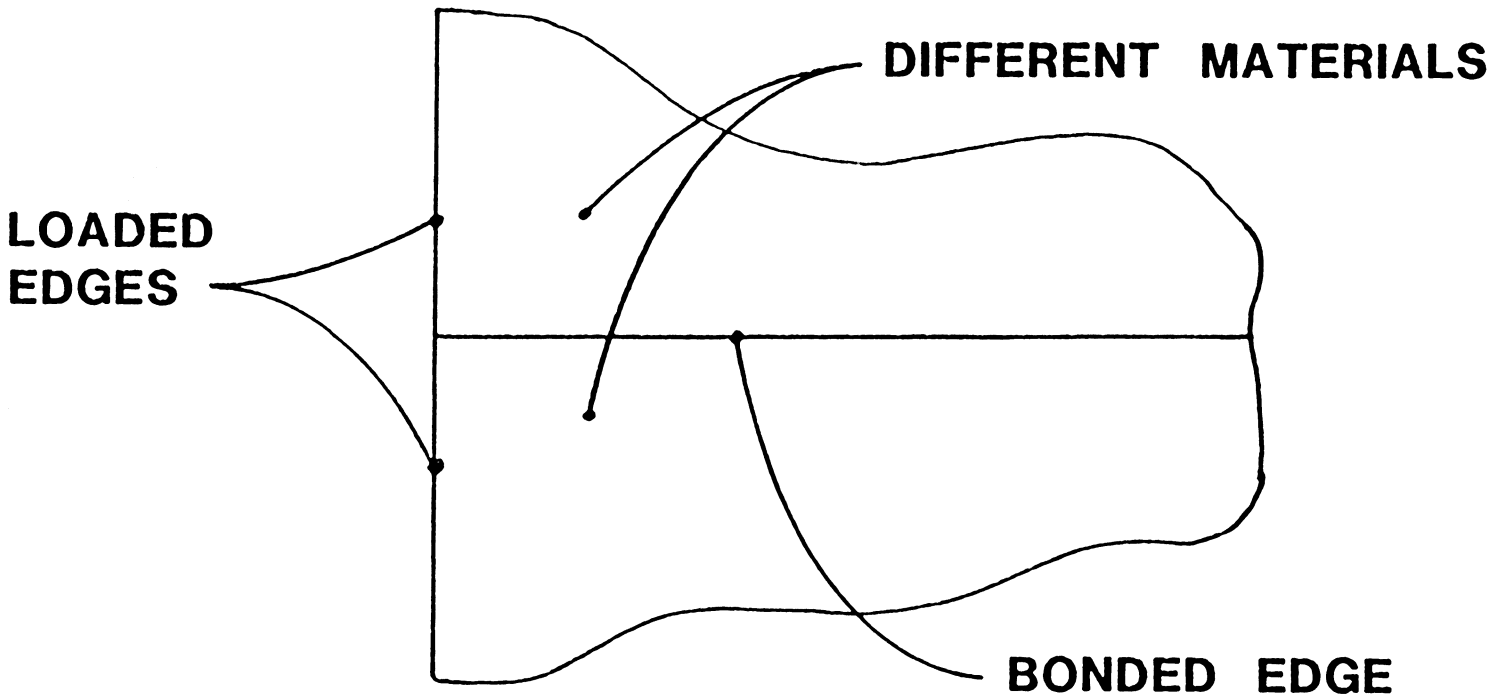

FIGURE 1-2 Problem Studied by Bogy [2]

be of questionable value.

In 1982, Kim [5] performed an experimental study to develop a technique for the prevention of free edge delaminations. By wrapping the edges of graphite-epoxy laminates with woven fiberglass cloth, Kim found that the onset of delaminations could be delayed or prevented. Kim did not correlate this experimental study with analysis of the edge stresses.

The concept of reinforcing free edges to prevent delaminations is attractive because it allows a designer the flexibility to choose lamination stacking sequences without being concerned about free edge effects. Although this project will be concerned only with flat tensile specimens, reinforcement techniques could be applied to any laminates with free edges, such as plates with holes or cutouts.

The goals of this project are

(1) to perform FE analysis of reinforced and unreinforced laminates and thus show theoretically the advantage of reinforcing the free edges,

(2) to make failure predictions based on the analysis results,

(3) to fabricate graphite-epoxy laminates and to reinforce the edges of some of these laminates without

having to introduce complex machining operations or specialized tooling,

(4) to subject the unreinforced and reinforced laminates to static and fatigue loading until they fail and thus show the effectiveness of the reinforcements, and

(5) to correlate the experimental results with the analysis.

The computer analysis is performed using the SAAS III finite element program [6]. A modification to the SAAS III program is necessary in order to analyze the generalized plane strain problem, which is an idealization of the free edge problem. This modification will be discussed in Section 2.2.

The composite material used for the laminates is T-300 graphite fibers preimpregnated with 5209 resin. This material is relatively well-characterized, with wide usage in the aerospace industry.

The stacking sequence of the laminates to be studied is selected so that the laminate will develop tensile Z-direction normal stresses near the edges when the laminate is subjected to a tensile axial load. In order to eliminate bending and shearing of the laminate when subjected to an axial load, only configurations which are symmetric about the

midplane and are balanced (for each lamina oriented at an angle of +theta degrees to the axis, there is a lamina oriented at -theta degrees) are considered. Classical lamination theory (CLT) is used in Section 2.1 to show that Z-direction stresses are created by stresses in the Y-direction. These Y-direction normal stresses are created if different layers in the laminate have different Poisson's ratios (i.e., if the individual laminae tend to contract different amounts in the Y-direction when subjected to an X-direction load. The Poisson's ratio discussed here is actually the apparent Poisson's ratio in global coordinates for a +/-theta layer and is a function of the orientation angle theta.) Therefore, for the interlaminar stresses to be maximized, extreme values of Poisson's ratio NU-XY are desired for the layers. For T-300-5209, the maximum value of Poisson's ratio occurs at about +/-27 degrees, with the minimum value occurring at 90 degrees, as shown in Figure 1-3. An angle of 30 degrees is preferred to an angle of 27 degrees because a 30 degree angle is easy to cut from the roll of material by using a 30-60-90 triangle. Thus, the laminate will contain +/-30 degree and 90 degree layers. NASA [7] uses an edge delamination tension specimen which contains 11 layers oriented at [+30/-30/+30/-30/90/90/90/-30/+30/-30/+30]. This stacking sequence will be utilized for this project. A sketch of the NASA edge delamination

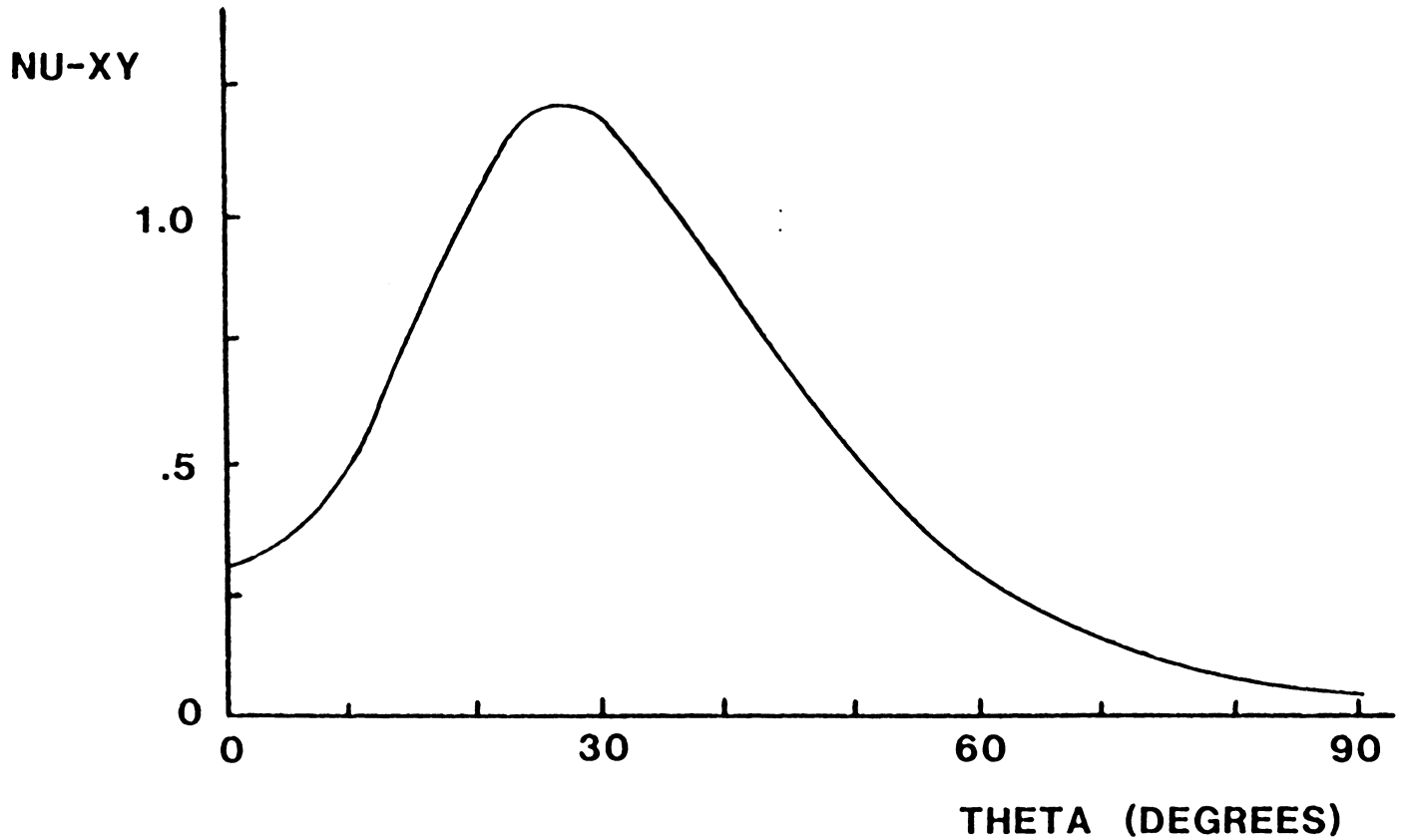

FIGURE 1-3 Poisson's Ratio NU-XY for +/-Theta Degree Pair of Laminae

tension specimen is shown in Figure 1-4.

The method of reinforcement to be used is a simple edge cap which is made by wrapping a single ply of Kevlar-49 style 120 woven cloth impregnated with F-155 resin around the edge, as shown in Figure 1-5. This Kevlar-epoxy cloth is chosen because of its good workability.

The methods of analysis which are used are discussed in Chapter 2, and analytical results are presented in Chapter 3. The experimental portion of the project is presented in Chapter 4, and the project is summarized in Chapter 5.

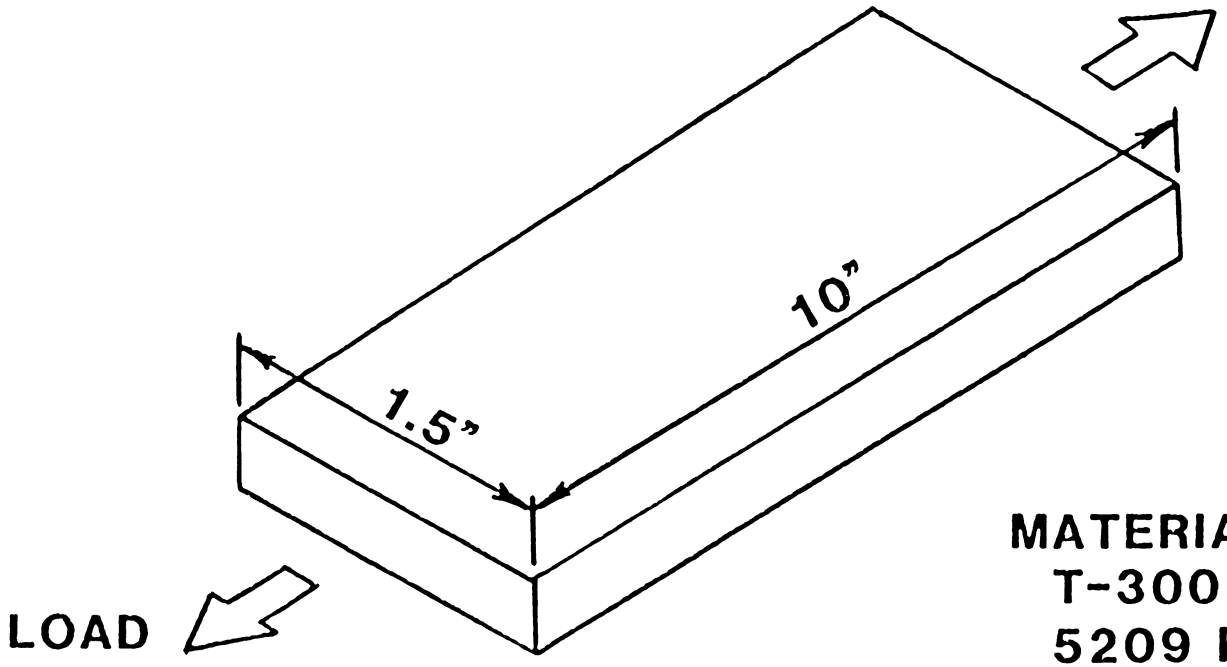

MATERIAL :
T-300 GRAPHITE
5209 RESIN

STACKING SEQUENCE :

$$[+30/-30/+30/-30/90/90/90/-30/+30/-30/+30]_T$$

FIGURE 1-4 NASA Edge Delamination Tension Specimen

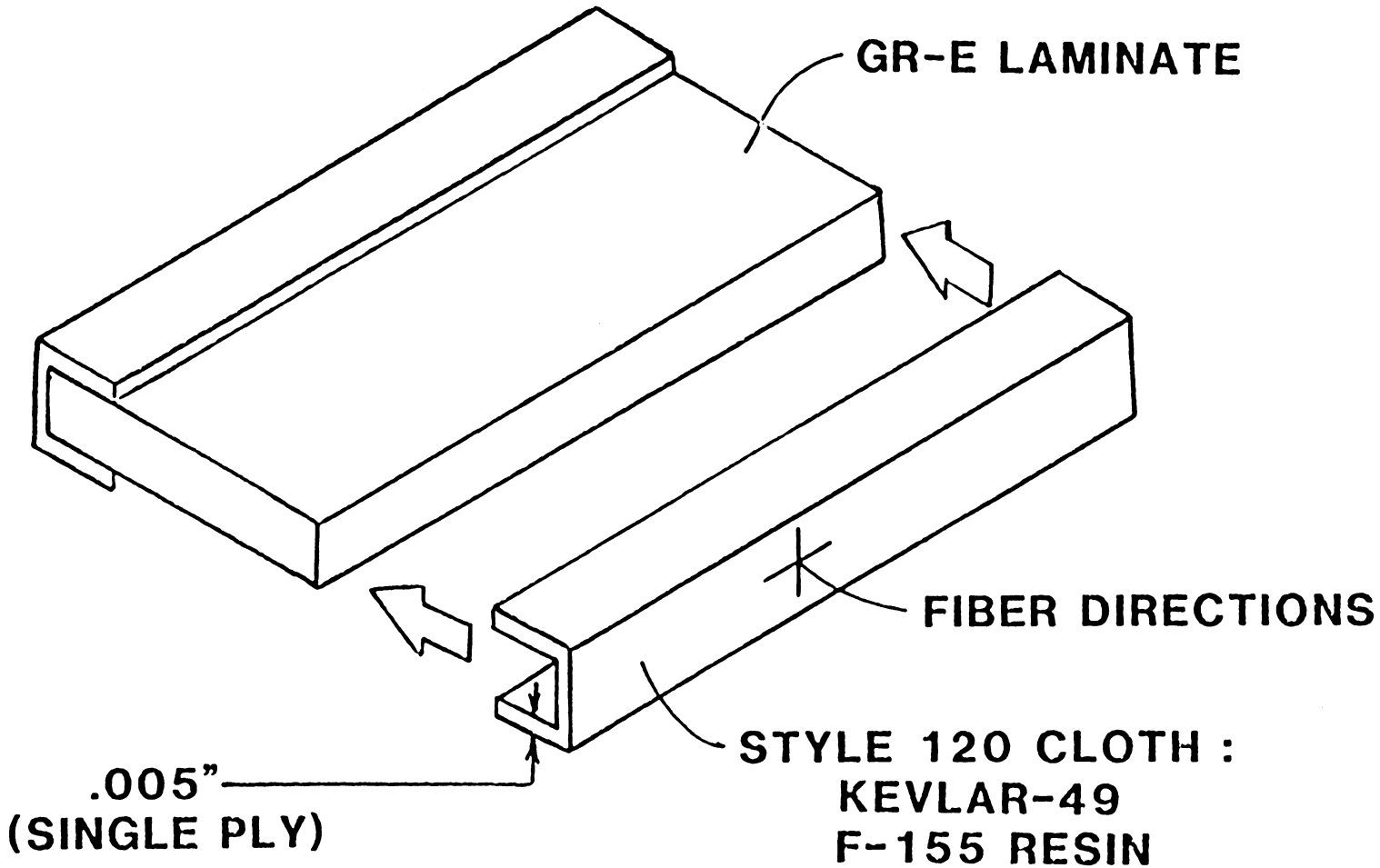

FIGURE 1-5 Kevlar-Epoxy Edge Cap

CHAPTER 2

ANALYSIS PROCEDURE

Classical lamination theory is used to calculate in-plane stresses in the laminate. These stresses can be used to calculate the interlaminar stress resultants near the free edges. However, to determine the distribution of interlaminar stresses near the free edge, finite element analysis or some other numerical approach must be used. The stresses which are calculated with the FE analysis, along with a 3-D composite failure criterion, are used to predict the failure load of each lamina. The lamina which is predicted to fail first has its properties degraded to reflect the failure, and then the finite element analysis of the laminate is repeated. This procedure is repeated until the failure of the entire laminate is predicted.

2.1 CLASSICAL LAMINATION THEORY

Classical lamination theory (CLT) can be used to determine the state of stress in the laminate plane of a thin laminate which is subjected to in-plane loads. CLT stresses are valid only at a sufficient distance away from free edges, points of applied loads, and other geometric discontinuities. For the free edge problem, however, CLT can be used to examine the

mechanism through which interlaminar stresses are created. The use of CLT to determine in-plane stresses will not be discussed here, but is explained by Jones [8].

Consider a balanced, symmetric laminate subjected to a uniform axial tensile load. No bending occurs, so the in-plane stresses will be uniform through the thickness of each lamina. Consider a block of material which is taken from the top lamina and is adjacent to a free edge, as shown in Figure 2-1. The symbol F represents a stress resultant (stress multiplied by the area of the face on which the stress acts). The in-plane stress resultants, which are calculated from CLT stresses, for the material block being considered are shown in Figure 2-1. Notice that on the top surface and on the free edge, the stress resultants are zero. This state of force is consistent with the boundary conditions for a free surface and a free edge.

In order for the material block to be in static equilibrium, interlaminar stress resultants must be present. These equilibrating stress resultants are two shear stress resultants, F-ZX and F-ZY, and a couple consisting of two Z-direction normal stress resultants which are equal in magnitude and opposite in direction. This couple will be referred to as M-Z, a moment. (This moment acts about the X-axis, but will be referred to as M-Z because it results

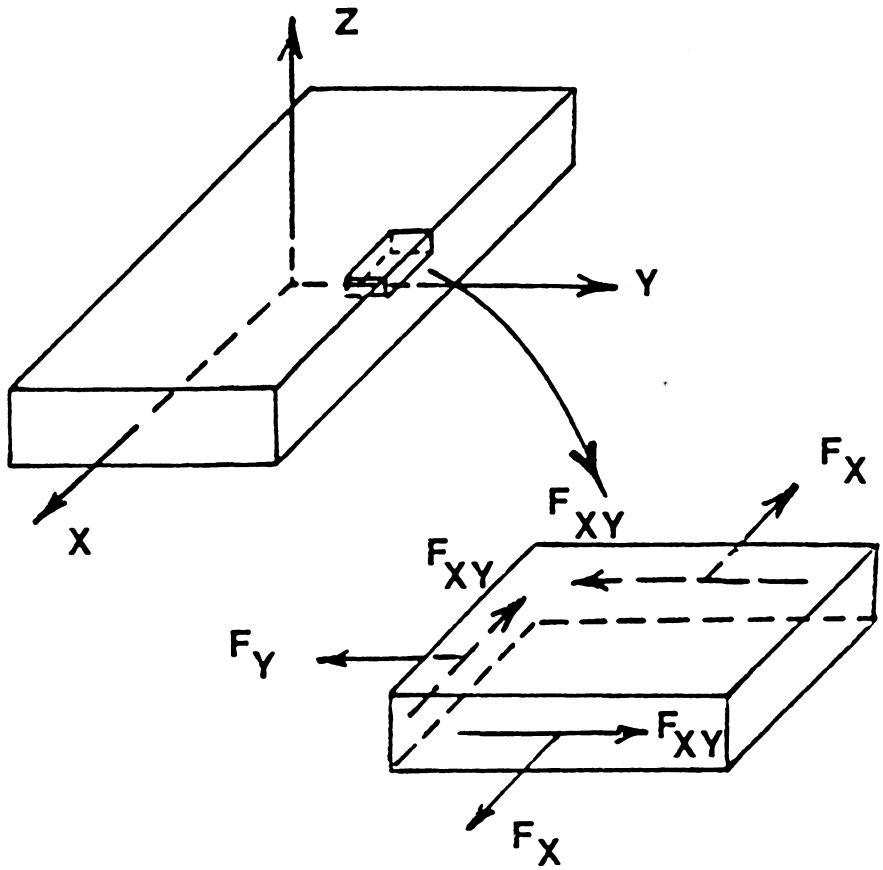

FIGURE 2-1 In-Plane Stress Resultants in Top Lamina

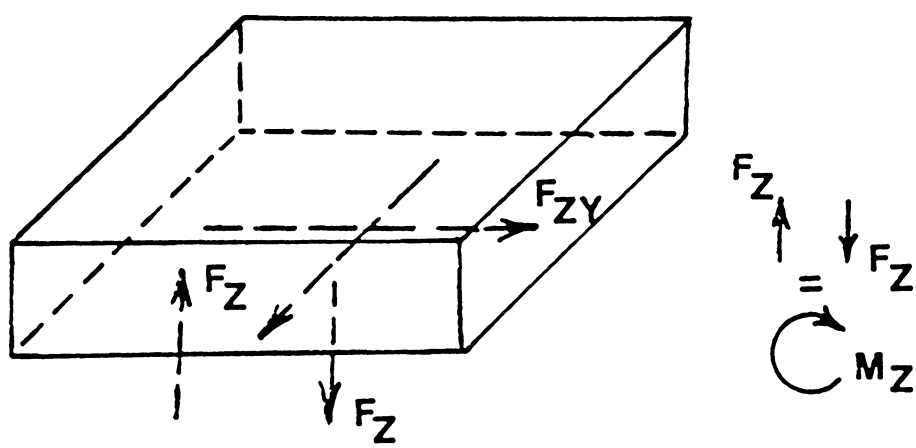

FIGURE 2-2 Interlaminar Stress Resultants at Bottom Surface of Top Laminate

from stresses in the Z-direction.) A positive value of M-Z indicates that the stress resultant F-Z which is closest to the free edge is acting downward, i.e., the Z-direction normal stresses adjacent to the free edge are tensile. The interlaminar stress resultants are shown in Figure 2-2. The values of these interlaminar stress resultants are obtained by summing the forces and moments:

$$F_{zx} = F_{xy} = \tau_{xy} t \tag{2.1}$$

where: t = laminate thickness

$$F_{zy} = F_y = \sigma_y t \tag{2.2}$$

$$M_z = F_y(t/2) = \sigma_y(t^2/2) \tag{2.3}$$

These results can be generalized for the interface between any two laminae in the laminate. We will restrict this discussion to laminates for which all laminae have equal thickness t. The lamina numbering system to be used is shown in Figure 2-3, with i denoting the lamina under consideration and j referring to the interface under consideration. The interlaminar stress resultants occurring at the n-th interface are:

$$F_{zx}^{i} = \sum_{j=1}^{i} F_{xy}^{j} = t \sum_{j=1}^{i} \tau_{xy}^{j} \tag{2.4}$$

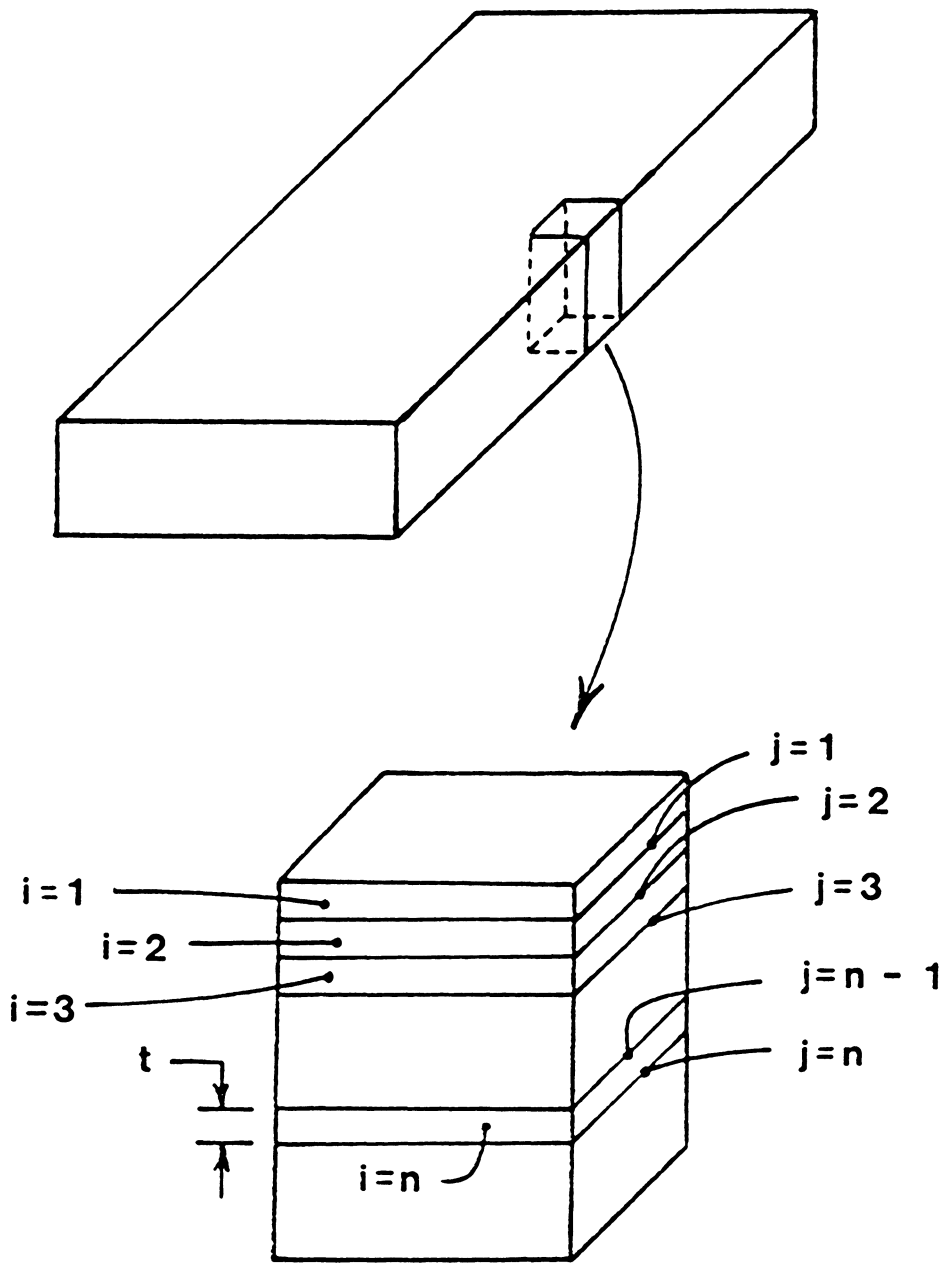

FIGURE 2-3 Lamina Numbering System for Calculation of Interlaminar Stress Resultants

$$F_{zy}^{i} = \sum_{j=1}^{i} F_{y}^{j} = t \sum_{j=1}^{i} \sigma_{y}^{j} \qquad (2.5)$$

$$M_{z}^{i} = \sum_{j=1}^{i} F_{y}^{j}(\text{MOMENT ARM})^{j} = (t^{2}/2) \sum_{j=1}^{i} \sigma_{x}^{j}(2j - 1) \qquad (2.6)$$

Calculation of the interlaminar stress resultants is useful for making a qualitative evaluation of the interlaminar stresses in a laminate or for examining the effects of changing the stacking sequence of a laminate. However, actual interlaminar stresses cannot be determined from CLT. Therefore, finite element analysis is used herein to predict the distribution of interlaminar stresses.

2.2 SAAS III FINITE ELEMENT PROGRAM

SAAS is an acronym for Stress Analysis of Axisymmetric Solids. The full name of the SAAS III computer program, which was developed by James G. Crose and Robert M. Jones, is "Finite Element Stress Analysis of Axisymmetric and Plane Solids With Different Orthotropic, Temperature-Dependent Material Properties in Tension and Compression" [6].

SAAS III has several features which make it suitable for the free edge reinforcement problem. A grid generator allows

the finite element grid to be created easily. Run times are generally less than for other medium-sized FE programs, so that computer costs are lower. A plotting subroutine allows graphical presentation of results. These features allow a large number of reinforcement concepts to be considered quickly and at an acceptable cost.

2.2.1 SAAS III CAPABILITIES

The SAAS III program can be used to analyze three basic problem types - axisymmetric stress, plane stress, and plane strain. Typical geometries, as well as the stress or strain assumptions made, are shown for each problem type in Figure 2-4. Because the problem of interest is a generalized plane strain problem, a modification to the SAAS III program was necessary in order to allow this problem type to be considered. This modification will be discussed in Section 2.2.2.

The finite element method allows a problem involving complex geometries and different material properties to be solved by breaking the body to be analyzed into a system of small elements. In SAAS III, a plane solid is approximated by a series of quadrilateral elements, each of which is subdivided into four triangular elements, as in Figure 2-5. The points at the corners of the quadrilateral elements are

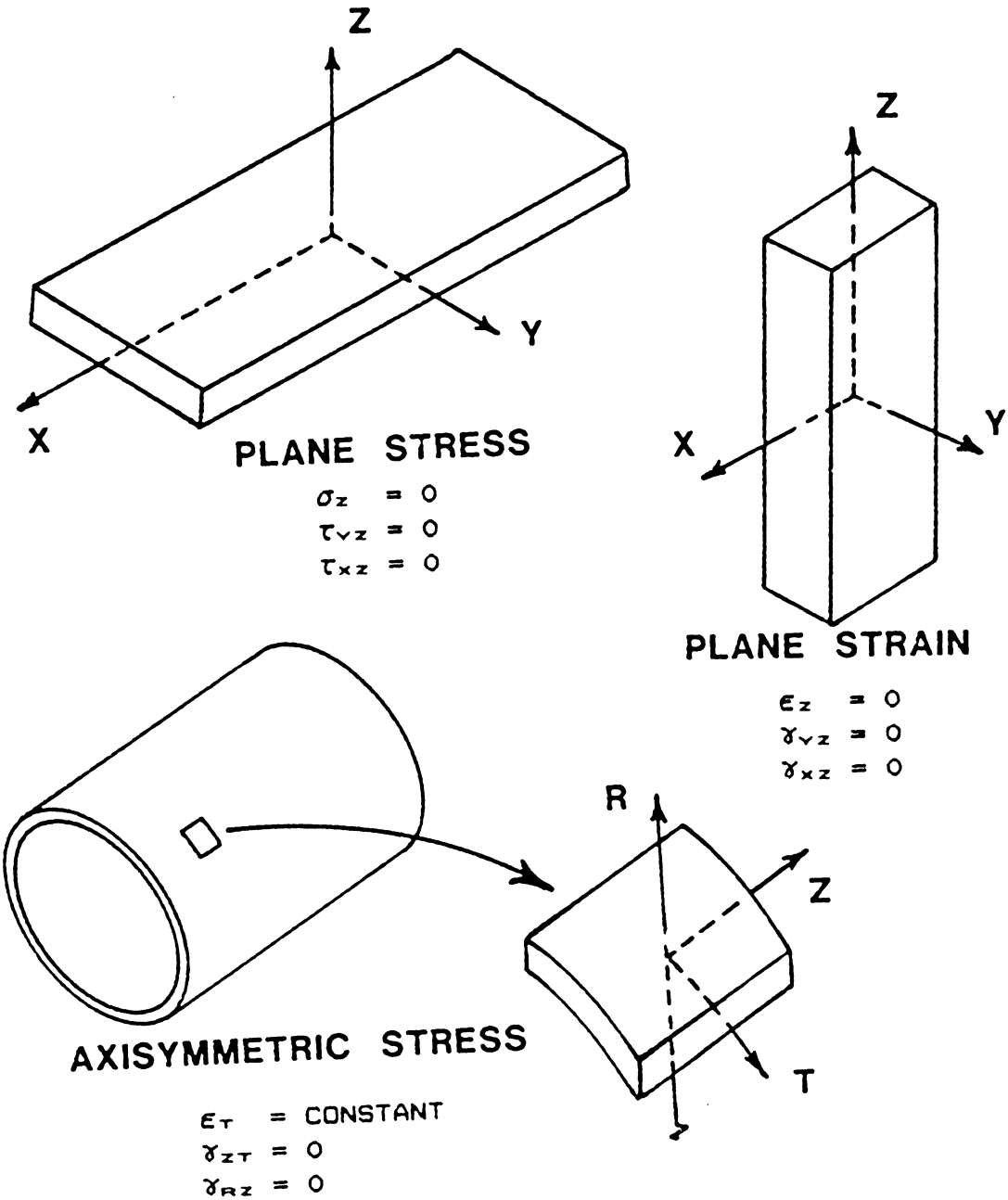

FIGURE 2-4 SAAS III Problem Types

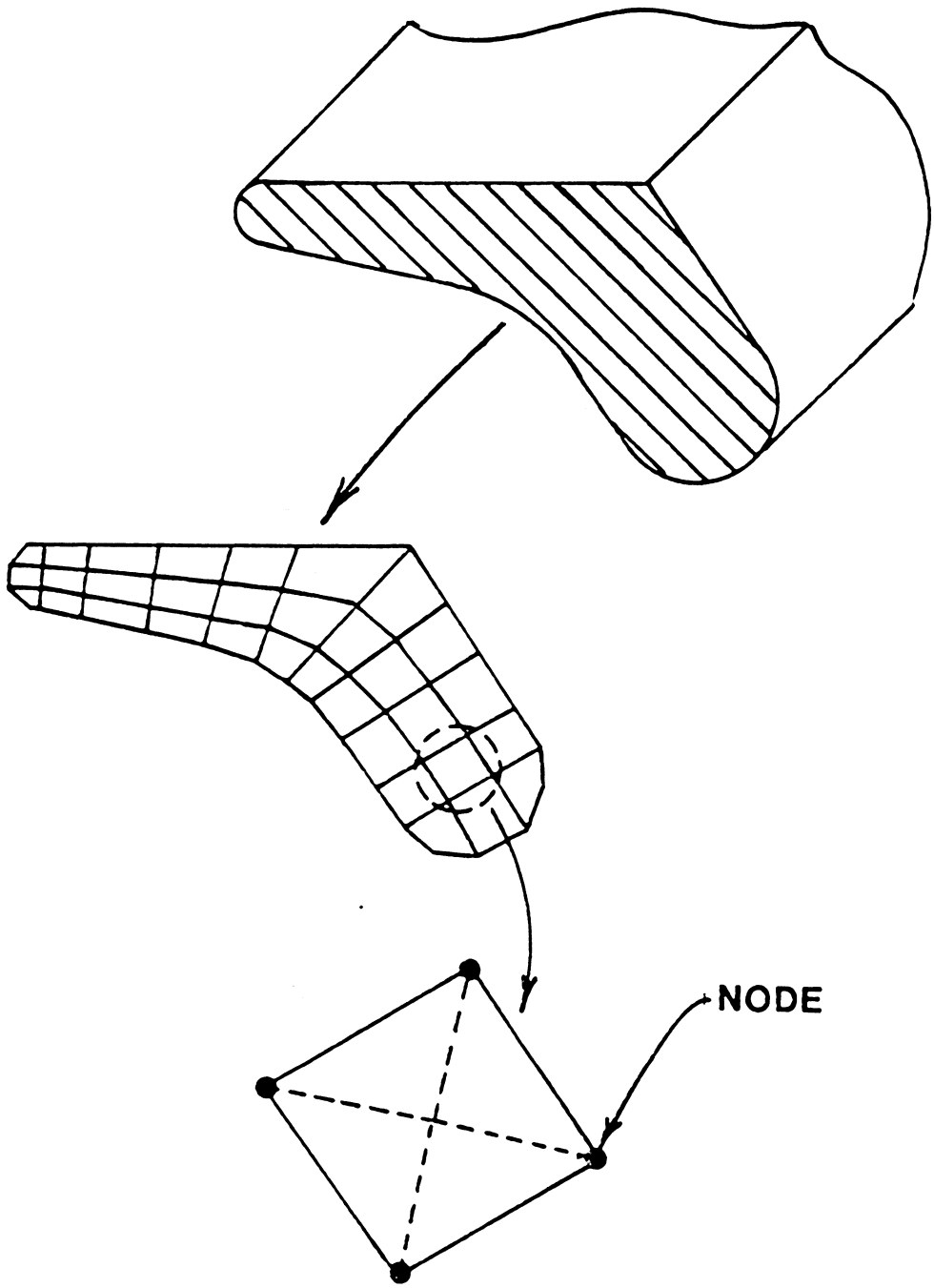

FIGURE 2-5 Finite Element Idealization of a Plane Solid

called nodes. Equilibrium equations for the displacements of the nodes are formulated for each element, and these equations are assembled to form a set of linear equations which when solved yield approximations for the displacements of each node. (See Appendix A for more detail.)

Element strains are calculated by a method developed by Cook [9]. In this method, a linear displacement function is derived from a least squares fit of the nodal point displacements. Stresses for each element are calculated by multiplying the material's stiffness (stress-strain) matrix by the element's strain matrix.

2.2.2 MODIFICATION FOR GENERALIZED PLANE STRAIN

In order to analyze the free edge problem, the SAAS III program was modified to handle generalized plane strain problems. Generalized plane strain is different from plane strain in that the out-of-plane strain is a constant, instead of zero.

In order to understand the generalized plane strain problem, it is helpful to consider the example of a homogeneous orthotropic material block subjected to a constant axial strain, as shown in Figure 2-6. Because there are no con-

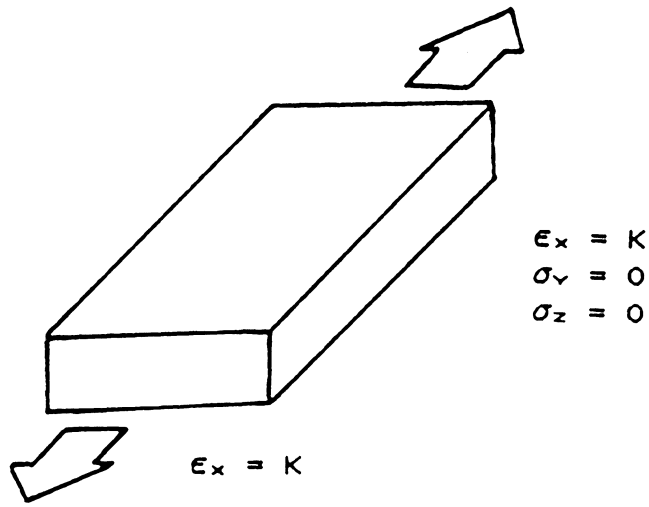

FIGURE 2-6 Material Block Subjected to Constant Axial Strain

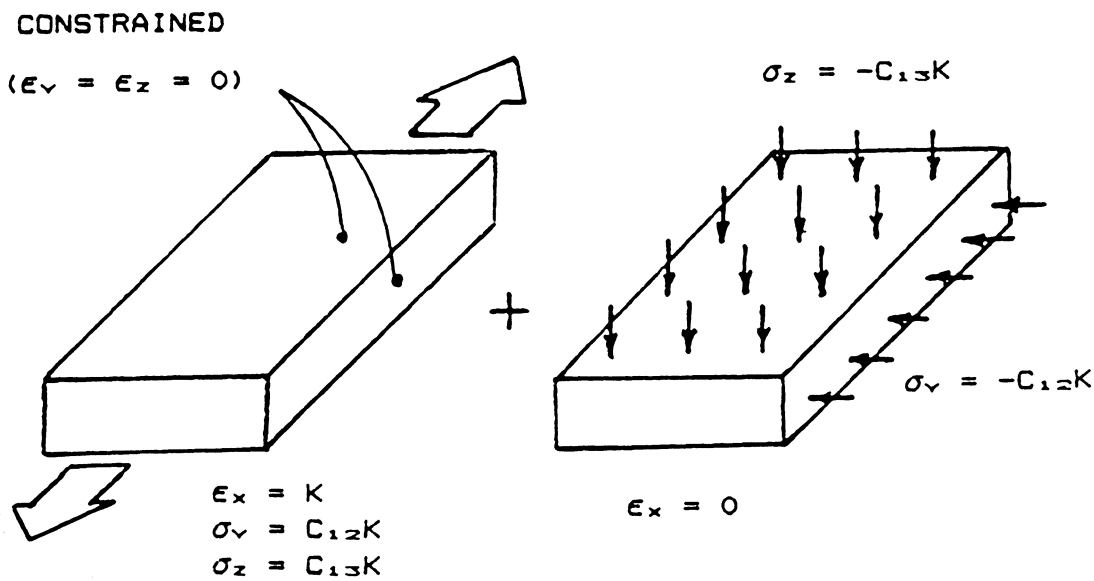

FIGURE 2-7 Superposition of Two Problems to Equal Generalized Plane Strain Problem

straints or applied forces on the edges of the block, the Y- and Z-direction stresses must be zero. This stress-strain state can be thought of as being the superposition of the two cases shown in Figure 2-7. In the first of these two cases, the X-direction strain has been set to K, a constant, with all other strains zero. Substitution of this state of strain into the material's stress-strain equations (See Appendix A) results in stresses in the Y- and Z-directions. These Y- and Z-direction normal stresses are restraint stresses resulting from the zero lateral strain boundary conditions. The second case is a plane strain problem, with applied stresses equal in magnitude and opposite in direction to the restraint stresses of the first case. The superposition of these two problems is identical to the generalized plane strain problem of Figure 2-6. That is, the Y- and Z-direction normal stresses disappear, and we are left with a block which is subjected to an X-direction normal strain with no other constraints.

This concept can be applied to the finite element analysis of generalized plane strain problems. The first step is to solve a plane strain problem with each element subjected to stresses similar to the constraint stresses mentioned above. Thermal and pore pressure stresses can also be included in the SAAS III plane strain analysis. Therefore, the total

stress of each element can be written as:

$$\left\{ \sigma \right\}_m = \left[\quad C \quad \right]_m \left\{ \epsilon \right\}_m - \left\{ \tau \right\}_m - \left\{ \sigma_G \right\}_m + \left\{ \sigma_P \right\}_m \qquad (2.7)$$

where: $\left[\quad C \quad \right]_m \left\{ \epsilon \right\}_m$ = mechanical stresses

$\left\{ \tau \right\}_m$ = thermal stresses

$\left\{ \sigma_G \right\}_m$ = generalized plane strain (GPS) stresses

$\left\{ \sigma_P \right\}_m$ = pore pressure stresses

The m subscript indicates that the corresponding quantity is for an individual element.

Equation (2.7) is the stress equation to be incorporated into the SAAS III plane strain problem, as is detailed in Appendix A. Strains for each element are calculated from the resulting displacements, and the input value of X-direction strain is added to each element's strain matrix. Stresses for each element are then computed.

The steps added to the SAAS III computer program to accomplish the foregoing procedure are:

(1) In the main program, when the generalized plane strain option has been selected, the value of the specified X-direction strain is read from the data.

(2) In the subroutine in which the body force matrix is assembled, the generalized plane strain (GPS) stresses are computed and added to the thermal stresses.

(3) In the subroutine in which element stresses are computed, the X-direction strain is added to the strains calculated for the plane strain problem.

Otherwise, the operation of the SAAS III program is unchanged from its plane strain operation.

2.2.3 ASSUMPTIONS AND LIMITATIONS

For a problem to be idealized as a generalized plane strain problem, there must be no coupling between axial extension and bending. For composite laminates, this restriction implies a symmetric layer stacking sequence. Because the SAAS III program does not handle problems involving monoclinic (one axis of symmetry) materials, single layers for which the angle between the fibers and the longitudinal axis is not 0 or 90 degrees are not allowed. Off-axis laminae may be included in SAAS III, however, if their use is restricted

to balanced, symmetric laminates. A balanced laminate contains a lamina oriented at an angle of -theta to the axis for every +theta lamina. When a +theta lamina and a -theta lamina are placed next to each other in a symmetric laminate, the two laminae, if considered as a single unit, exhibit orthotropic material behavior in extension. This observation can be verified by using CLT to show that the extension-shear coupling terms for a -theta layer are equal in magnitude and opposite in sign to those of a +theta layer. Therefore, the +/- theta unit exhibits no extension-shear coupling. The symmetric laminate restriction ensures that there will be no extension-bending coupling. Because these coupling terms are absent, the +/-theta pair can be modeled as an orthotropic material as long as no bending loads are present (even within a symmetric laminate, there will be bending-twist coupling).

2.3 FAILURE CRITERIA

Classical lamination theory and FE analysis are used to determine the state of stress in a laminate. In order to relate the stresses to the failure of the laminate, a failure criterion must be used. The three criteria which are presented here - the Tsai-Hill [10], Hoffman [11], and Tsai-Wu [12] criteria - are among the most widely accepted failure

criteria. More detail on these criteria can be found in Appendix B.

For plane stress problems, the values of five material strengths are required. These strengths are the two uniaxial tensile strengths, X-T and Y-T, the two uniaxial compressive strengths, X-C and Y-C, and the pure shear strength, S-XY. The X-, Y-, and Z-axes are the lamina's principal material directions, with the X-axis coincident with the longitudinal axes of the fibers. The material is regarded as transversely isotropic, so properties in the Z-direction are the same as those in the Y-direction.

The Tsai-Hill criterion for failure is:

$$\frac{\sigma_x^2}{X_T^2} - \frac{\sigma_x\sigma_y}{X_T^2} + \frac{\tau_{xy}^2}{S_{xy}^2} = 1 \qquad (2.8)$$

The X-T and/or Y-T in Equation (2.8) changes to X-C and/or Y-C if the corresponding stress is negative (compressive). The Hoffman failure criterion is:

$$\frac{\sigma_x^2 - \sigma_x\sigma_y}{X_TX_C} + \frac{\sigma_y^2}{Y_TY_C} + \frac{(X_C - X_T)\sigma_x}{X_TX_C} + \frac{(Y_C - Y_T)\sigma_y}{Y_TY_T} + \frac{\tau_{xy}^2}{S_{xy}^2} = 1 \qquad (2.9)$$

The Tsai-Wu criterion for failure is:

$$\frac{\sigma_x^2}{X_T X_C} + \frac{\sigma_y^2}{Y_T Y_C} + \left[\frac{1}{X_T} - \frac{1}{X_C}\right]\sigma_x + \left[\frac{1}{Y_T} - \frac{1}{Y_C}\right]\sigma_y +$$

$$F_{12}\sigma_x\sigma_y + \frac{\tau_{xy}^2}{S_{xy}^2} = 1 \qquad (2.10)$$

The Tsai-Wu criterion contains one parameter, F-12, which must be determined by a combined-stress test. Usually this test is not practical, so a value for F-12 must be assumed. Narayanaswami and Adelman [13] recommend that a value of zero for F-12 be used to obtain adequate results. Another common assumption for F-12 is:

$$F_{12} = -\frac{1}{2X_T X_C} \qquad (2.11)$$

With this value, the Tsai-Wu criterion is identical to the Hoffman criterion. For the remainder of this report, a value of zero for F-12 will be used for failure predictions with the Tsai-Wu criterion.

All of the criteria mentioned above are for the prediction of the failure of a single lamina. For progressive laminate failure, the criterion is applied to each lamina individually, and the lamina which will fail first is eliminated or has its properties degraded. Then the loading is increased, and the process is repeated until all of the laminae have failed. Such a procedure is necessary because the failure of a single lamina is not necessarily critical. That is, fail-

ure of a single lamina does not necessarily mean that the entire laminate fails at the corresponding load.

For example, consider a cross-ply laminate (all laminae oriented with their fibers either parallel to or perpendicular to the laminate's X-axis) subjected to a uniform tensile load in the X-direction. A failure analysis of each lamina is performed, and matrix failure in the laminae with fibers perpendicular to the X-axis is identified as the earliest failure mode. The material properties of these laminae are degraded to account for this failure, and a second failure analysis of each ply is performed. The next failure mode encountered as load is increased is fiber breakage in the laminae with fibers parallel to the axis. This mode is clearly the critical mode for the laminate.

Because the region of interest in the free-edge problem is subjected to a three-dimensional state of stress, a 3-D failure criterion must be used. The Hoffman criterion has been chosen for this purpose because its allowance of different strengths in tension and compression makes it an improvement over the Tsai-Hill criterion, and the three interaction terms of the Tsai-Wu criterion do not have to be evaluated.

Hoffman's 3-D criterion, which is given as Equation (B.5)

of Appendix B, can be applied to materials with transverse isotropy in the form:

$$\frac{\sigma_x^2}{X_T X_C} + \frac{\sigma_y^2}{Y_T Y_C} + \frac{\sigma_z^2}{Y_T Y_C} - \frac{\sigma_x \sigma_y}{X_T X_C} - \left[\frac{2}{Y_T Y_C} - \frac{1}{X_T X_C}\right]\sigma_y \sigma_z +$$

$$\frac{\tau_{yz}^2}{S_{yz}^2} + \frac{1}{S_{xy}^2}(\tau_{xz}^2 + \tau_{xy}^2) +$$

$$\left[\frac{1}{X_T} - \frac{1}{X_C}\right]\sigma_x + \left[\frac{1}{Y_T} - \frac{1}{Y_C}\right](\sigma_y + \sigma_z) = 1 \qquad (2.12)$$

Substitution of stresses calculated for a given loading condition in Equation (2.12) will only show whether or not failure is predicted at this load level. Usually it is desirable to find the load level at which failure is expected. In order to find this load level, a load factor R is introduced. If stresses are known for a certain loading condition, failure is regarded to occur when the loading is increased to R multiplied by the known load level. For linear analysis, the stresses at failure are simply the stresses at the known load level multiplied by R. If the failure stresses are substituted into Equation (2.12) and the equation is solved for R, then:

$$R = \frac{-B \pm \sqrt{B^2 + 4A}}{2A} \qquad (2.13)$$

where:

$$A = \frac{\sigma_x^2}{X_T X_C} + \frac{\sigma_y^2}{Y_T Y_C} + \frac{\sigma_z^2}{Y_T Y_C} - \frac{\sigma_x \sigma_y}{X_T X_C} - \left[\frac{2}{Y_T Y_C} - \frac{1}{X_T X_C}\right]\sigma_y \sigma_z + \frac{\tau_{yz}^2}{S_{yz}^2} + \frac{1}{S_{xy}^2}(\tau_{xz}^2 + \tau_{xy}^2)$$

$$B = \left[\frac{1}{X_T} - \frac{1}{X_C}\right]\sigma_x + \left[\frac{1}{Y_T} - \frac{1}{Y_C}\right](\sigma_y + \sigma_z)$$

Equation (2.13) yields two values for R corresponding to tensile and compressive loadings.

Equation (2.13) has been programmed into a post-processor for the SAAS III FE program. This post-processor:

(1) reads stresses and strains in global (laminate) coordinates for each element.

(2) calculates XY-shear stress for a + or - theta lamina from the +/- theta unit's strains.

(3) rotates stresses into the lamina principal material directions.

(4) solves Equation (2.13) for each element.

The lowest positive value of R is then selected (only tensile loads are of interest), and the predicted failure load of the corresponding lamina is R multiplied by the load for which

the laminate was analyzed.

In this chapter the analytical tools are discussed which are used to study the free edge problem and the reinforcement concept. In the next chapter, results obtained by applying these tools are presented.

CHAPTER 3

ANALYSIS RESULTS

Classical lamination theory is used to show that the NASA edge delamination specimen is expected to have significant strength-reducing edge delaminations when it is subjected to only a modest-sized tensile axial load. The stacking sequence of a laminate is shown to affect the nature of interlaminar stresses. Large, perhaps singular, stresses are predicted at the free edge when the laminate is analyzed with a linear finite element program. The addition of edge caps is shown to greatly reduce interlaminar normal stresses. A manufacturing defect, namely a gap between the cap and the edge of the laminate, is incorporated in an FE model in order to simulate as closely as possible the actual as-built laminate. The 3-D Hoffman failure criterion is used to predict the failure load of the capped laminate.

3.1 Classical Lamination Theory

In Section 2.1, equations for calculating interlaminar stress resultants are given (Equations (2.4), (2.5), and (2.6)). These equations are used to to calculate interlaminar stress resultants for the NASA edge delamination tension specimen subjected to a uniform axial load of 1000

pounds. The resulting stress resultants are shown in Figure 3-1. The moment M-Z is positive, indicating tensile normal stresses near the free edge. The greatest values of M-Z occur at the interfaces which are closest to the centerline of the laminate. The largest values of the ZY-shear stress resultant occur at the interfaces which separate the 90 degree and the -30 degree laminae. The ZX-shear stress resultant is nonzero only within the +/-30 degree laminae. This result occurs because the XY-shear stress is equal in magnitude and opposite in direction for the -30 degree laminae as compared to the +30 degree laminae.

The importance of stacking sequence is shown by rearranging the laminae of the NASA edge delamination specimen. When a 90 degree lamina is moved from the interior of the laminate to the top of the laminate and another 90 degree lamina is moved to the bottom of the laminate, the stress resultants are drastically changed, as shown by comparing the stress resultants for the new sequence in Figure 3-2 with those for the old sequence in Figure 3-1. The moment M-Z becomes negative throughout the thickness of the laminate, indicating compressive normal stresses adjacent to the free edge. The ZY-shear stress resultants have been redistributed, also, by this stacking sequence change.

CLT analysis is used to show that the NASA edge delam-

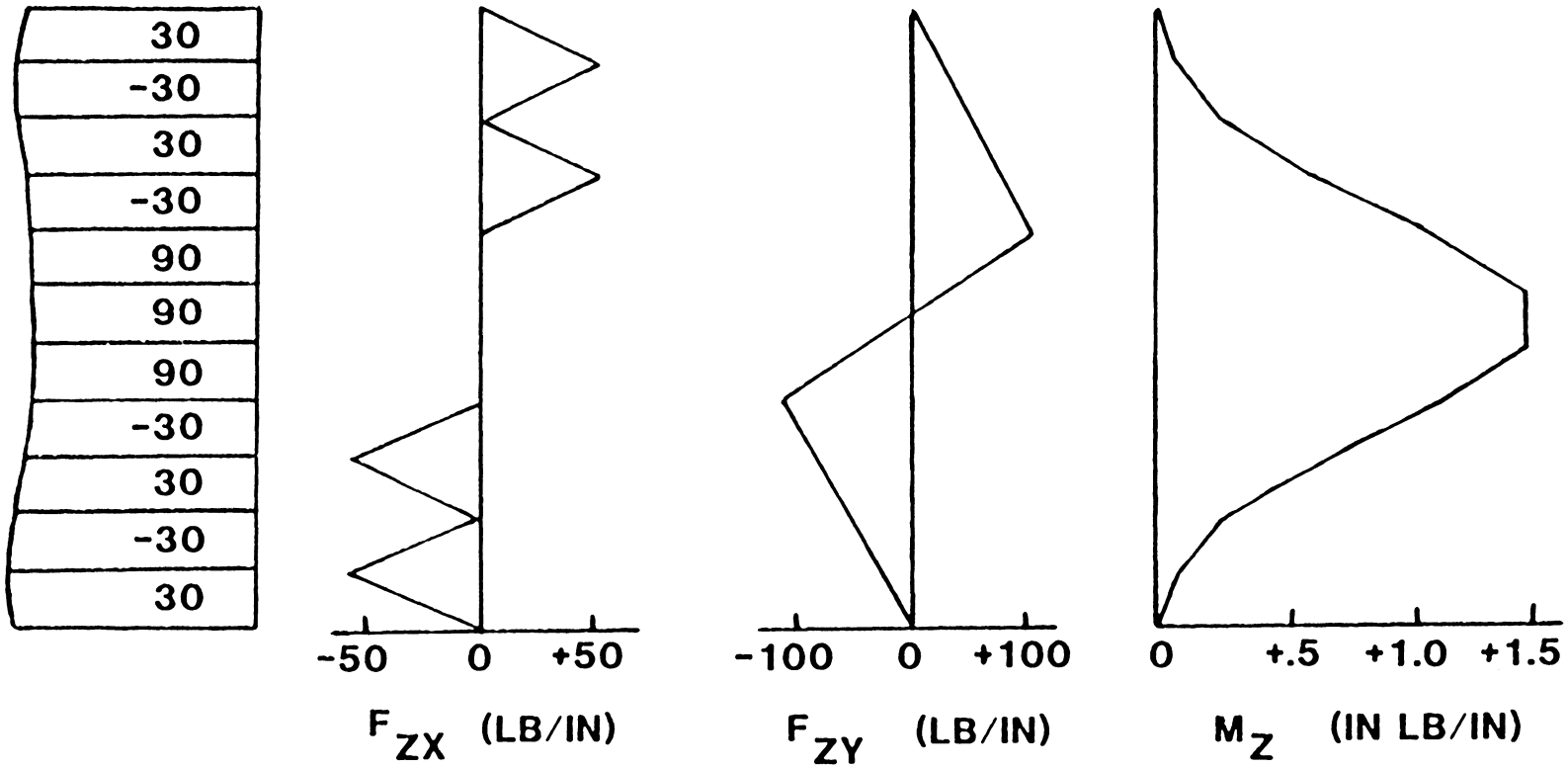

FIGURE 3-1 Interlaminar Stress Resultants for NASA Edge Delamination Tension Specimen

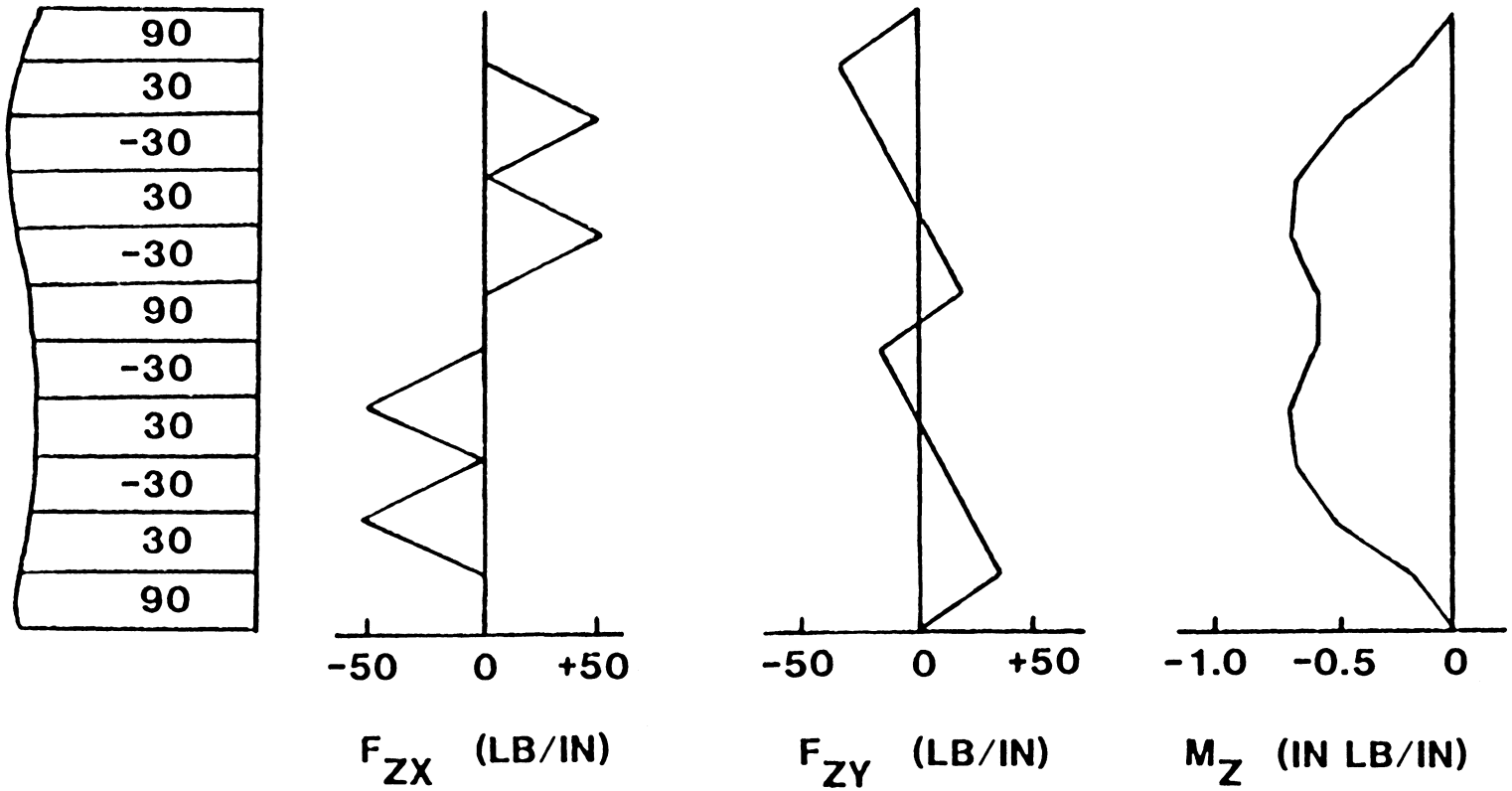

FIGURE 3-2 Interlaminar Stress Resultants for NASA Laminate with Altered Stacking Sequence

ination specimen is expected to have tensile normal stresses near the free edges when the specimen is subjected to a uniform axial tensile load; therefore, edge delaminations are expected. This is not a surprising result because the NASA laminate was originally selected for its tendency to delaminate under tensile loading. Finite element analysis is now used to determine stress distributions within the laminate.

3.2 FINITE ELEMENT MODELS

Because the NASA laminate is symmetric about both the Y- and Z-axes, only one-fourth of the laminate cross-section must be analyzed, as shown in Figure 3-3. Each lamina is represented by two rows of elements so that stress variations within the laminae can be identified. Because interlaminar stresses occur only near the free edge, the number of elements per unit of width of the laminate is large near the free edge and small away from the edge. The grid which was selected consists of elements with a 1:1 aspect ratio (length-to-width ratio) near the free edge, a 10:1 aspect ratio near the center of the laminate, and a 2:1 ratio in a transition zone, as shown in Figure 3-4. To demonstrate the adequacy of the grid selected, SAAS computer runs are made with baseline grid described above (grid #1) and three

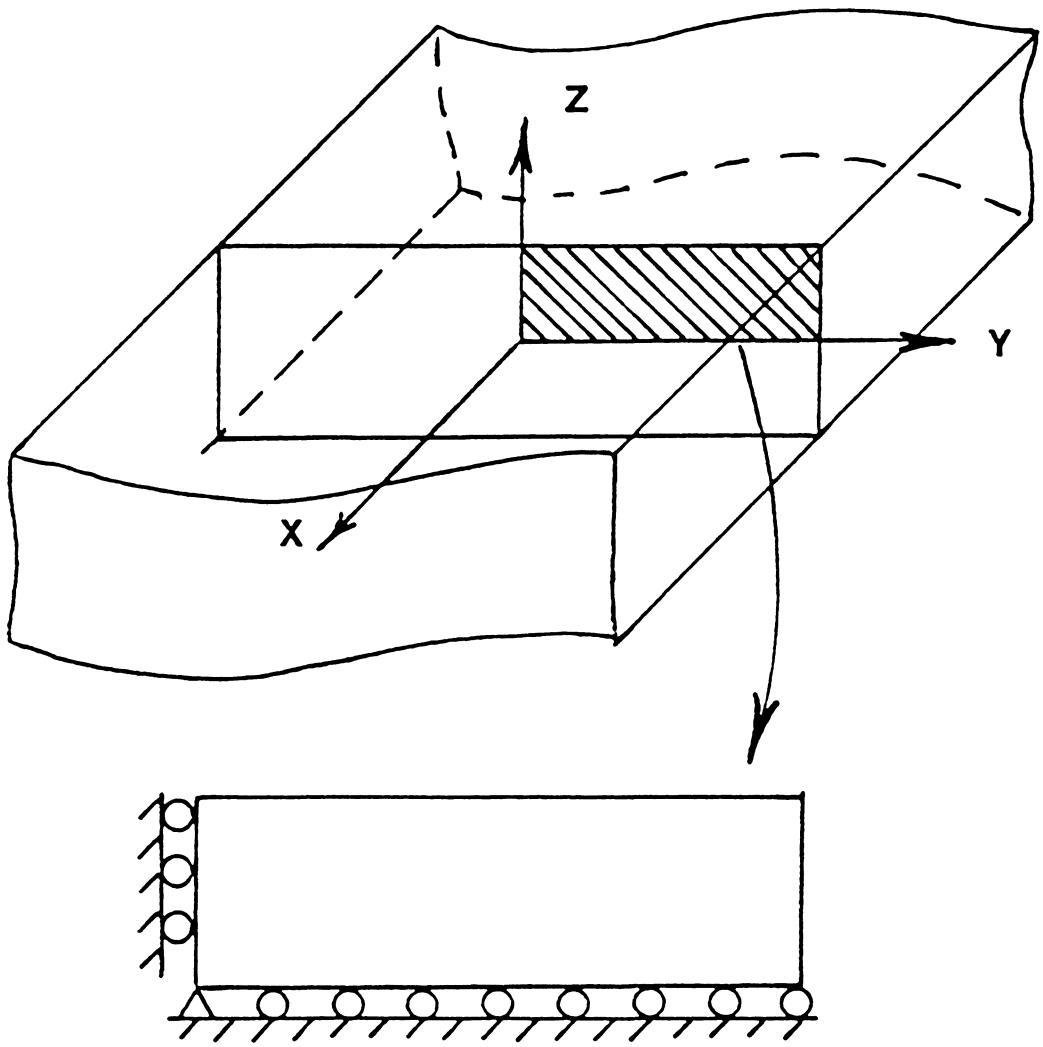

FIGURE 3-3 Portion of Laminate Cross-Section to be Analyzed

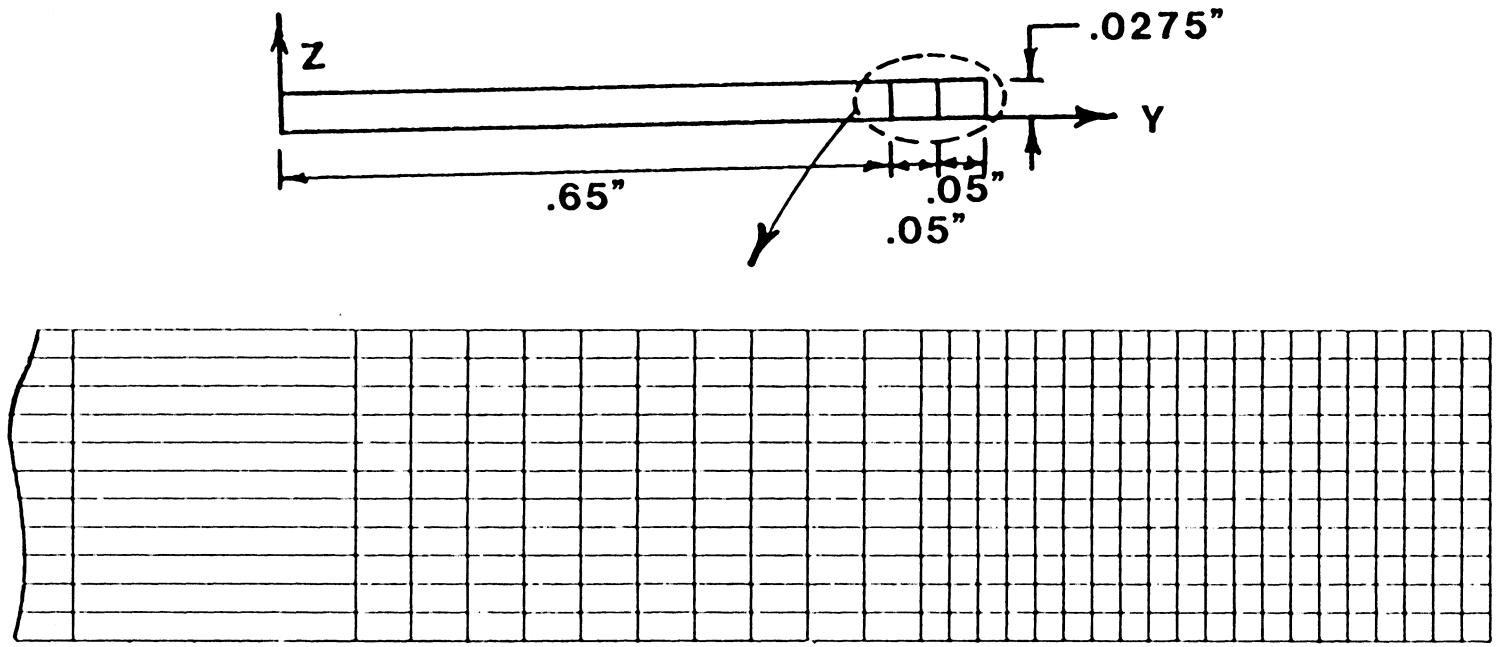

FIGURE 3-4 Unreinforced Laminate Finite Element Grid

alternative grids. Grid #2 has fewer elements near the free edge. Grid #3 has 10:1 aspect ratio elements across the full width of the laminate. Grid #4 has more elements near the free edge than does the baseline grid #1. The four grid designs to be considered are shown in Figure 3-5.

Predictions of the Z-displacements along the top surface of the laminate are shown in Figure 3-6. The results for grid #1 and grid #2 are nearly identical. Grid #3 clearly does not contain enough elements to accurately predict the displacements near the free edge. Results for grid #4 are not plotted, but the displacements are within 0.2% of the displacements calculated using grid #1. In addition, the interlaminar normal stresses predicted with grid #1 and grid #4 are compared. Among the stresses considered are those for the elements which are adjacent to the laminate midplane and near the free edge. Good agreement exists between the two sets of stresses as seen in Figure 3-7. In particular, the normal stresses at the free edge (from linear extrapolation of the stresses for the two elements closest to the edge) differ by only 1.6%.

The conclusion from these studies is that grid #1 is an acceptable grid because increasing the number of elements does not change the displacements or the stresses a great deal. Grid #2 also appears to be an adequate grid, but grid

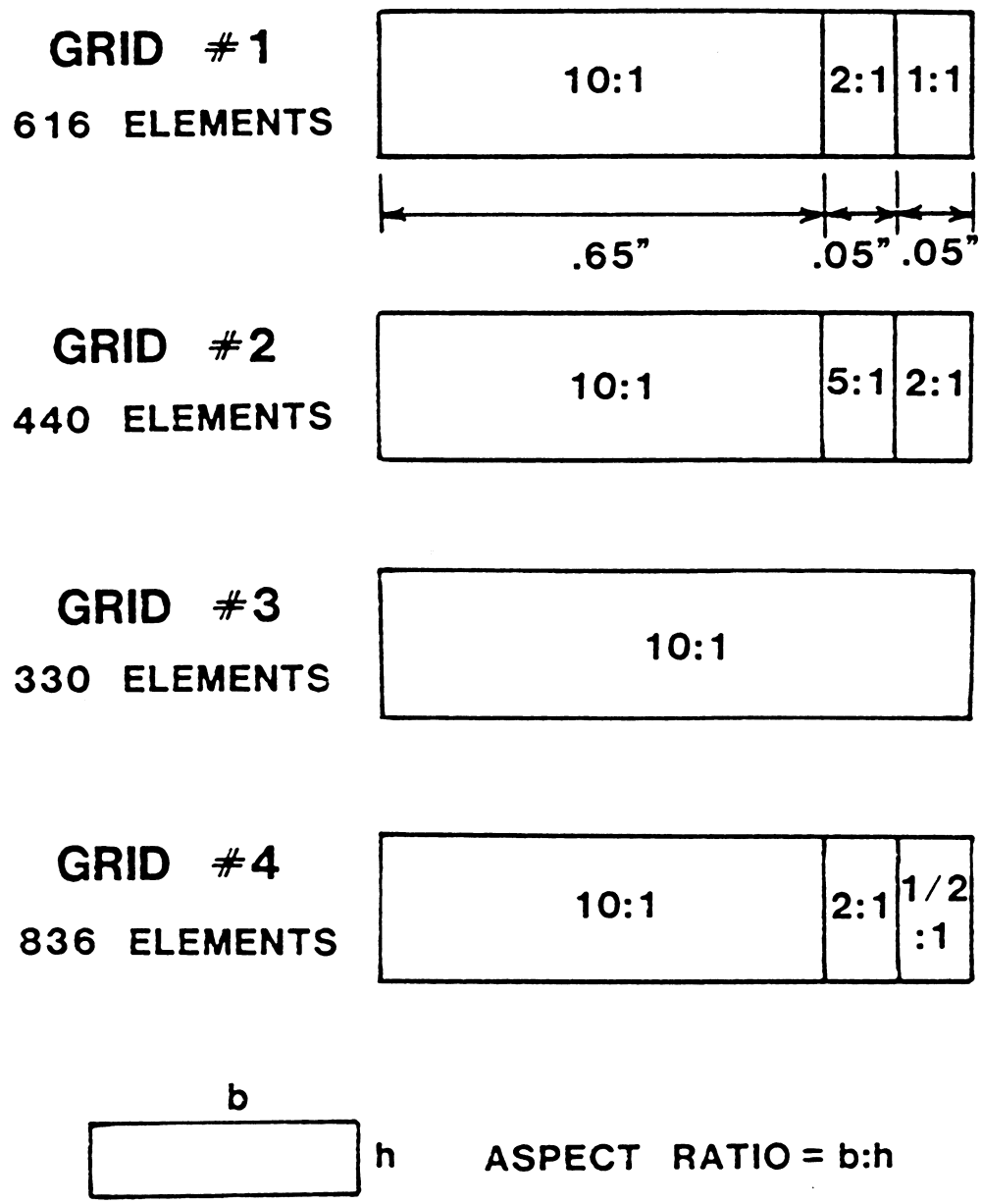

FIGURE 3-5 Element Aspect Ratios of Alternative FE Grids

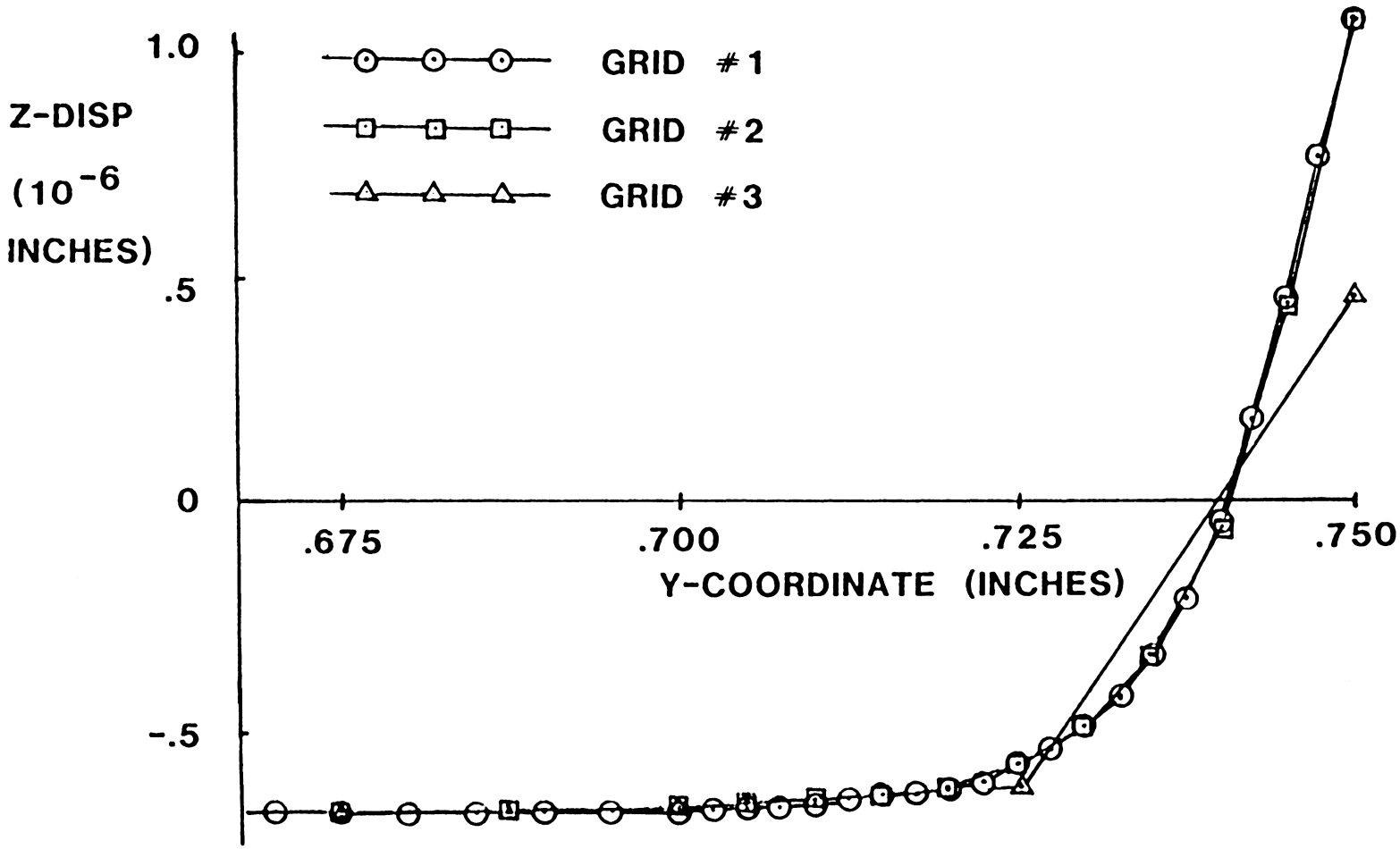

FIGURE 3-6 Top Surface Displacements Predicted with Grid #'s 1, 2, and 3

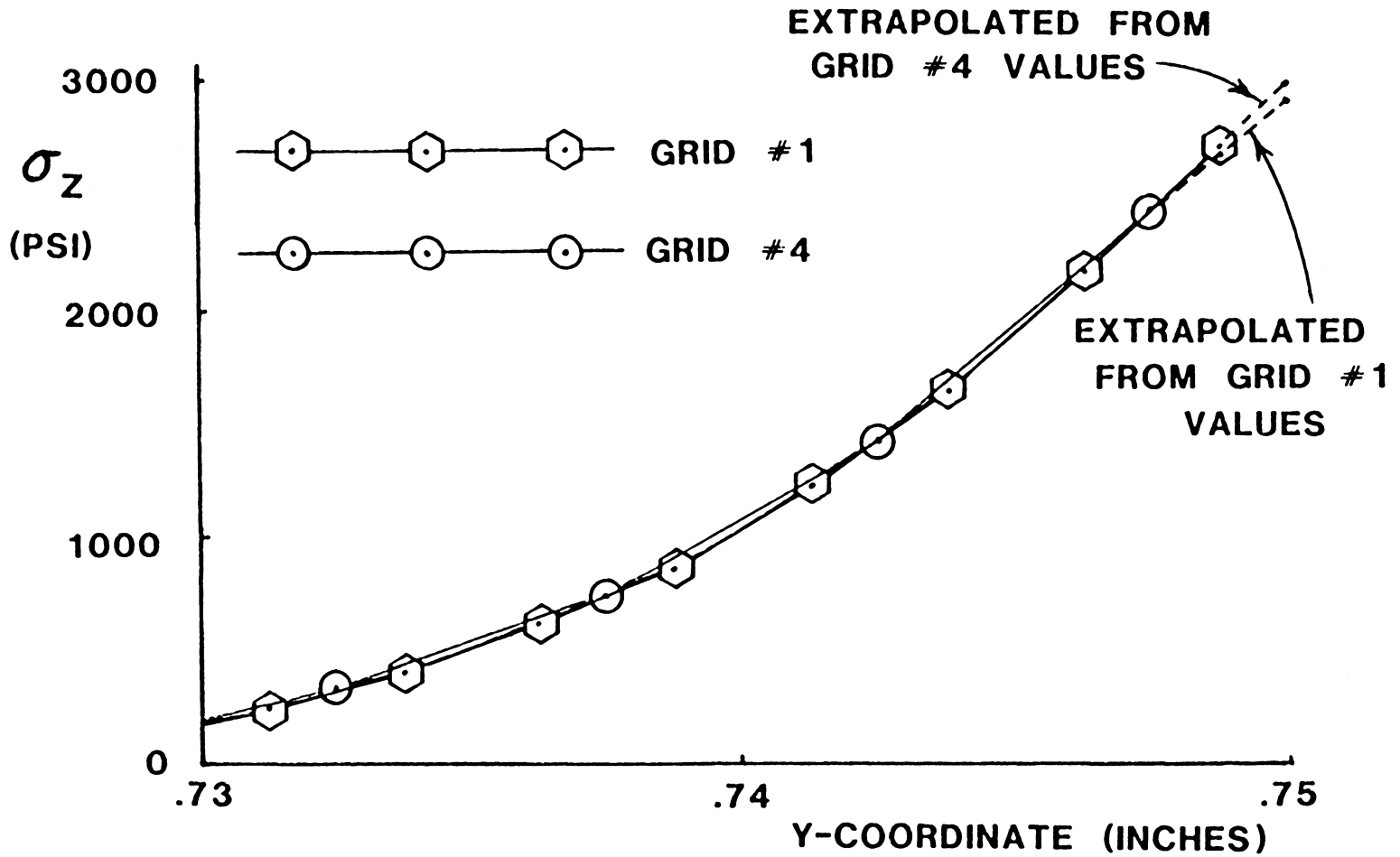

FIGURE 3-7 Interlaminar Stresses Near Midplane of Laminate Predicted with Grid #'s 1 and 4

#1 is preferred because its greater number of elements near the free edge allows for the edge cap to be modelled more exactly when the reinforced laminate is to be analyzed. Grid #1, then, is selected to be the FE grid used to model the NASA edge delamination specimen.

In order to develop the grid for the edge cap, a procedure similar to that described above is used. A trial grid is selected and compared to a more refined grid to determine whether the trial grid is acceptable. A grid with one row of elements through the thickness of the cap is not considered because differences in stresses through the thickness of the cap cannot be identified if only one row of elements is used. Grids containing two and four rows of elements are compared, and the displacements and stresses within the laminate calculated using each grid are nearly identical. The stresses within the cap itself, which are calculated using a 2-row grid, are somewhat different from those calculated using the 4-row grid, but the same general trends are shown, as seen in Figure 3-8. The stresses in the cap are low compared to those in the laminate, so the cap is not expected to fail when the laminate is loaded. Therefore, the cap stresses are not critical, and the 2-row grid is acceptable. The final reinforced NASA laminate FE grid is shown in Figure 3-9.

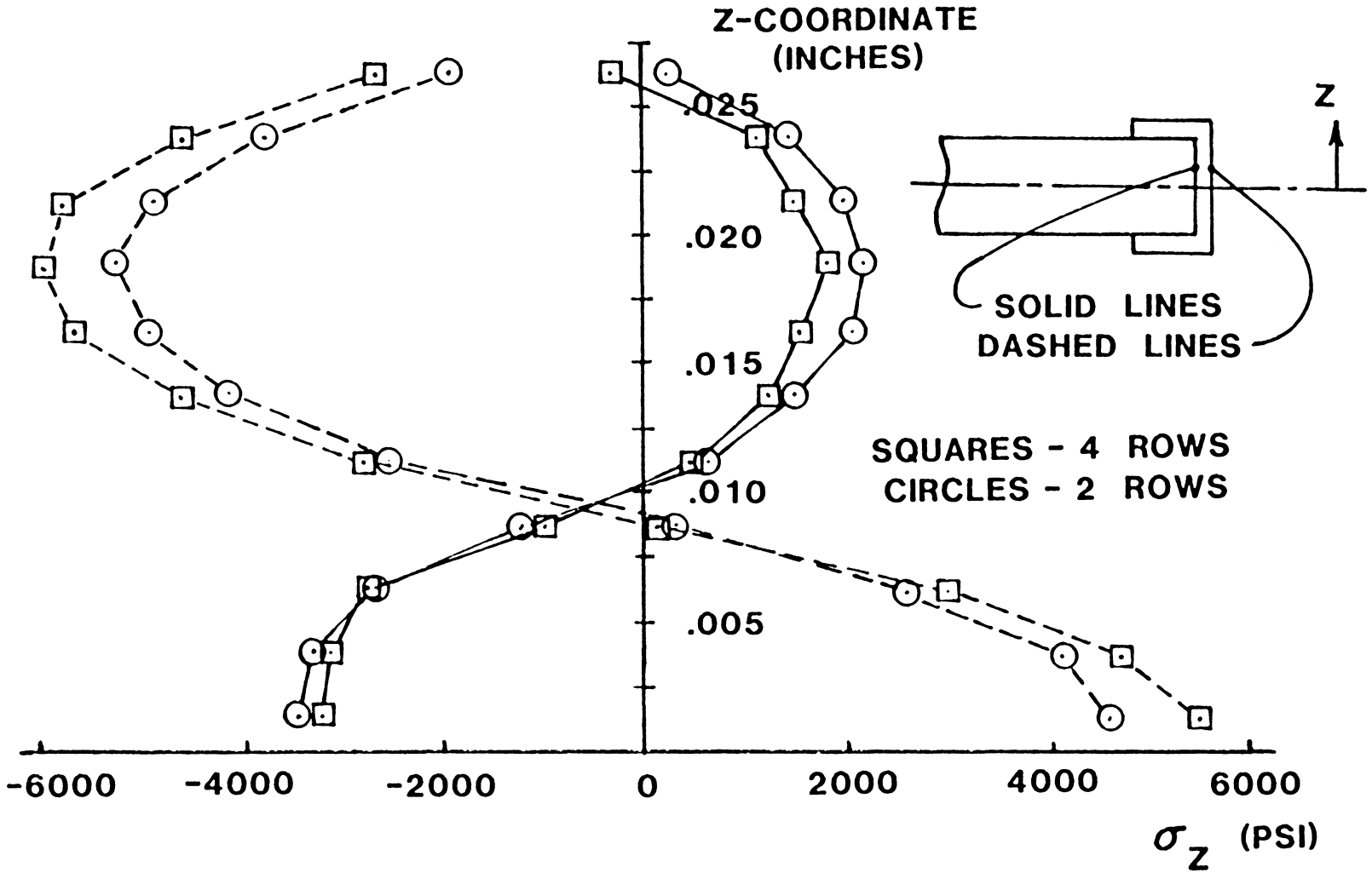

FIGURE 3-8 Z-Direction Normal Stress in Cap - 2 and 4 Rows of Elements in Cap Grid

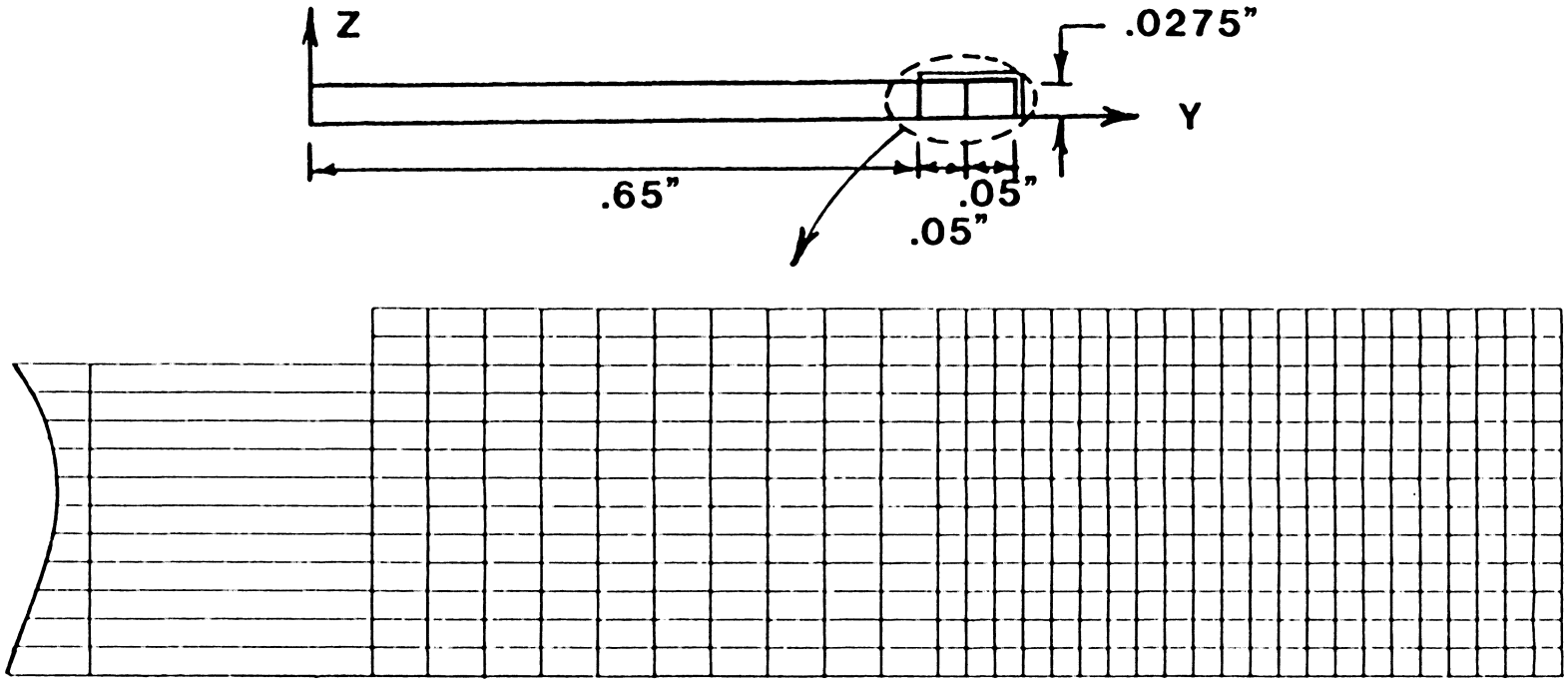

FIGURE 3-9 Reinforced Laminate Finite Element Grid

A manufacturing defect was observed during the fabrication process for the capped laminates. The cap could not be fully bonded to the edge of the laminate because no pressure causing such a bond was applied. Instead, a gap occured between the laminate edge and the cap. (This gap is discussed in Chapter 4 and is shown in Figure 4-2.) In order to simulate as closely as possible the actual laminates which were loaded, this gap is incorporated into an FE grid, as shown in Figure 3-10. The value of .01 inches for the gap opening is selected arbitrarily; two other gap openings are considered, as shown in Figure 3-11. The largest interlaminar normal and shear stresses predicted by using these three grids differ by a maximum of 10%.

The material properties which are input into the SAAS program are calculated from principal material direction properties, as described in Appendix A. The principal material direction properties for the T-300-5209 unidirectionally reinforced graphite-epoxy material were provided by Mr. Mark Shuart of NASA Langley Research Center [14]. The principal material direction properties for the K-49-F-155 Kevlar-epoxy woven cloth material were obtained from Lubin [15]. The input properties are listed in Table 3-1.

The value of the X-direction extensional strain which is input into the SAAS program is .001. This strain corresponds

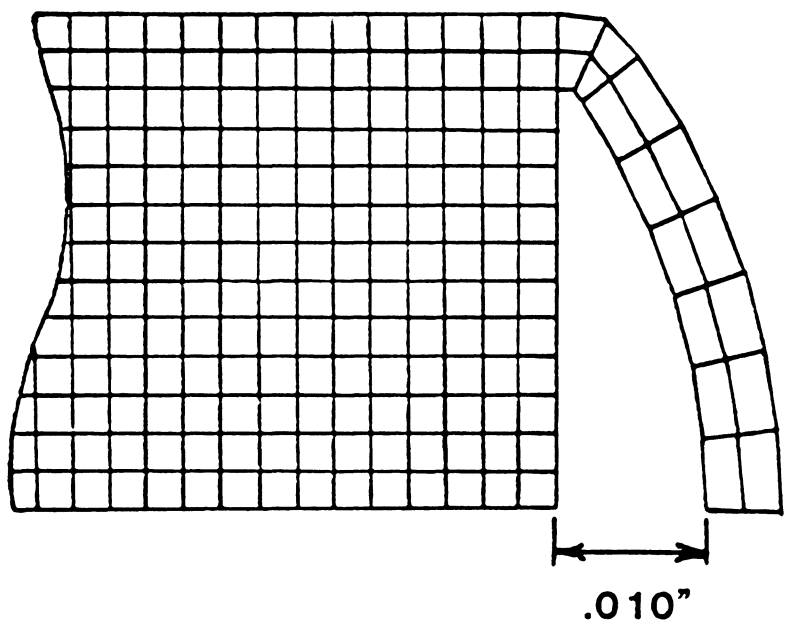

FIGURE 3-10 Finite Element Grid for Reinforced Laminate with Gap Between Laminate Edge and Cap

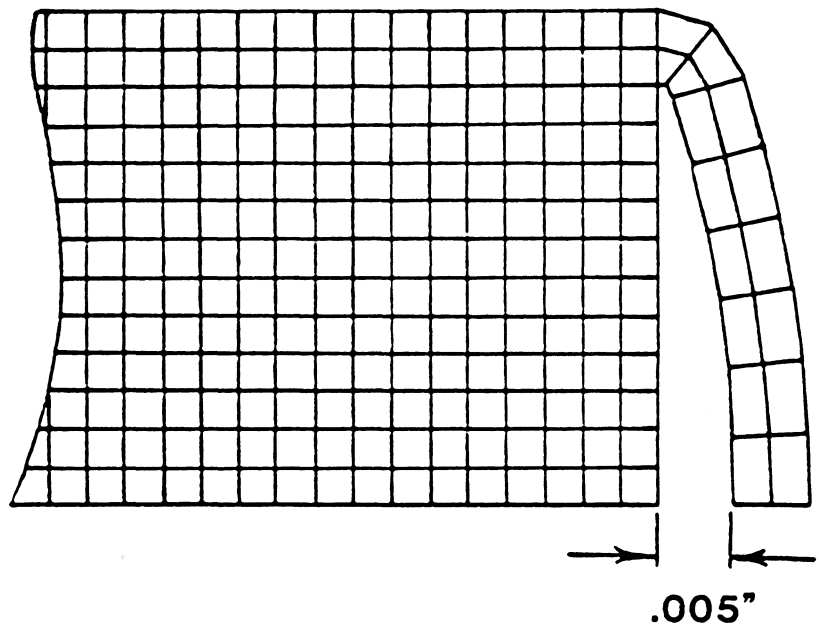

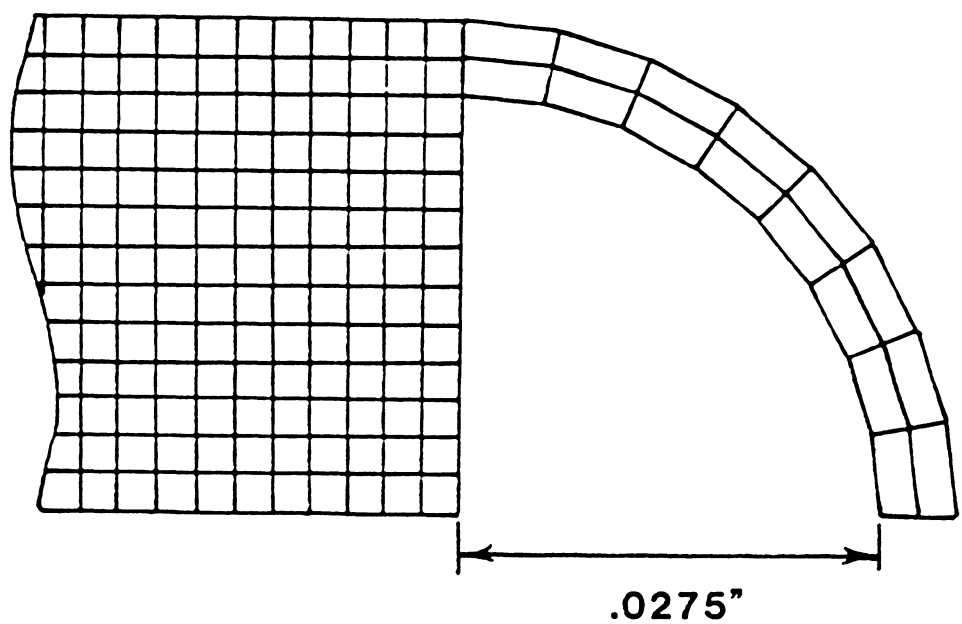

FIGURE 3-11 Alternative FE Grids for Modelling Gap

TABLE 3-1

Material Properties Input to SAAS III Computer Program

Material Principal Direction Properties

Property	Graphite-Epoxy (from Shuart [14])	Kevlar-Epoxy (from Lubin [15])
E-1 (Msi)	18.5	7.9 *
E-2 (Msi)	1.64	.74
NU-12	.30	.31
G-12 (Msi)	.87	.26
NU-23	.36	.40 **

* Lubin [15] gives E-1 as 11.86 psi for 60% fiber volume. This number has been reduced to represent 40% fiber volume (woven cloth).

** Assumed value

Input 3-D Properties

Property	Graphite-Epoxy		Kevlar-Epoxy
	90 Degree Layers	+/-30 Degree Layers	0/90 Degree Cloth
E-Z (Msi)	1.64	1.64	.74
E-Y (Msi)	1.88	18.5	4.35
E-X (Msi)	7.34	1.64	4.35
NU-ZY	.23	.027	.077
NU-ZX	-.011	.36	.077
NU-YX	.30	.30	.053
E-T' (Msi) *	.99	2.25	.766

* modulus in YZ-plane 45 degrees from Y-axis

to a total axial load on the specimen of 643 pounds, as calculated using CLT analysis. Throughout this report, all stresses and displacements which are reported correspond to this load level. For linear elastic analysis, stresses and displacements can be scaled to any load.

The finite element models discussed in this section are used to calculate the stress distributions within unreinforced and reinforced laminates. Finite element results are presented in the next section.

3.3 SAAS III RESULTS

Classical lamination theory was used in Section 3.1 to show that tensile interlaminar Z-direction stresses are predicted near the free edge of the NASA free edge delamination specimen, with the largest stresses occurring at the laminate midplane. This prediction is verified with the SAAS III finite element results.

Under load, the unreinforced laminate is predicted to increase in thickness near the free edge, as is shown in the deformed grid plot of Figure 3-12. The Z-direction normal stresses are largest near the laminate midplane and the free edge, as shown in Figure 3-13. The letter "K" is used to

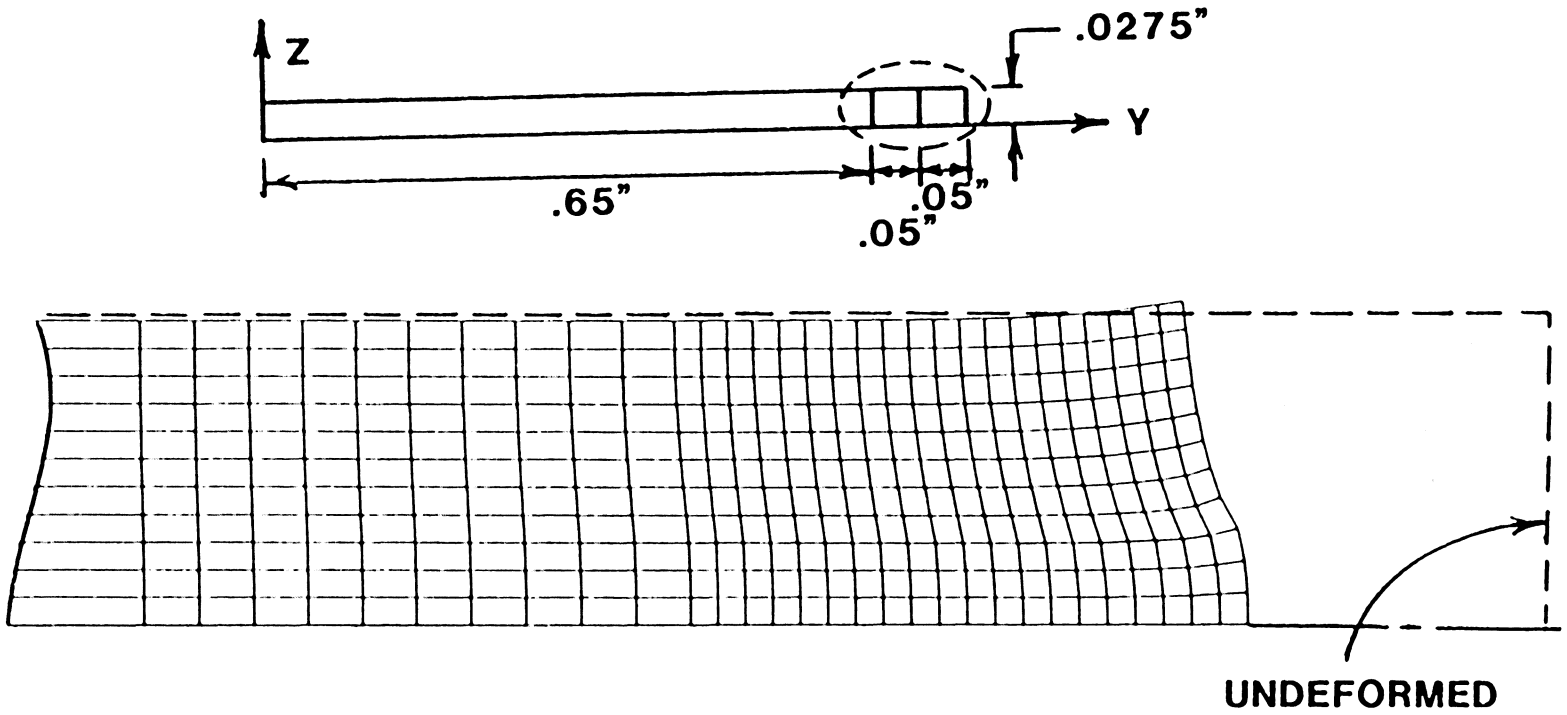

DISPLACEMENTS MULTIPLIED BY 100

FIGURE 3-12 Deformed SAAS III Grid - Unreinforced Laminate

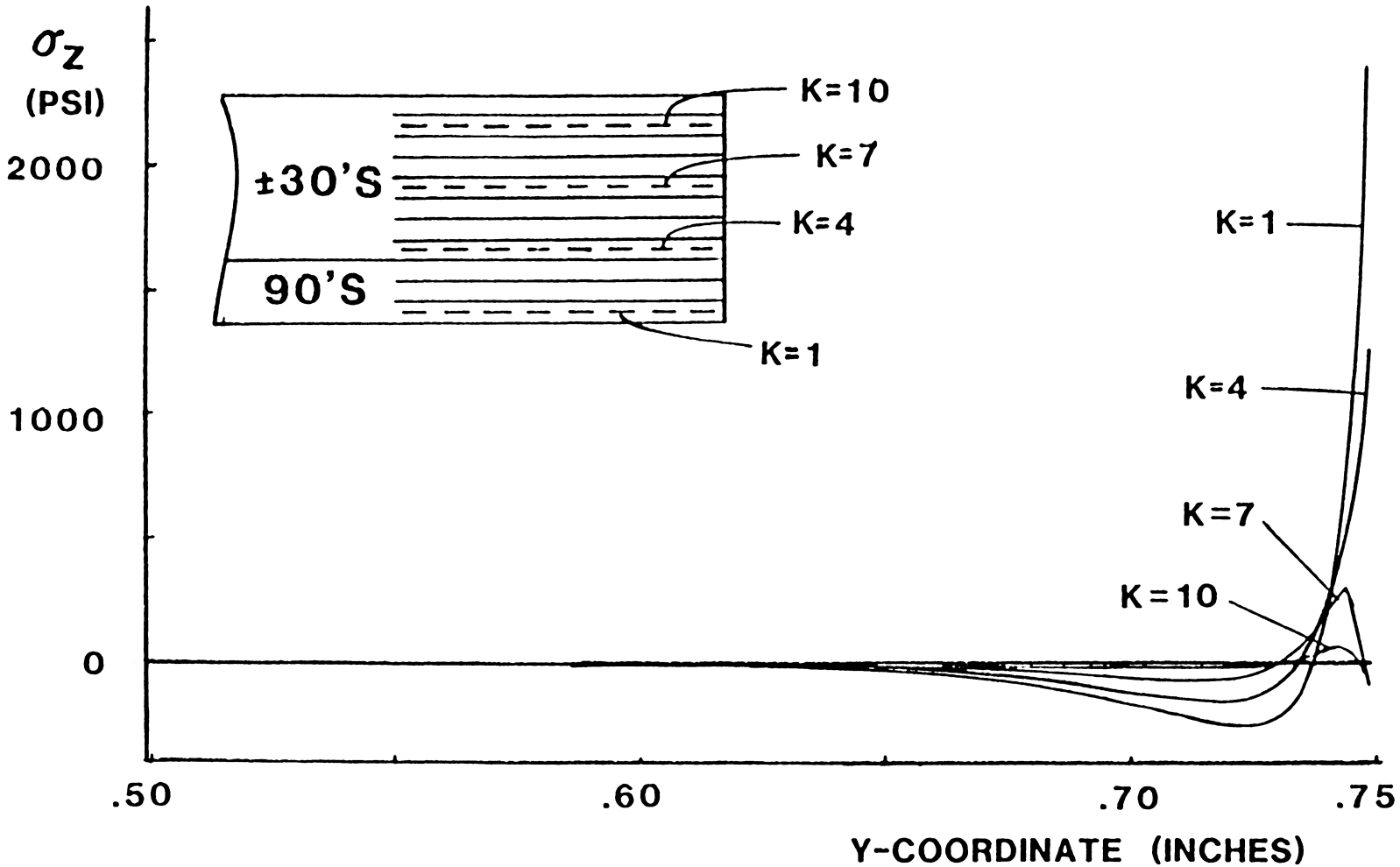

FIGURE 3-13 Z-Direction Normal Stress - Unreinforced Laminate

denote the row of elements for which the stresses are plotted. The row of elements which is adjacent to the midplane has a K-value of one. The Z-direction normal stresses near the midplane are increasing very rapidly near the free edge, suggesting the presence of the mathematical singularity which was theorized by Pipes and Pagano [1]. The Z-direction normal stresses decrease near the top surface. This result is consistent with the traction-free boundary condition of the top surface. The maximum values of the YZ-shear stress occur at the interface between the +/-30 degree layers and the 90 degree layers. This condition is shown in Figure 3-14. These shear stresses decrease near the free edge and near the top surface. These results are also consistent with the boundary conditions of a traction-free top surface and free edge.

The edge cap is predicted to prevent the edge of the laminate from increasing in thickness as shown for the deformed reinforced laminate in Figure 3-15. The Z-direction normal stresses, which are shown in Figure 3-16, are much lower than those for the uncapped laminate (Figure 3-13). The YZ-shear stresses, however, are almost unchanged in magnitude. This result can be seen by comparing the shear stresses for the capped laminate (Figure 3-17) with those for the uncapped laminate (Figure 3-14).

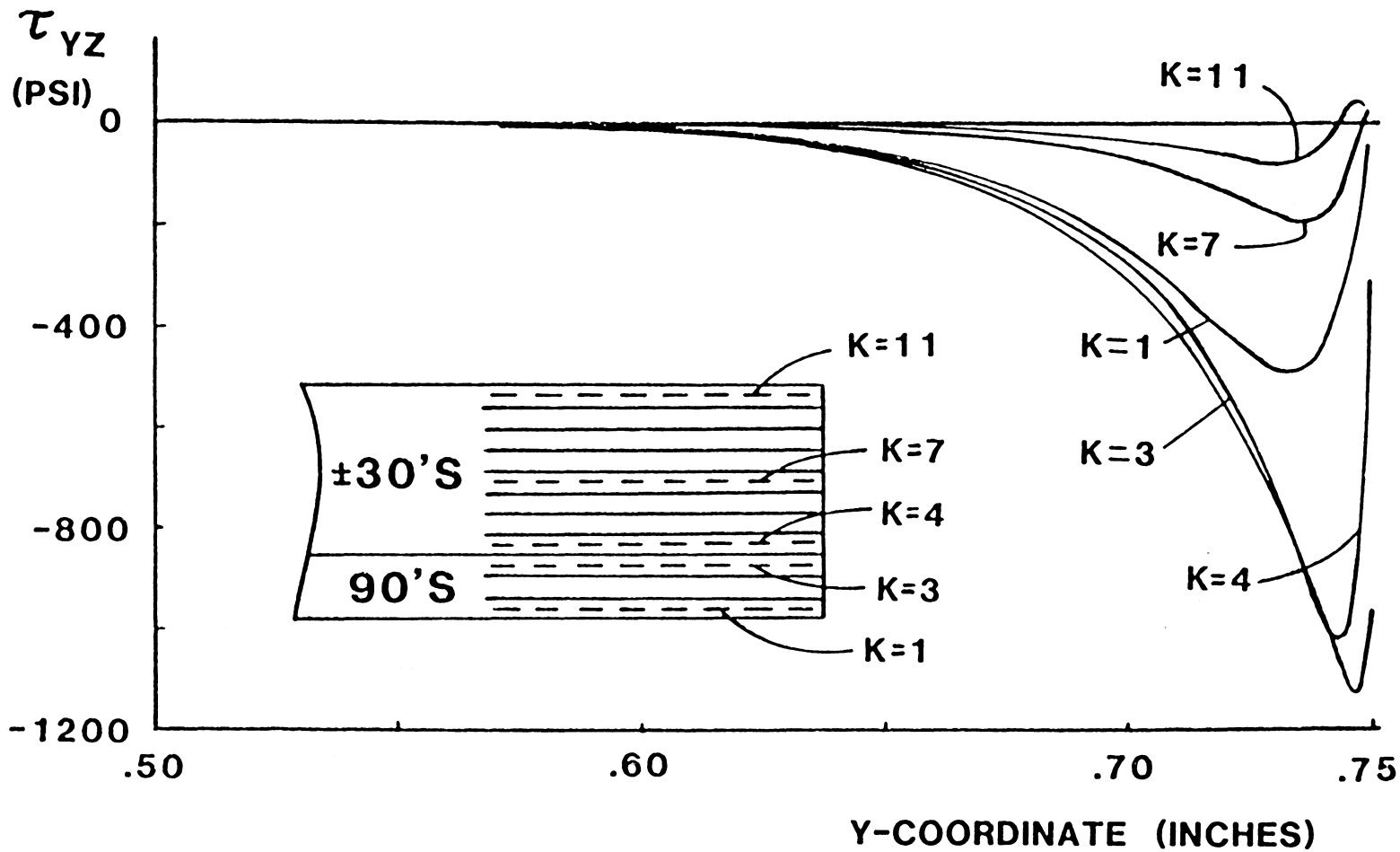

FIGURE 3-14 YZ-Shear Stress - Unreinforced Laminate

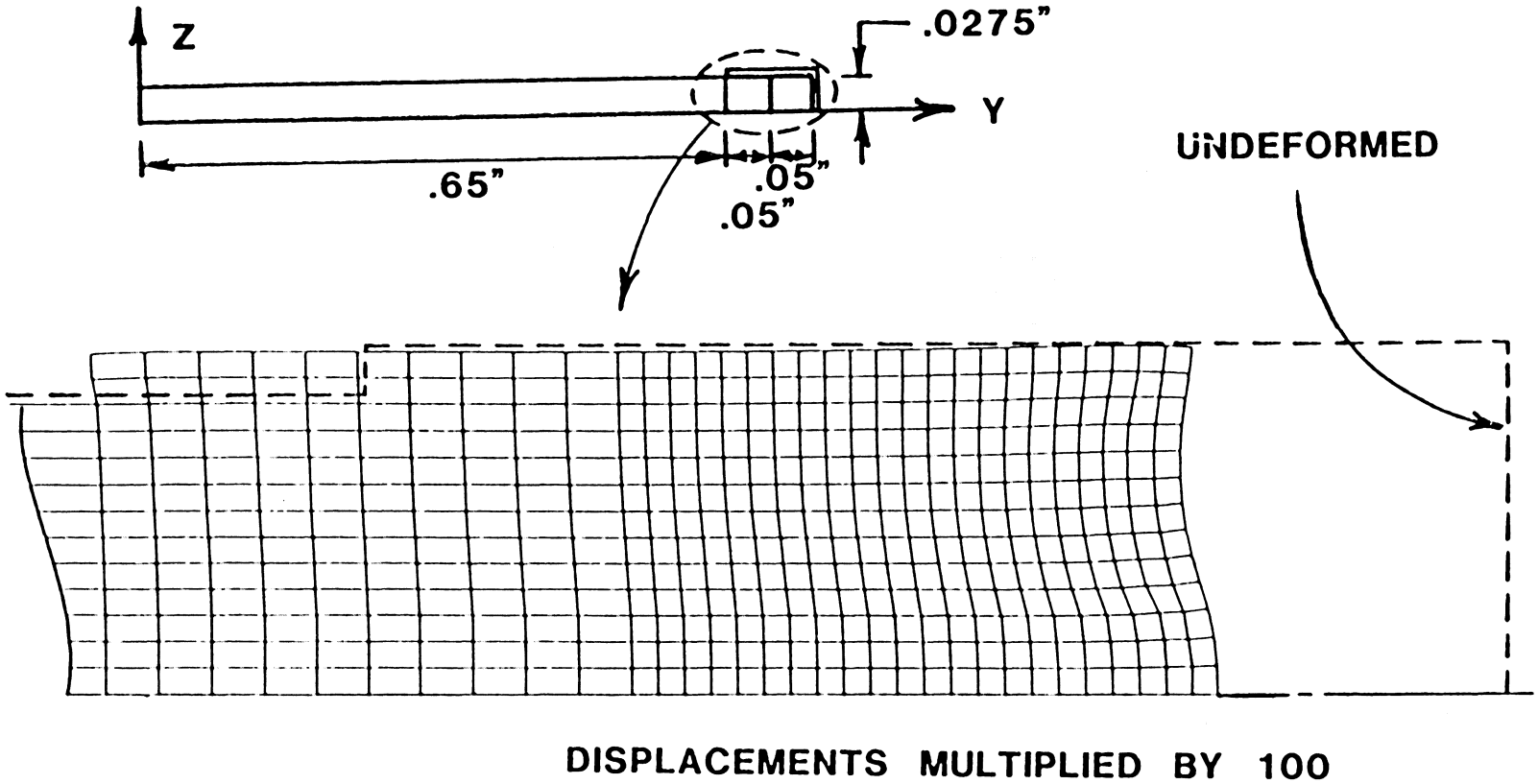

FIGURE 3-15 Deformed SAAS III Grid - Reinforced Laminate

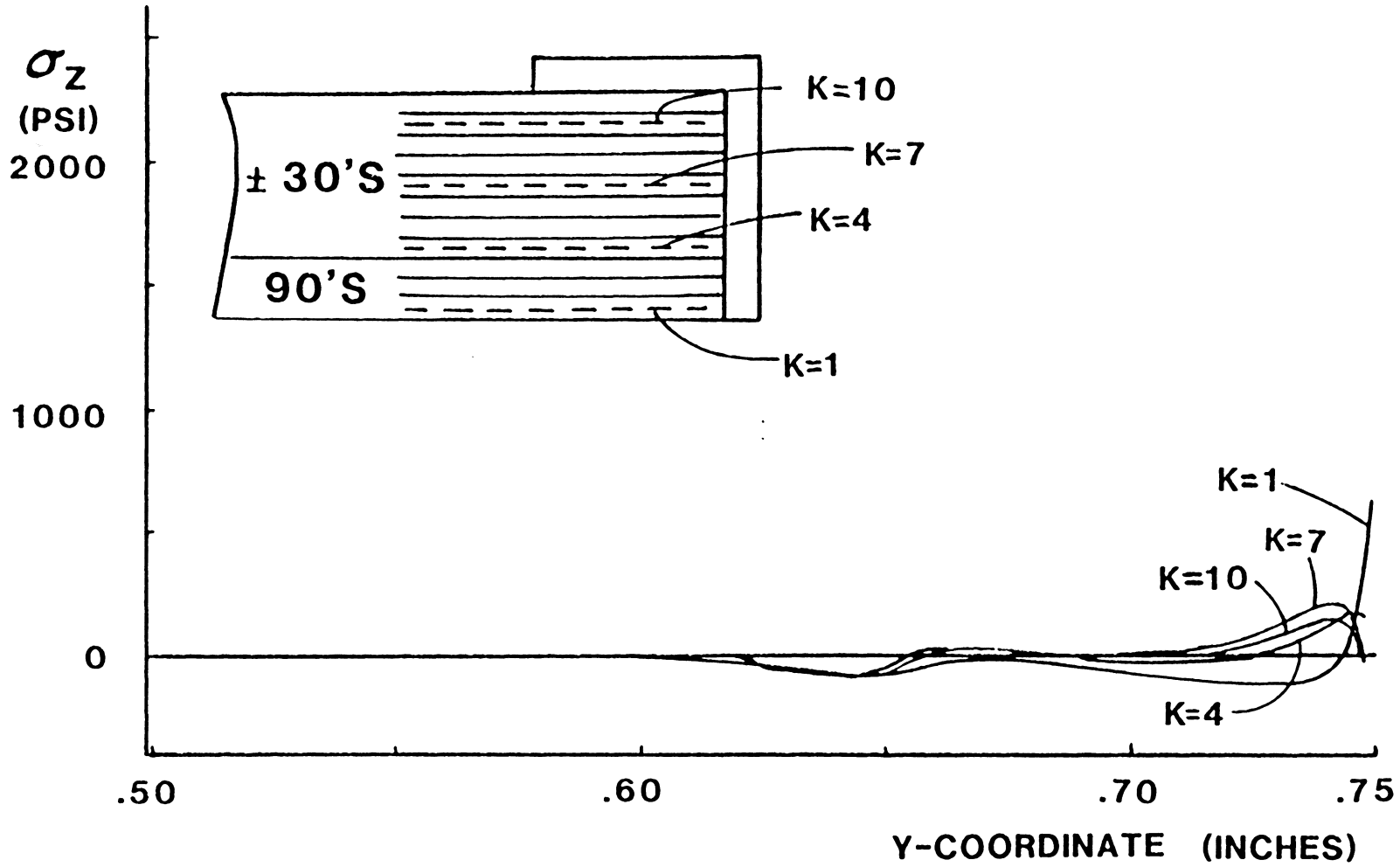

FIGURE 3-16 Z-Direction Normal Stress - Reinforced Laminate

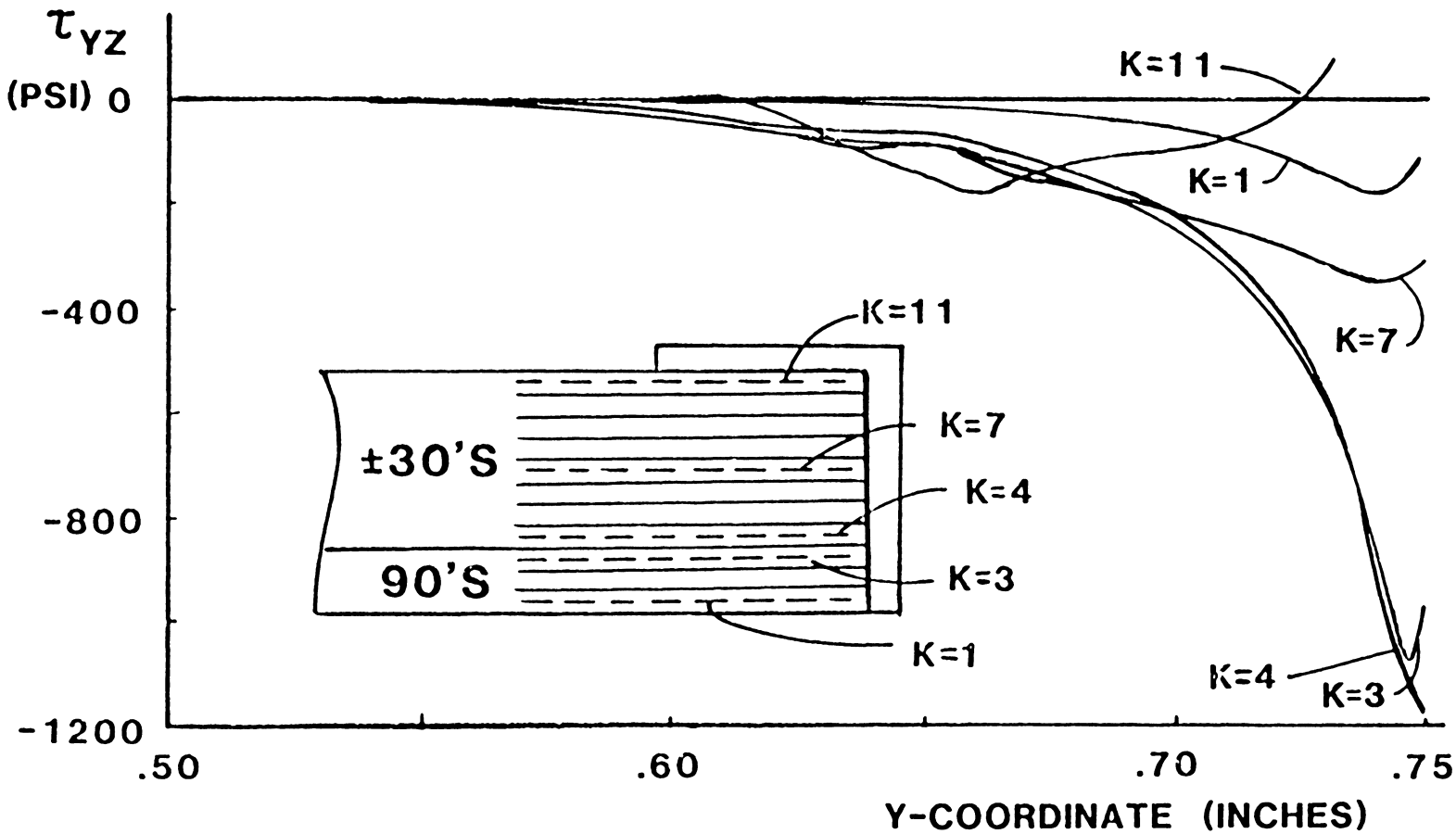

FIGURE 3-17 YZ-Shear Stress - Reinforced Laminate

The Z-direction stresses in the part of the cap which is bonded to the edge of the laminate are relatively low, as shown in Figure 3-18. Because these stresses are in the direction of some of the fibers in the cap, the corresponding tensile strength is much higher than the through-the-thickness tensile strength of the laminate. When the Hoffman 3-D failure criteria is applied to both the stresses within the laminate and the stresses within the cap, it is predicted that the laminate will fail at a much lower load than the failure load of the cap. Therefore, cap stresses are not important in the evaluation of an edge cap.

The shear stresses between the top surface of the laminate and the edge cap are shown in Figure 3-19. Notice in Figure 3-19 that the area under the curve is small, as the positive and negative parts of the curve nearly cancel each other. This result would seem to indicate that the net load which is transferred from the cap to the laminate is small. To illustrate this observation, SAAS III analyses were performed for two problems involving dissimilar materials which are bonded together. The first problem, the "shear lag" problem, has the load being transferred from the top material to the bottom material, as shown in the first sketch of Figure 3-20. In the second problem, the "strain compatibility" problem, the loading and the reactions both occur in the

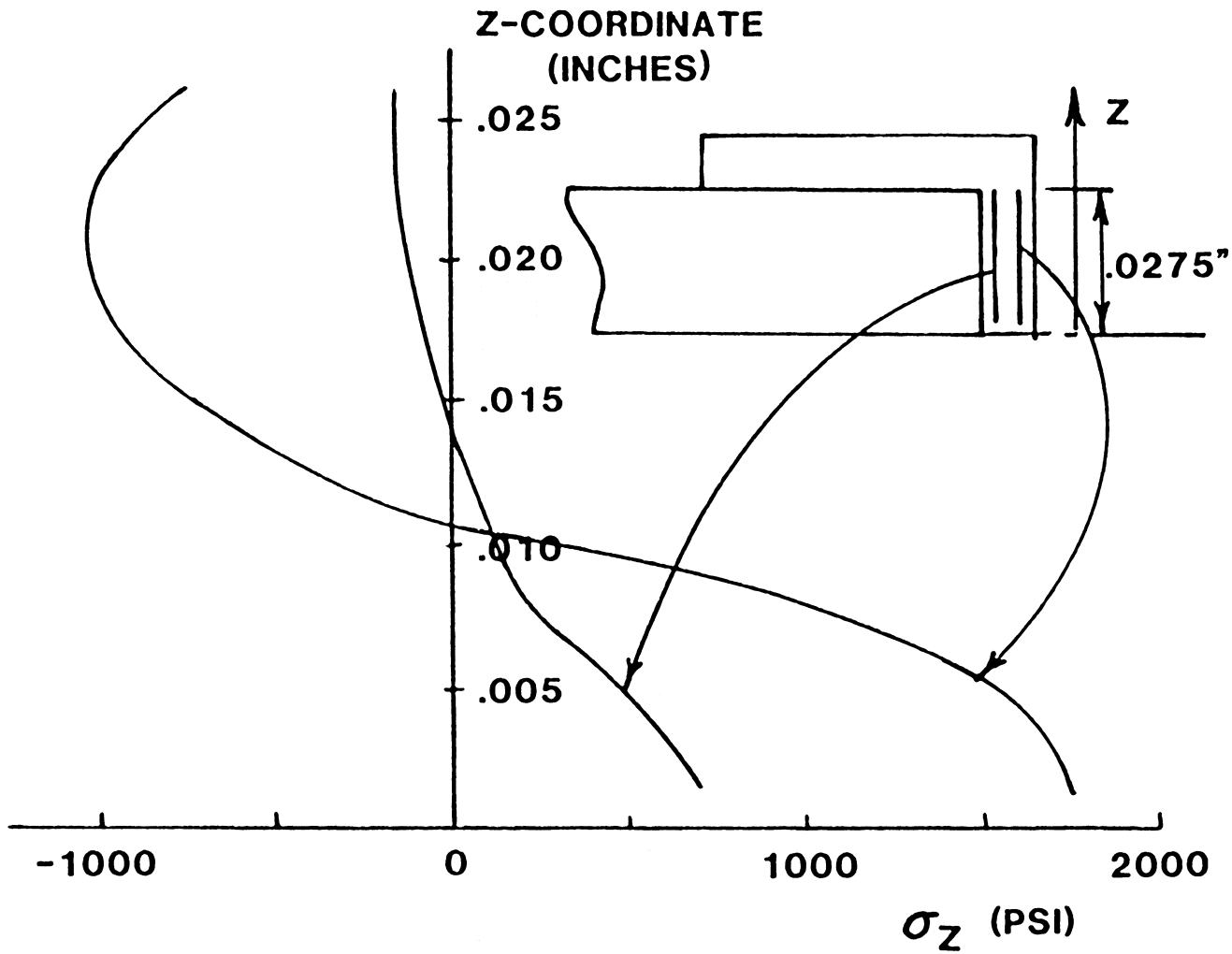

FIGURE 3-18 Z-Direction Normal Stress in Cap

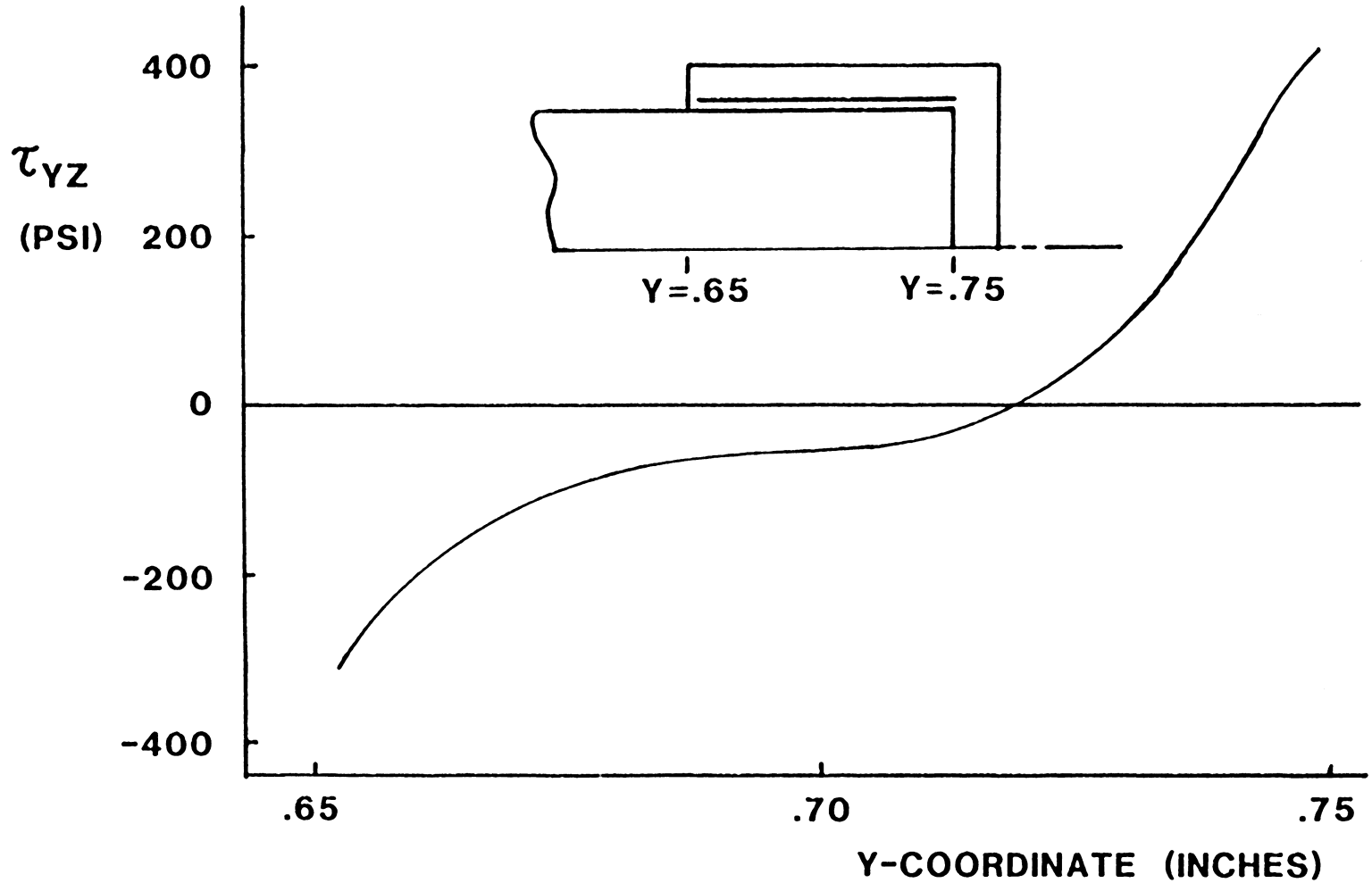

FIGURE 3-19 YZ-Shear Stress in Cap Adjacent to Cap-to-Laminate Interface

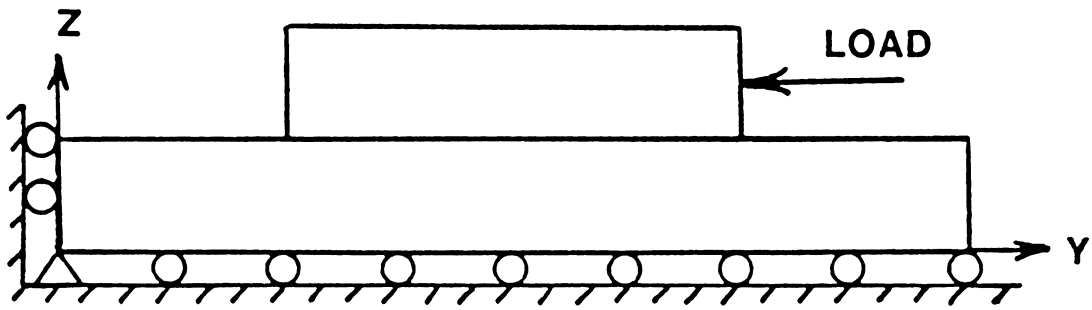

SHEAR LAG PROBLEM

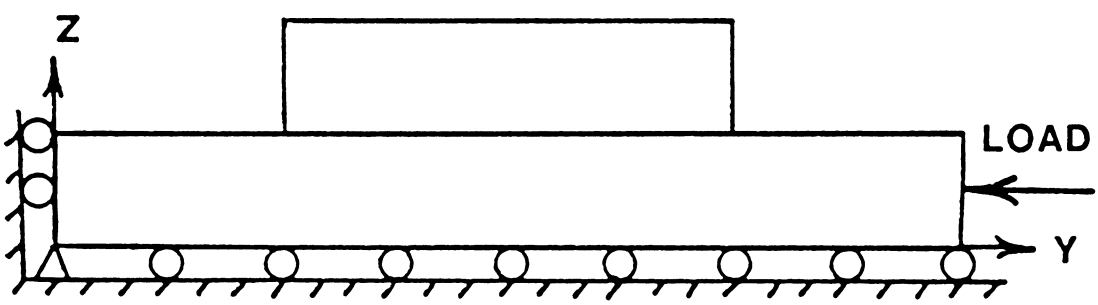

STRAIN COMPATIBILITY PROBLEM

FIGURE 3-20 Shear Stress Example Problems

bottom material, as shown in the second sketch of Figure 3-20. The shear stresses between the material layers, as predicted using the SAAS III plane strain option, are shown in Figure 3-21. The shear stresses for the edge cap-to-laminate top surface interface (Figure 3-19) closely resemble those for the "strain compatibility" case. This result leads to the observation that the top part of the cap is not a load-transferring member. Therefore, the bond length of the cap onto the laminate is probably not an important parameter.

Cap-to-laminate bond length is one of the design parameters which is varied in SAAS III analyses and compared to the "baseline" edge cap results. The other design parameters are cap thickness and cap material or fiber orientation. The baseline cap is one layer of K-49-F-155 Kevlar-epoxy style 120 woven cloth with the fibers oriented parallel to the X- and Z-axes. The bond length is .10 inches. The changes to be considered are extending the bond length to .25 and .50 inches, doubling the cap thickness, changing the cap material to T-300-5209 graphite-epoxy, and changing the orientation of the Kevlar-epoxy cloth so that the fibers are oriented at +/-45 degree angles to the X-axis. These alternative cap designs are shown in Figure 3-22. The effect of each design parameter on the performance of the cap is shown by comparing

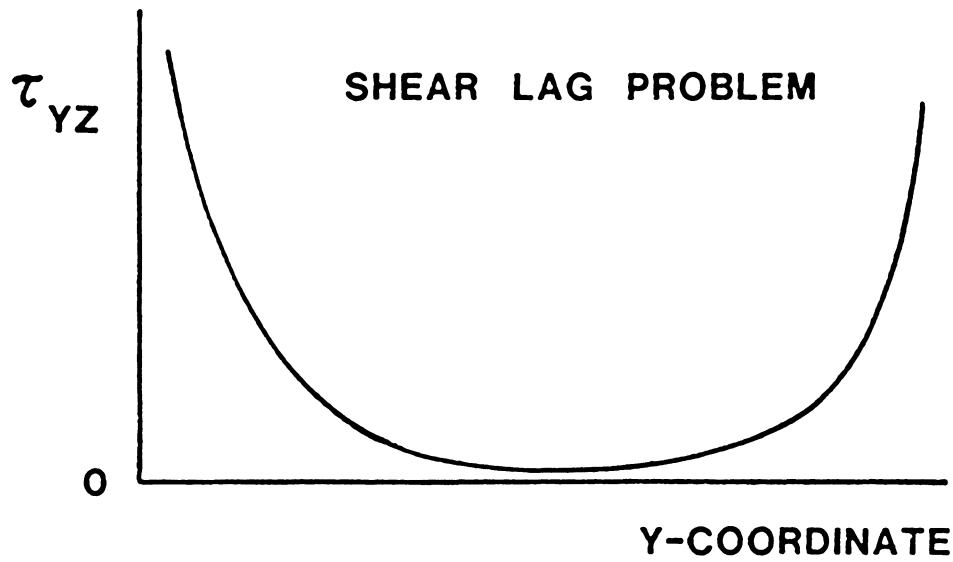

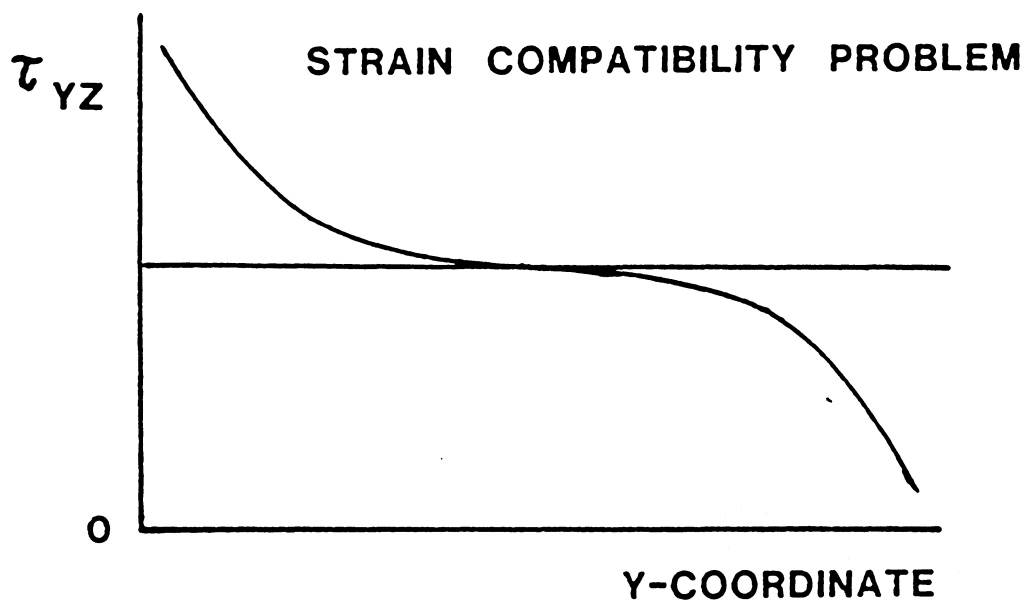

FIGURE 3-21 Shapes of YZ-Shear Stress Plots for Example Problems

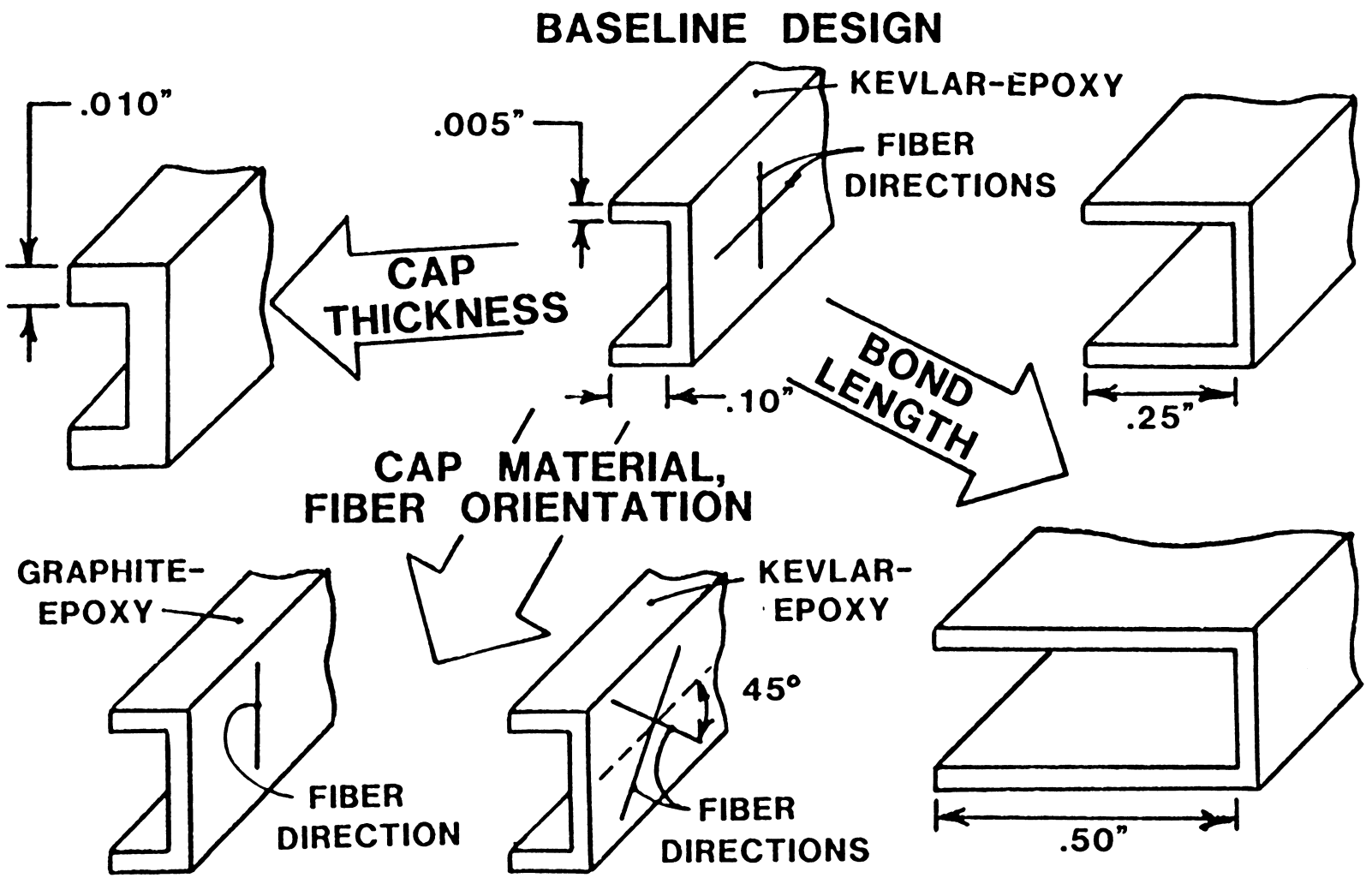

FIGURE 3-22 Alternative Edge Cap Designs

the values of three stresses to those predicted for the baseline design: (1) the maximum value of the Z-direction normal stress in the 90 degree plies near the laminate midplane, which contributes to delaminations, (2) the maximum value of the Z-direction normal stress in the +/-30 degree layers, which contributes to the ultimate failure of the laminate, and (3) the maximum value of the YZ-shear stress near the +/-30-90 interface, which also contributes to the ultimate laminate failure. These stress values associated with each cap design are listed in Table 3-2.

The cap-to-laminate bond length has little effect on the laminate stresses, as was predicted earlier. Increasing the bond length from .10 inches to .25 or .50 inches causes almost no change in the interlaminar stresses. It should be noted that the specimens which were fabricated had a 1/2" bond length because it was deemed impractical to fabricate an edge cap from a narrower piece of material.

The use of two layers of material in the cap instead of one caused the interlaminar stresses to be lower, but only by 5 - 10% at most. The conclusion drawn from this result is that the use of more than one layer of material for the edge cap is of little benefit for reinforcing this thin (11-layer) laminate.

TABLE 3-2

Maximum Stress Values- Alternative Cap Design Study

Cap Design	σ_z 90 Degree Layers (psi)	σ_z +/-30 Degree Layers (psi)	τ_{yz} +/-30-90 Interface (psi)
No Cap	2927	1528	1108
Baseline Cap	819	212	1199
Thick Cap (2 layers)	748	202	1081
.25" Bond Length	838	219	1213
.50" Bond Length	840	219	1213
Kevlar-epoxy +/-45 Degree Cap	659	48	1250
Graphite-epoxy Cap	249	289	1151

The selection of the cap material and its orientation is the design parameter which is shown to be the most important. The two alternative cap materials represent two different reinforcement strategies: (1) stiffening the cap (increasing the modulus E-Z) in order to provide more resistance to through-the-thickness deformations and (2) increasing the Poisson's ratio NU-XZ in order to cause the cap to "shrink" onto the laminate when loaded as does the braided Chinese finger torture device that clamps harder on your fingers when you try to pull them apart. (The coordinates which are used here are for the part of the cap which is bonded to the edge of the laminate, i.e., the fibers lie in the XZ-plane.) The graphite-epoxy material represents the first strategy. It has an E-Z of 18.5 Msi, compared to 4.35 Msi for the 0/90 degree Kevlar-epoxy and .93 Msi for the +/-45 degree Kevlar-epoxy. The +/-45 degree Kevlar-epoxy material represents the second design strategy. It has a Poisson's ratio NU-XZ of .80, compared to .053 for the 0/90 degree Kevlar-epoxy and .027 for the graphite-epoxy. Although the lowest values of the Z-direction normal stress in the 90 degree layers and the YZ-shear stress correspond to the graphite-epoxy cap, the +/-45 degree Kevlar-epoxy cap is shown to be the most effective for reducing the Z-direction normal stress in the +/-30 degree layers. Therefore, neither of these two cap designs can be identified as the "best"

choice. Based on the stress predictions, the graphite-epoxy cap should delay the onset of delaminations better than the other caps, while the +/-45 degree Kevlar-epoxy cap should improve the laminate's ultimate strength the most. It should be noted that these results are for tensile loading only. The +/-45 degree Kevlar-epoxy cap will shrink onto the laminate when subjected to a tensile load, but will expand a great deal when subjected to a compressive load. Therefore, the graphite-epoxy cap is preferred for compressive loading or tension-compression fatigue loading.

The FE model for the capped laminate with a manufacturing defect (see Section 3.2) is analyzed in order to determine the effect of the defect, or gap, on the stresses in the laminate. In general, all of the interlaminar stresses for the cap with a gap fall between those predicted for the uncapped laminate and those predicted for the "ideal" (no gap) capped laminate. This result is shown for the Z-direction normal stresses in Figure 3-23. The conclusion drawn from these results is that the cap which is not bonded to the edge does reduce the interlaminar stresses, but not as effectively as the "ideal" cap.

The results of the SAAS III analyses lead to the conclusion that the addition of edge caps lowers interlaminar normal stresses in the NASA edge delamination tension specimen. In

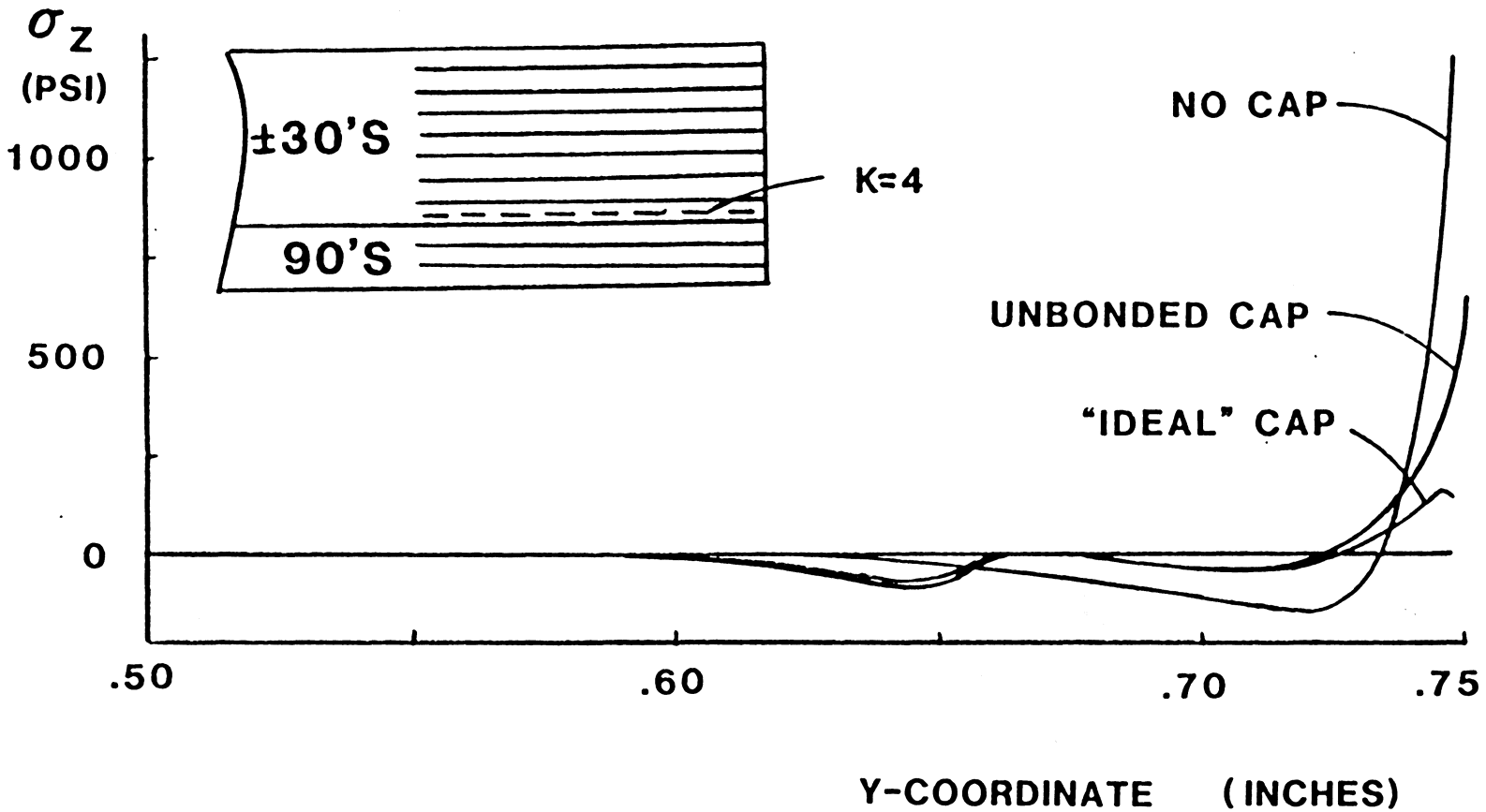

FIGURE 3-23 Stress Reduction Due to Unbonded Cap

order to correlate these results to the ultimate strength of the specimen, stresses calculated using SAAS III must be used in a three-dimensional failure criterion.

3.4 FAILURE PREDICTIONS

A progressive laminate failure analysis is used to calculate the failure load of the NASA edge delamination tension specimen. The failure criteria which are presented in Section 2.3 are used to predict the failure loads of individual laminae. The lamina with the lowest failure load has its material properties degraded to reflect the associated failure mode, and the analysis is repeated. A new failure load is then calculated for each lamina. This process is repeated until no laminae remain intact.

3.4.1 FAILURE PREDICTIONS BASED ON 2-D STRESSES

Predicted failure loads which are calculated using CLT-calculated stresses are too high because CLT does not include interlaminar stresses. These failure loads are of interest, however, because they represent the theoretically highest laminate strength which is possible, i.e., the strength which would be obtained if the interlaminar stresses did not

influence or cause failure.

The failure sequence which is outlined here results from using the Hoffman criterion. Similar procedures are used to predict the failure load using the Tsai-Hill and the Tsai-Wu failure criteria. An axial load per unit width of 1000 pounds/inch (1500 pounds total load) is arbitrarily selected, and CLT is used to predict the in-plane stresses in principal material directions which are shown in Table 3-3. Because linear analysis is used, these stresses can be linearly scaled to obtain the state of stress at any load value at or below the first-ply failure. The stresses for each lamina are scaled to the load value at which the failure polynomial is equal to one (the condition for lamina failure). Failure loads which result from this scaling are 2617 pounds for the 90 degree layers and 5594 pounds for the +/-30 degree layers. Therefore, the 90 degree layers are the first to fail. Each term of the failure polynomial is then evaluated for the 90 degree lamina failure load to determine the failure mode. The largest terms are those which involve the stress component transverse to the fibers (in the X-direction), as shown in Table 3-4. This result indicates that the matrix (resin) of the 90 degree layers will fail.

To account for this failure in a progressive laminate failure analysis, the Z-direction modulus and the in-plane

TABLE 3-3

CLT Stresses for a 1500 Pound Axial Load

90 Degree Layers	+/-30 Degree Layers
σ_1 = -14,849 psi	σ_1 = 28,618 psi
σ_2 = 3,433 psi	σ_2 = 662 psi
τ_{12} = 0	τ_{12} = -/+ 2406 psi

TABLE 3-4

Value of Each Term of Hoffman's Failure Criterion for 90 Degree Layer Failure Load

$(C_2 + C_3)\sigma_1^2$ =	.0156
$(C_1 + C_3)\sigma_2^2$ =	.2748
$-2C_3\sigma_1\sigma_2$ =	.0036
$C_4\sigma_1$ =	.0042
$C_5\sigma_2$ =	.7019
$C_6\tau_{12}^2$ =	.0000
	1.0001

shear modulus of the 90 degree layers are reduced by a factor of ten. Stress values are recalculated, and new failure loads are computed: 5294 pounds for the +/-30 degree layers and 13,875 pounds for the 90 degree layers. The individual terms of the failure polynomial are calculated, and it is seen that the +/-30 degree layers are predicted to fail in a combined fiber tension and in-plane shear mode. Because this mode can result in broken fibers, the laminate will be left with no load-carrying capability. Therefore, 5294 pounds is the predicted failure load of the laminate. For the Tsai-Hill and the Tsai-Wu criterion, the corresponding predicted laminate failure loads are 5798 pounds and 5275 pounds, respectively.

3.4.2 FAILURE PREDICTIONS BASED ON 3-D STRESSES

A procedure similar to that described above for CLT stresses is used to predict failure based on FE results. The Hoffman three-dimensional failure criterion is used to predict lamina failures. Stresses which are rapidly increasing near the free edge cannot be used to calculate the laminate failure load because of the possible mathematical singularity which exists at the free edge. This restriction prevents calculation of a failure load based on FE results

for the unreinforced NASA edge delamination tension specimen. For the capped specimen, however, the ultimate load prediction is based on stresses which are calculated for a point away from the free edge. At this point, the Z-direction normal stresses reach a maximum value. Here is the failure sequence for the capped specimen, as predicted with FE results and the 3-D Hoffman failure criterion:

(1) The 90 degree layers fail in the X-direction (transverse to the fibers). The properties E-X, NU-XY, NU-XZ, G-XY, and G-XZ are then reduced in the FE model.

(2) The 90 degree layers fail in the Z-direction (delamination). To simulate this failure mode, E-Z, NU-ZY, NU-ZX, and G-YZ are reduced in the row of elements closest to the midplane. Another iteration results in the second row of elements having its properties degraded as in step (1). In both cases, the material properties are degraded only in a region near the edge. The width of this region is equal to the laminate thickness because almost all of the interlaminar stresses occur within this region.

(3) A +/-30 degree layer fails due to fiber tension, in-plane shear, Z-direction tension, and interlaminar shear. This mode corresponds to the failure of the

laminate because no load-carrying fibers remain.

The calculated failure load is 3920 pounds. It should be noted that this failure prediction is based on several assumptions and approximations, especially concerning the simulation of delaminations in step (2). The simulation of X-direction failure in the 90 degree layers, step (1), is relatively straightforward in that when some of matrix material fails, the rest of the material is strained more. Therefore, it is reasonable to expect all of the matrix material to fail at approximately the same time. This is not the case for delamination because a through-the-thickness failure in some of the material reduces the stresses in the remainder of the laminate. The way in which the delamination process is simulated will have an effect on the calculated failure load. Therefore, it should be kept in mind that this failure load is calculated for comparison purposes and should not be construed as a failure prediction with a high degree of confidence.

The failure load which is predicted using FE results is 74% of the failure load which is predicted using CLT results. The conclusion is that interlaminar normal stresses make a large contribution to the failure of the laminate, even for the capped laminate with interlaminar normal stresses which are much lower than those for the uncapped laminate.

Similar failure analyses can be performed to evaluate further the alternative edge cap designs studied in Section 3.3 (see Figure 3-22 and Table 3-2). The predicted failure loads based on 3-D stresses are 3710 pounds for a laminate reinforced with the +/-45 degree Kevlar-epoxy cap and 3980 pounds for a laminate reinforced with the graphite-epoxy cap. These results are obtained from FE models which include a gap between the cap and the laminate edge, while the results in Table 3-2 are for "ideal" caps. In Section 3.3, the +/-45 degree Kevlar-epoxy cap was shown to be the best design for reducing stresses in the +/-30 degree layers, while the graphite-epoxy cap is shown to be the best choice when the gap is present and a progressive laminate failure analysis is used. Therefore, when the gap is present the stiffness of the cap in the Z-direction appears to be the best edge cap design philosophy.

Finite element analysis is used to show that the inter-laminar normal stresses are lower for the capped laminate than for the uncapped laminate. This result leads to the qualitative conclusion that the capped laminate should be stronger than the uncapped laminate. A comparison of failure predictions based on CLT and FE results in the conclusion that interlaminar normal stresses are large enough to cause a significant decrease in laminate strength, even for the

capped laminates. These analytical conclusions are verified by an experimental program which is described in the next chapter.

CHAPTER 4

EXPERIMENTAL VERIFICATION

Fifteen NASA edge delamination tension specimens were fabricated and loaded to failure. Of these 15, eight had edge caps. Three of these capped specimens were loaded in static tension, and the other five were loaded in tension-tension fatigue. Of the seven remaining uncapped specimens, four were loaded in static tension, and three were loaded in fatigue. For both the static and fatigue loadings, the capped specimens were significantly stronger than the uncapped specimens. The addition of edge caps to the static-test specimens also caused the coefficient of variation of the failure strength to decrease.

4.1 FABRICATION OF SPECIMENS

The specimens were cut from cured 12" X 12" flat laminates. The laminates were laid up from unidirectional composite material composed of T-300 graphite fibers in a 5209 epoxy resin matrix. This material was cut from a 12"-wide roll. It should be noted here that the graphite-epoxy material had been stored well beyond its expiration date (by about 10 years). All of the specimens were fabricated from the same roll of material.

After the laminates were laid up, they were prepared for curing by being placed in the curing assembly which is shown in the schematic diagram of Figure 4-1. The purpose of the bleeder cloth is to absorb excess resin during cure. The glass skrim cloth prevents the bleeder cloth from sticking to the graphite-epoxy plate, and the mylar sheets prevent the bleeder cloth from sticking to the steel plates. The curing assembly was placed in a hot press which had been heated to 170 degrees F, and the press was closed. A small force was applied on the press to ensure contact between the components of the curing assembly. The temperature was held at 170 degrees F for 30 minutes to allow the temperature to equilibrate. The force on the press was then increased until the graphite-epoxy plate was subjected to a 100 psi pressure, and the temperature was increased to 260 degrees F. The temperature was held at 260 degrees F for one hour and 35 minutes, and then the heaters were turned off. The pressure was held at 100 psi until the temperature dropped to 180 degrees F. Then, the press was opened, the curing assembly was removed from the press, and the laminate was separated from the rest of the curing assembly.

The cured laminates were cut into 1.5" wide by 10" long specimens using a diamond-tipped saw. One-inch wide Kevlar reinforcements were cut from a sheet of style 120 woven

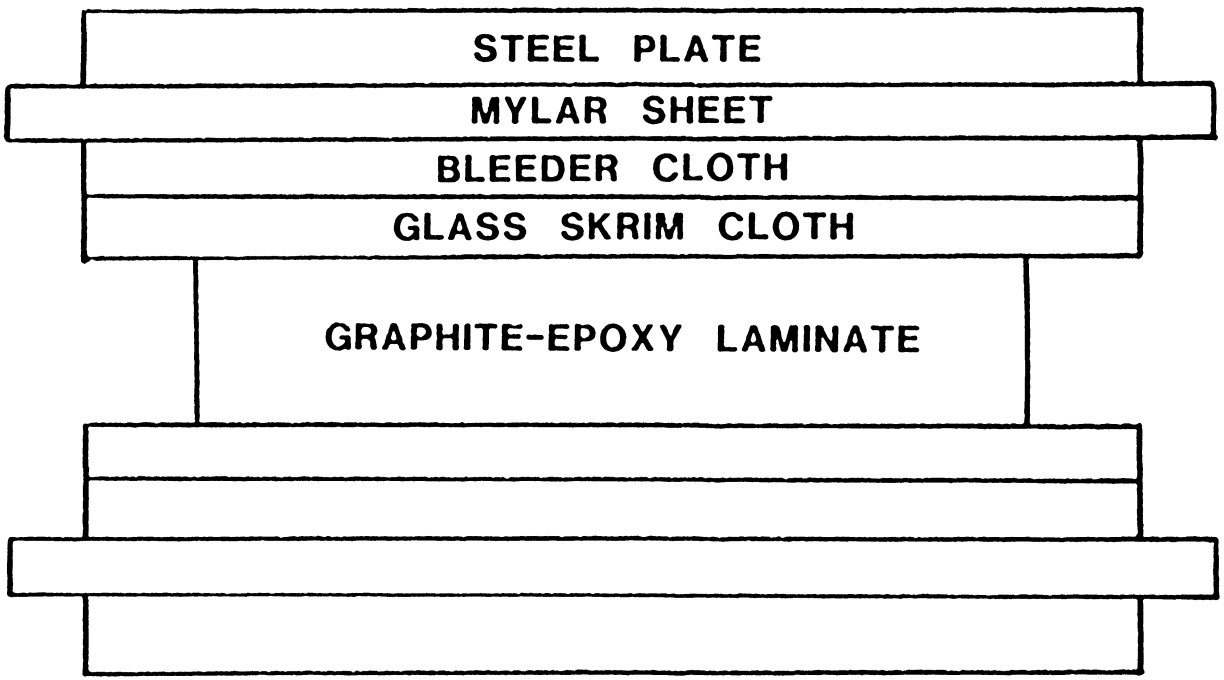

FIGURE 4-1 Curing Assembly

Kevlar-49-F-155 epoxy cloth and placed over the free edges of the laminates to be reinforced. These capped laminates were then subjected to a cure cycle similar to the earlier cure cycle. It should be noted that the total force on the hot press was calculated as though the total laminate surface area, rather than the surface area of the caps, was the load-bearing area. This calculation error resulted in a pressure of 150 psi, rather than the specified 100 psi, being applied to the caps during cure. This anomaly did not seem to affect the curing of the edge caps. The unreinforced laminates were not subjected to a second cure cycle.

During the cure of the edge caps, no direct pressure was exerted inward to force the cap against the laminate edge. As a result, a gap between the laminate edge and the cap was present in all of the reinforced specimens (see Figure 4-2). For laminates which are thicker than the NASA edge delamination tension specimen, this gap could be prevented by use of a curing apparatus through which pressure is applied to the laminate edges or by which the cap is restrained from moving away from the edge, as in Figure 4-3. For the thin laminates used in this project, such an apparatus would probably not prevent the gap because the Kevlar fibers could not be bent at a small enough radius. No excess resin was evident in the gap, so the gap was modelled as a void area in the finite

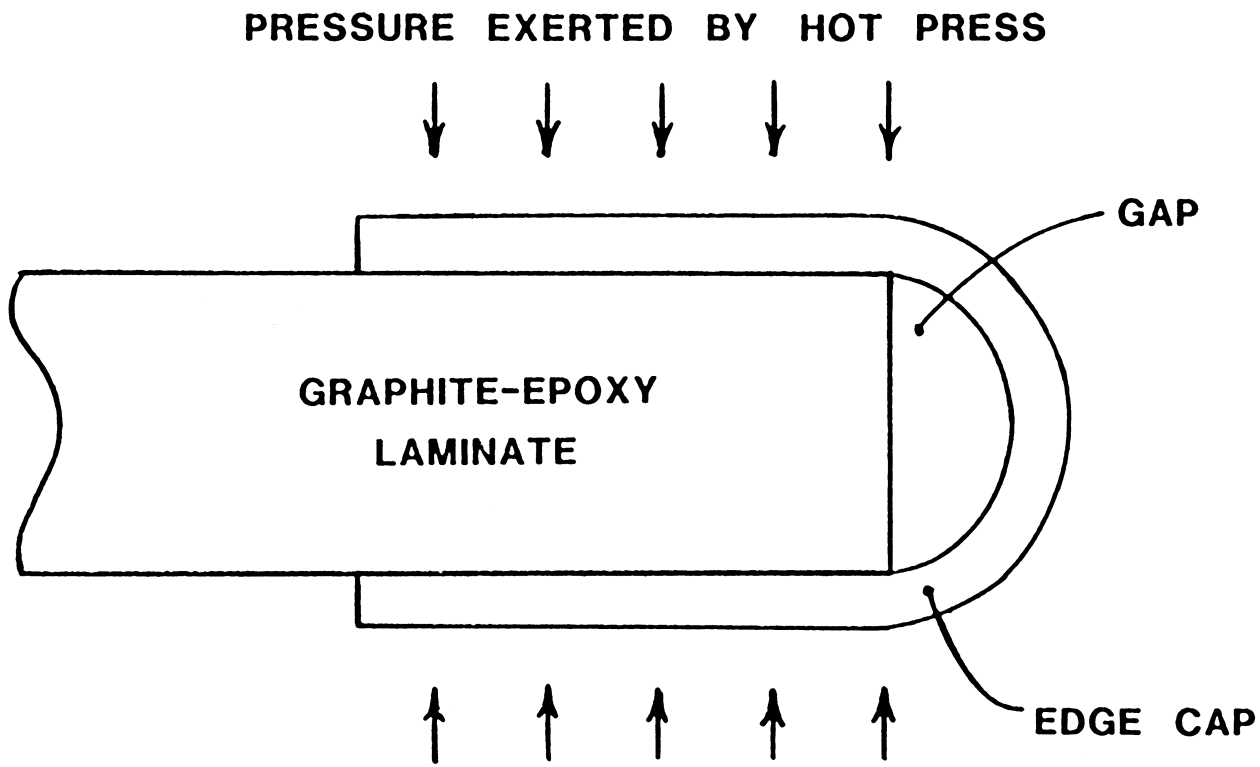

FIGURE 4-2 Gap Which Developed During Curing

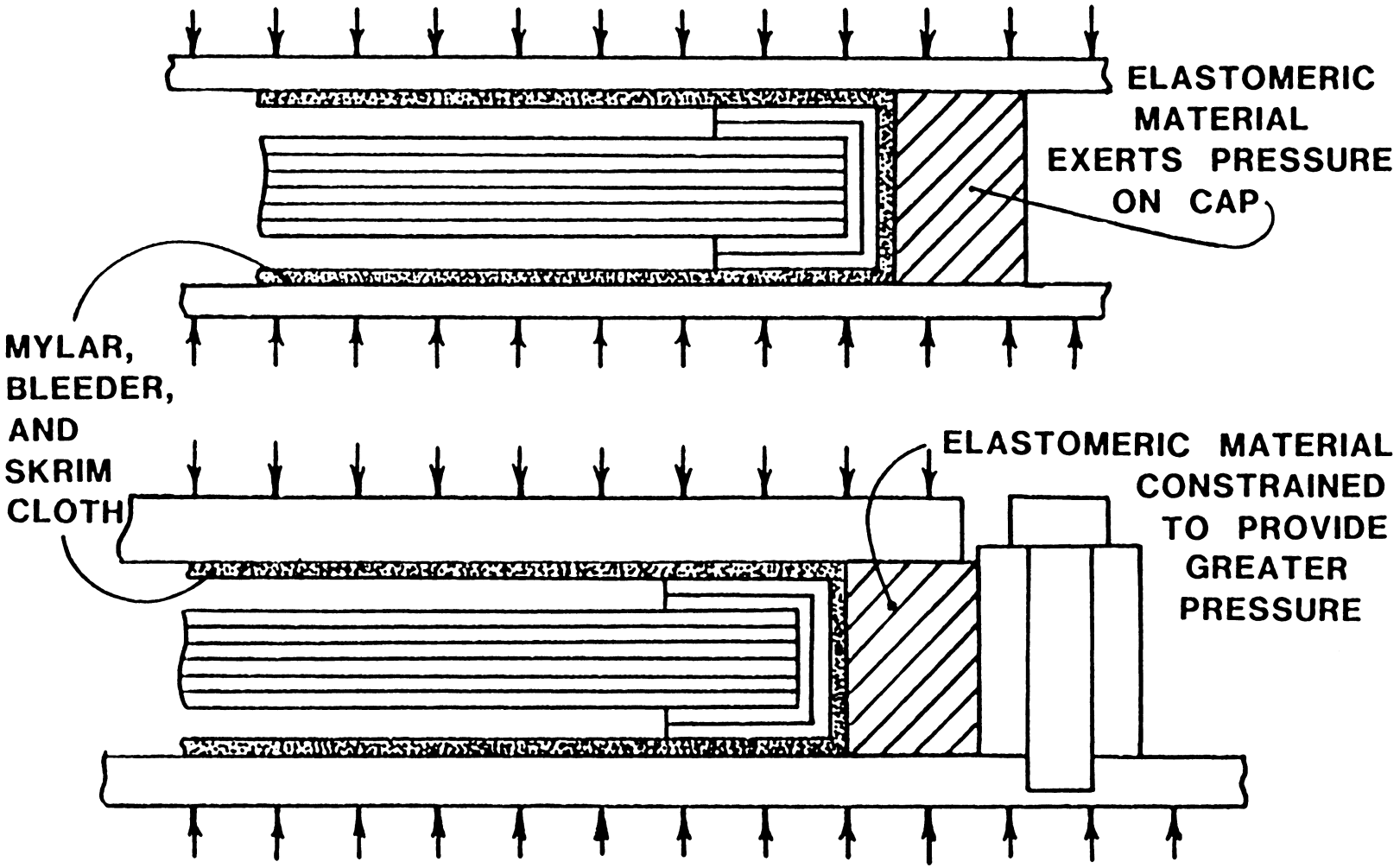

FIGURE 4-3 Curing Assemblies Which Prevent Gap

element analysis of the reinforced specimens with gaps present (see Section 3.2).

4.2 TEST APPARATUS AND PROCEDURES

The static and fatigue tests described below were performed in an MTS hydraulic tension-compression-fatigue machine with a 20,000 pound capacity. This machine can be operated so that either the load on the specimen or the displacement of the crosshead can be controlled by the machine's function generator.

Each specimen was placed in 2"-wide grips, so that both ends were clamped across the full width of the specimen. The MTS machine was operated in the load-control mode. The loading rate for the static tension tests was 25 pounds per second. The load on the specimen was monitored by a digital voltage readout from the function generator as well as an XY-plotter with input from the load cell. No strains were measured.

For the fatigue tests, the machine was also operated in the load-control mode. The fatigue tests were performed as follows:

(1) The specimen was loaded to the average of the high

and low loads. The low load was always 100 pounds to ensure that load variations did not cause the load to go below zero, placing the specimen in compression. The high load was selected to obtain a variety of stress levels for the S-N curve.

(2) Load indicators were set so that an indicator light would come on when either the high or low load was reached.

(3) The function generator was set to generate a sine wave at a loading frequency of 10 cycles/second. The span knob of the controls was set so that initially the amplitude of the sine wave was zero.

(4) The sine wave loading was begun, and the span (amplitude of the sine wave) was slowly increased until one of the load indicator lights was turned on, indicating that the desired loading had been reached. The number of cycles to reach this loading were recorded, and later subtracted from the number of cycles to reach failure. Normally, 200 - 300 cycles were required to reach the desired loading.

(5) The specimen was loaded until failure occurred, and then the number of cycles to failure was recorded.

This loading sequence is represented in the sketch of Figure 4-4. Because of the high frequency of the load cycling, the XY-plotter could not be used to monitor the loading.

4.3 TEST RESULTS

The average static tension failure load of the four uncapped specimens was 1808 pounds. There was a large variation in the failure loads of the specimens, with a range of 1380 to 2250 pounds and a coefficient of variation of 24%. The three capped specimens failed at an average load of 4367 pounds. The highest failure load obtained was 4650 pounds, the lowest 3950 pounds, and the coefficient of variation was 8%. These static test results are summarized in Table 4-1.

Results for the three uncapped and five capped specimens which were loaded in tension-tension fatigue are shown in Table 4-2. These results, along with those for the static tension tests, are plotted on an S-N (stress or load verses number of cycles to failure) curve in Figure 4-5. The lines which are shown on the S-N curve represent straight-line least-squares fits of the data points. The same results are shown in bar graphs in Figure 4-6. The results corresponding to 10,000 load cycles were obtained from the least-squares fits of the data points. The strength increase from the

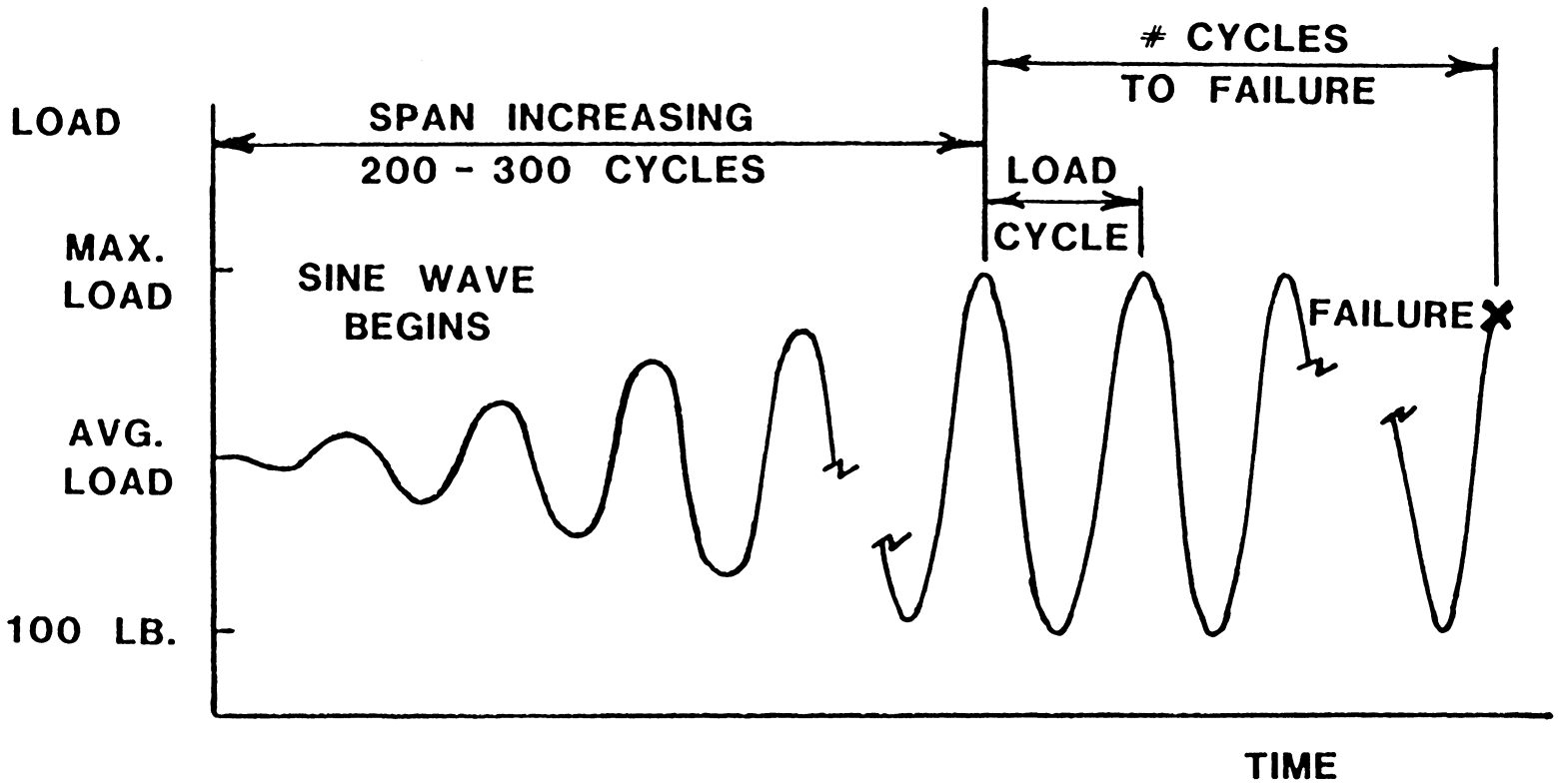

FIGURE 4-4 Fatigue Loading Diagram

TABLE 4-1

Static Loading Results

	Failure Load (pounds)	Mean Failure Load (pounds)	Coefficient of Variation
Uncapped	2250 1380 1500 2100	1808	24%
Capped	3950 4650 4500	4367	8%

TABLE 4-2

Fatigue Loading Results

	Maximum Load (pounds)	Cycles to Failure
Uncapped	1400	100,000 *
	1400	6,650
	1300	4,530
Capped	3500	2,580
	3300	2,920
	3300	4,810
	3100	12,290
	3000	11,460

* specimen did not fail during 100,000 load cycles

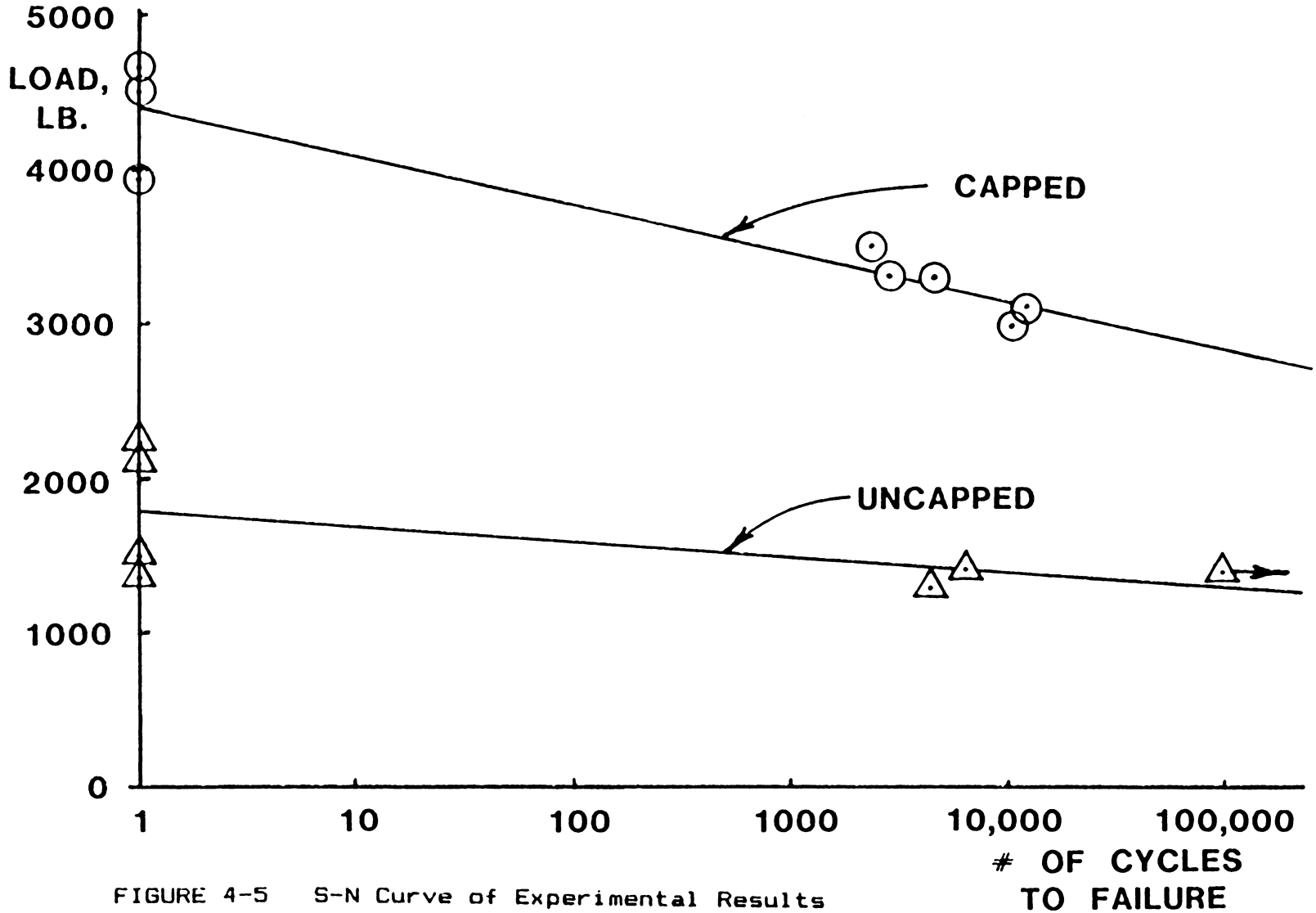

FIGURE 4-5 S-N Curve of Experimental Results

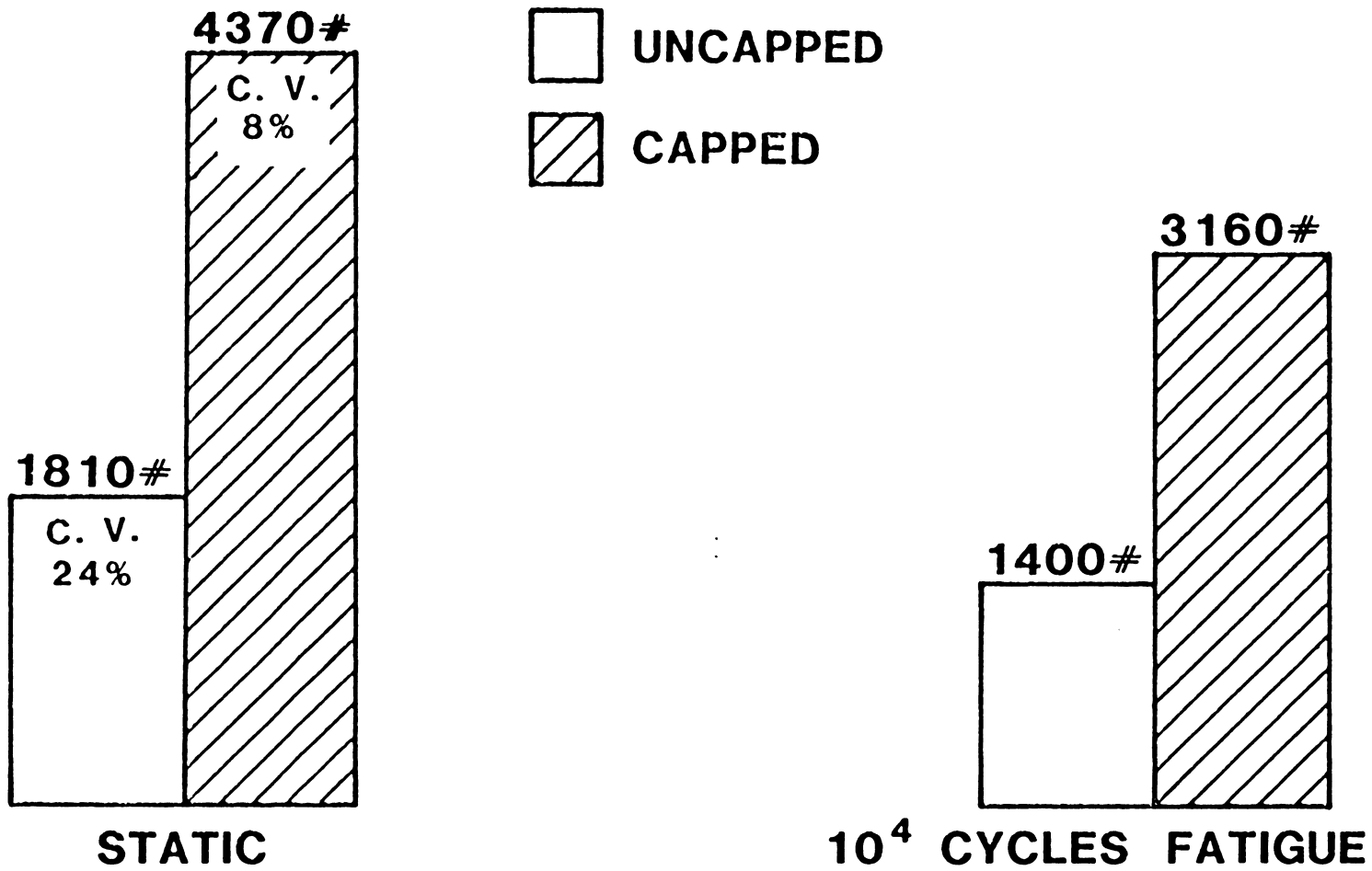

FIGURE 4-6 Capped Versus Uncapped Static and Fatigue Loading Results

unreinforced to the reinforced specimens was almost the same for 10,000 cycles (about 130%) as for the static tests (about 140%).

A visual inspection of the failed specimens revealed that the failure modes of the uncapped and the capped specimens were different. The failed, uncapped laminates had delaminations along the free edges, and failed along directions parallel to the fibers, as seen in the photograph of a typical uncapped failed laminate in Figure 4-7(a). No fiber breakage was evident in the uncapped specimens. The failed, capped laminates had broken graphite fibers in the +/- 30 degree layers. These broken fibers are visible in the photograph of a typical capped failed specimen in Figure 4-7(b).

The results of the experimental portion of this project are used to show that the addition of edge caps increases laminate strength and lowers the coefficient of variation of the strength. These experimental results are correlated with the analytical results in the next section.

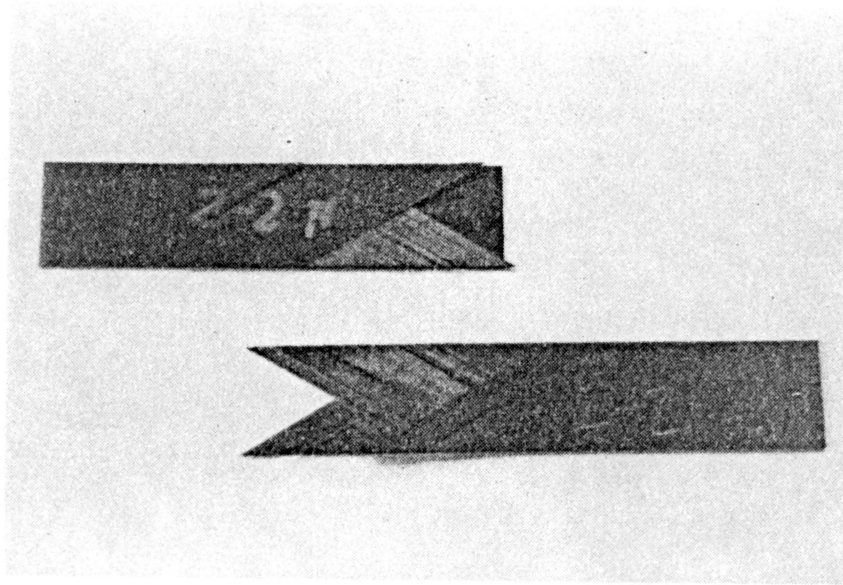

(a) Uncapped

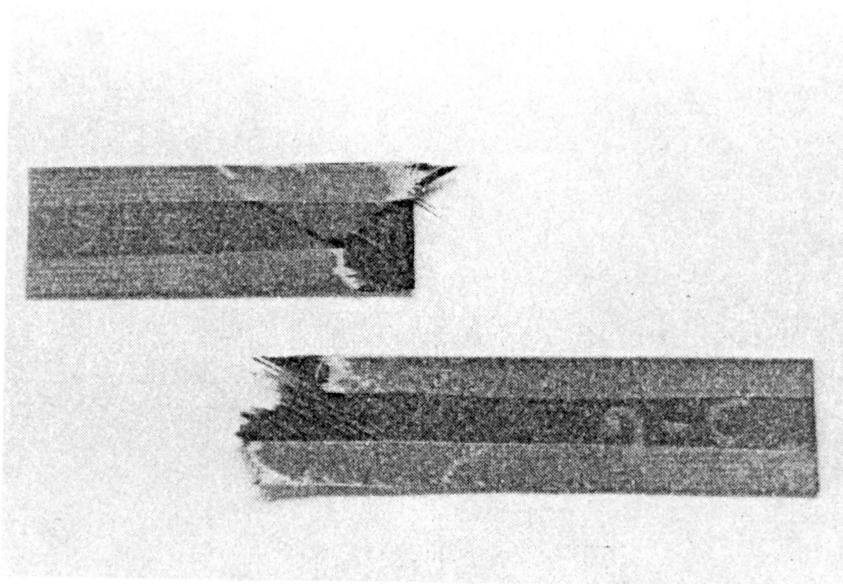

(b) Capped

FIGURE 4-7 Failed Specimens

4.4 CORRELATION OF ANALYSIS AND EXPERIMENTS

SAAS III analyses were used in Section 3.3 to show that adding edge caps to the NASA edge delamination tension specimen causes a significant reduction in the Z-direction normal stress in the specimen. Thus, the capped specimen should achieve a higher failure load than an uncapped specimen. A SAAS III model which incorporates a gap between the cap and the edge of the specimen is used to show that the Z-direction stresses can be reduced even by adding imperfect edge caps to the specimens. The experimental results are in agreement with these qualitative analytical results. The capped specimens, all of which had gaps between the caps and the specimen edges, failed at an average static tension load of 4367 pounds, whereas the uncapped specimens failed at an average load of 1808 pounds.

The Hoffman failure criterion was used in an attempt to relate the failure of the specimens to the interlaminar stresses which were calculated using SAAS III. The two-dimensional form of the criterion was used to predict the failure of the specimen in a region where no interlaminar stresses exist. Then, the three-dimensional form of the criterion was used to predict the failure of the capped specimen by taking into account the actual cap geometry in a

finite element analysis. The same procedure could not be used for the uncapped laminate because stresses which are calculated for the region adjacent to the free edge must be used in the failure prediction. These stresses are increasing very rapidly near the edge, which is indicative of a possible mathematical singularity. Because such a singularity is a manifestation of the linear mathematical model and not representative of physical reality, the stresses which are calculated for this region cannot be considered accurate.

For the capped specimen, the predicted failure load calculated using the 3-D criterion is 74% of the load calculated using the 2-D criterion. In the static load tests, the capped specimens failed at an average of 82% of the 2-D failure prediction. Therefore, the analysis was used effectively to show the relative impact of the interlaminar stresses, but could not be used to accurately predict the failure load (the predicted failure load was 10% different from the actual failure load). The test results and the predicted failure loads are summarized in Table 4-3.

Several possible reasons exist for the difference between the predicted and actual failure loads. One is the possibility that the material's unidirectional strengths were different from those which were used in the calculations. In

TABLE 4-3

Summary of Actual and Predicted
Static Tension Failure Loads

			Failure Load (pounds)	% of Failure Load Predicted by 2-D Hoffman Criterion
Predicted	2-D	Hoffman Criterion	5294	100
		Tsai-Hill Criterion	5798	109.5
		Tsai-Wu Criterion	5275	99.6
	3-D	Hoffman Criterion (Capped Specimen)	3920	74.1
Actual	Uncapped Specimens		1808	34.2
	Capped Specimens		4367	82.5

addition to the uncertainty of these strength numbers, the material used was stored about 10 years beyond its expiration date. The actual specimen strength, however, was higher than the predicted strength, so degradation of the material was not a factor. The most likely reason for the difference between the analytical and the experimental results is the difficulty in simulating delaminations in the SAAS analysis. The method in which delaminations are simulated affects the stress distribution in the laminate. A good method for accounting for delaminations in finite element analysis must be developed before accurate failure predictions can be made for laminates in which interlaminar stresses are significant.

In summary, FE analysis was used to qualitatively predict the strength increase obtained by reinforcing the edges of the NASA edge delamination tension specimen. Accurate failure predictions, however, are not possible until better techniques for accounting for delaminations are developed.

CHAPTER 5

SUMMARY

The conclusions drawn from the work in this report are summarized. Next, possible applications of the reinforcing concept are given. Finally, several problems are identified which could be examined in future research efforts.

5.1 CONCLUSIONS

Several conclusions have been drawn from the analytical and experimental results of this project. These conclusions are:

(1) Effective edge caps for thin laminates can be fabricated easily. No special tooling or complex procedures are required for the manufacture of the caps.

(2) Reinforcement of the free edges increases the strength of the specimens over the unreinforced edge laminate strength. The strength increase which was measured for the statically loaded specimens was about 140%. A similar increase (130%) occurred for fatigue loaded specimens at a specific life (10,000 cycles). The coefficient of variation of static tensile strength is reduced from 24% to 8% by capping the edges. This

reduction in coefficient of variation allows the allowable load of the structure to increase because the structure has been made more reliable.

(3) Finite element analysis was used to qualitatively show the effectiveness of the reinforcements. FE analysis was also used to evaluate and compare different edge cap designs. Cap-to-laminate bond length and cap thickness were shown to have little effect on the effectiveness of the cap, but the cap material and fiber orientation were shown to affect the cap performance a great deal.

(4) Linear finite element stress analysis cannot be used to predict the failure load of the unreinforced laminates. The failure is expected to occur at the free edge where the calculated stresses are increasing very rapidly. The question of whether a mathematical singularity in the stresses exists at the free edge has not been answered.

(5) The predicted failure load based on FE results and a progressive laminate failure analysis utilizing the Hoffman 3-D failure criterion for the reinforced laminate was 10% lower than the actual failure load. The major problem in predicting this load is the uncertainty

in simulating the delaminations within the laminate.

The work in this project dealt only with a particular laminate, the NASA edge delamination tension specimen, which was selected because it has a strong tendency to delaminate. Thus, the very large increases in strength shown here should not be expected for general laminates. However, it is possible to apply the edge reinforcement concept to practical structures which have free edges. Some possible applications are presented in the next section.

5.2 POSSIBLE APPLICATIONS

The edge reinforcement concept can be applied to many structures which contain free edges. Some possible applications are presented here.

Composite panels are often reinforced by laminated stiffeners which have free edges. Edge caps could be added to these stiffeners as shown in Figure 5-1. The cap on the bottom extends across the full width of the stiffener so that the stiffener can be placed flat against the panel. Composite ailerons are being used increasingly in the aerospace industry, and the trailing edge of an aileron is a free edge which could be capped, as shown in Figure 5-2. Aircraft

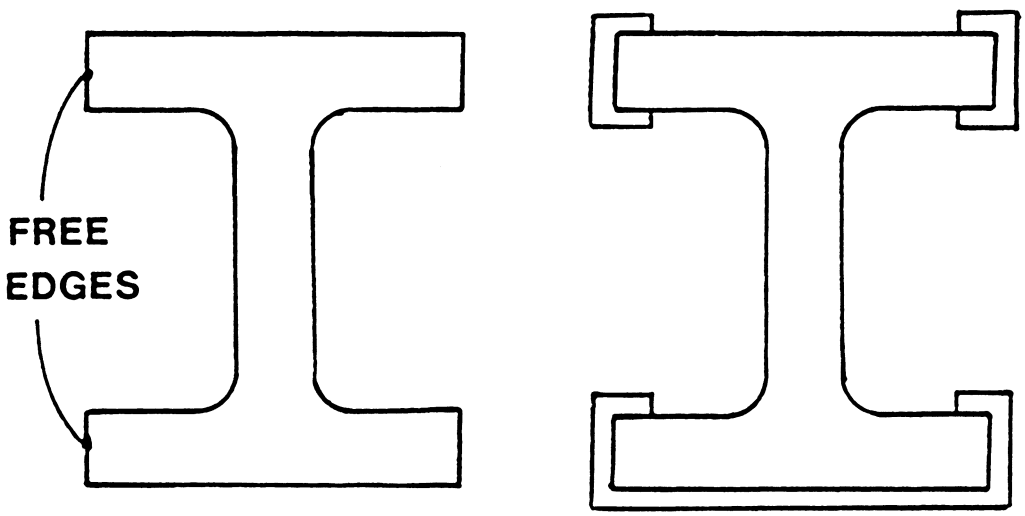

FIGURE 5-1 Laminated Stiffener

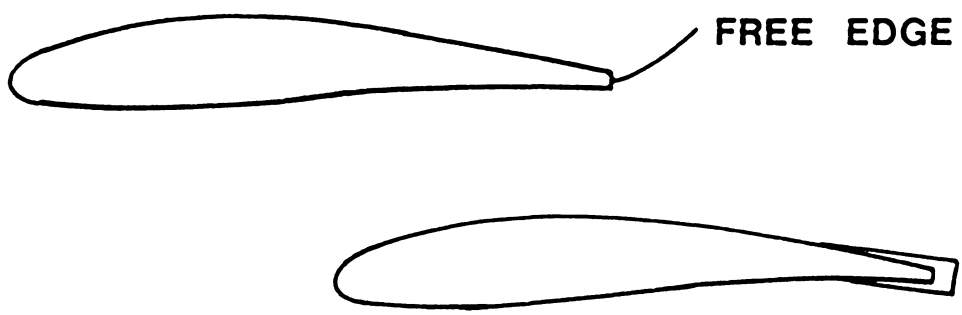

FIGURE 5-2 Trailing Edge of Aileron

fuselage panels could be joined together by edge caps, as shown in Figure 5-3. In all of these applications, the edge cap would also serve as a moisture barrier.

Although circular holes would be more difficult to reinforce than straight edges, it might be possible to reinforce circular holes. First, an oversized hole would be drilled through the laminate. The reinforcements would be rectangular pieces of material (probably woven) with a length equal to the circumference of the hole. The reinforcement would be slotted perpendicular to the edges so that small areas of the material could be folded over and bonded to the top and the bottom of the laminate, as shown in Figure 5-4. The slots must be closely spaced so that the reinforcing material will conform to the hole shape. To obtain the proper hole diameter, an expanding device or a fixed-diameter plug would then be placed in the hole and would remain during the curing process. Although several problems might arise from this method of reinforcement (clearance problems at the top and the bottom of the laminate, quality assurance problems, etc.), it has the potential of strengthening a laminate which has holes.

Cutouts in laminates could easily be reinforced with edge caps. Because cutouts are usually not load-bearing holes, their shapes are not dictated by fastener shapes. Therefore,

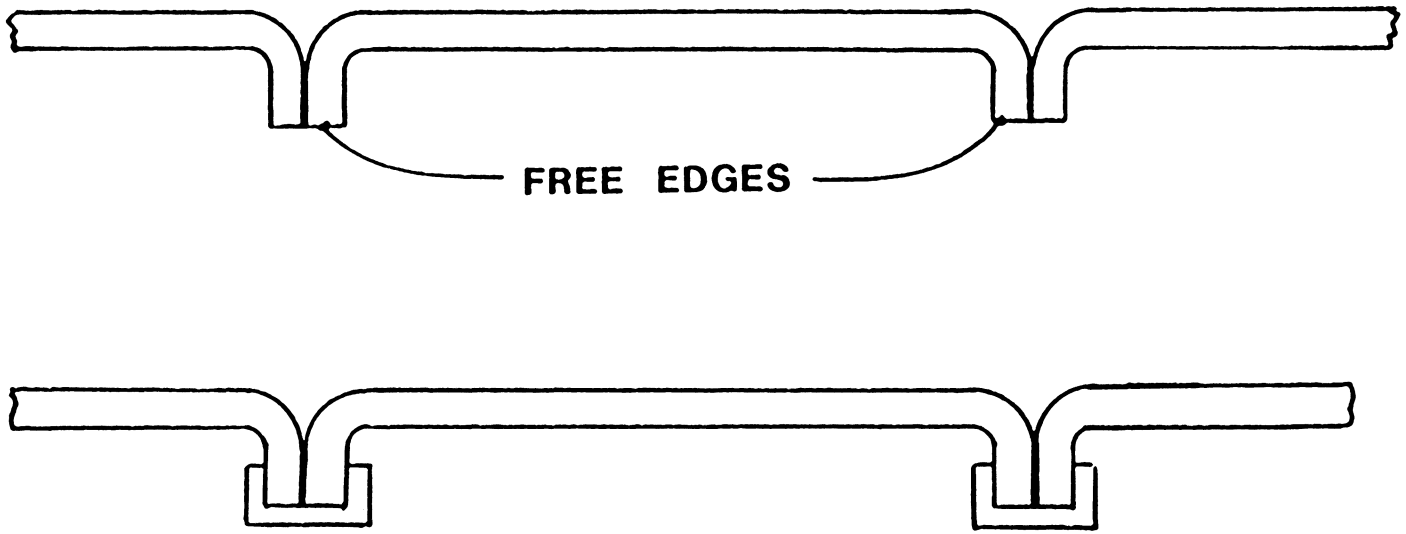

FIGURE 5-3 Aircraft Fuselage Panels

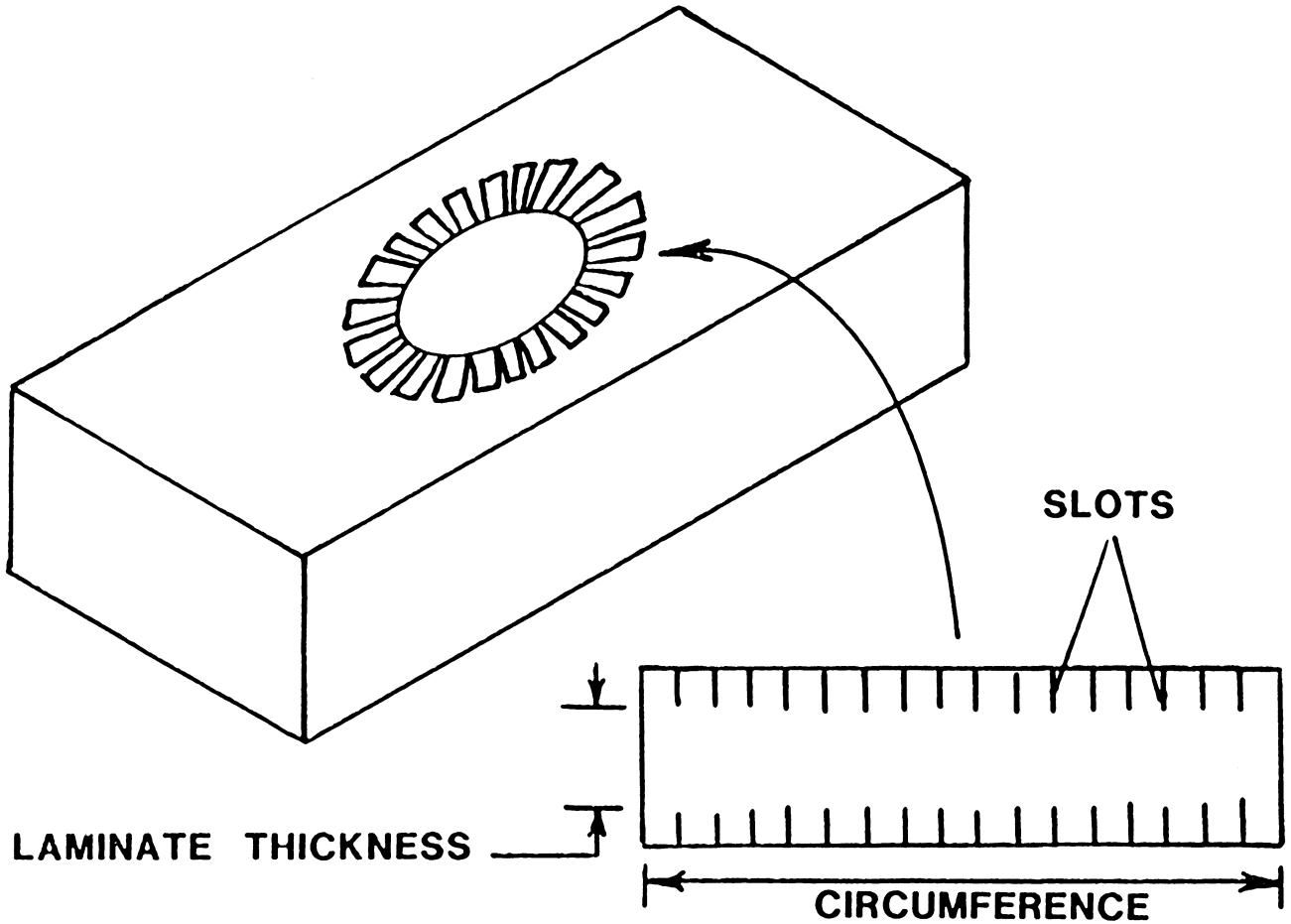

FIGURE 5-4 Reinforcement of Hole

rectangular cutouts (with rounded corners) are not uncommon. These rectangular cutouts could be reinforced easily. An edge cap along each side of the rectangle, as shown in Figure 5-5, could be used. An example of a possible use of this concept is a rocket motor skirt. A skirt is a cylindrical structure which is attached to one end of a rocket motor. The skirt must be capable of reacting a compressive load equal to the rocket motor thrust. Cutouts are placed so that wiring, hydraulic lines, etc. can be passed through the skirt to the rocket ignitor or the nozzle actuation system. Reinforcing the free edges of these cutouts could strengthen the skirt and thus allow a thinner, lighter skirt to be used.

Another structure which is a good candidate for free edge reinforcements is a tag end test specimen which is used to determine the strength of a filament-wound cylinder. When filament-wound cylinders are fabricated, they usually are made longer than the final product must be. The length of cylinder which is cut off from the final product is called the tag end. Test specimens which are used to characterize the cylinder material are cut from the tag end. These specimens are representations of the final product because they were made with the same manufacturing processes. The test specimens, however, have free edges while the final product does not (see Figure 5-6). Reinforcing the free

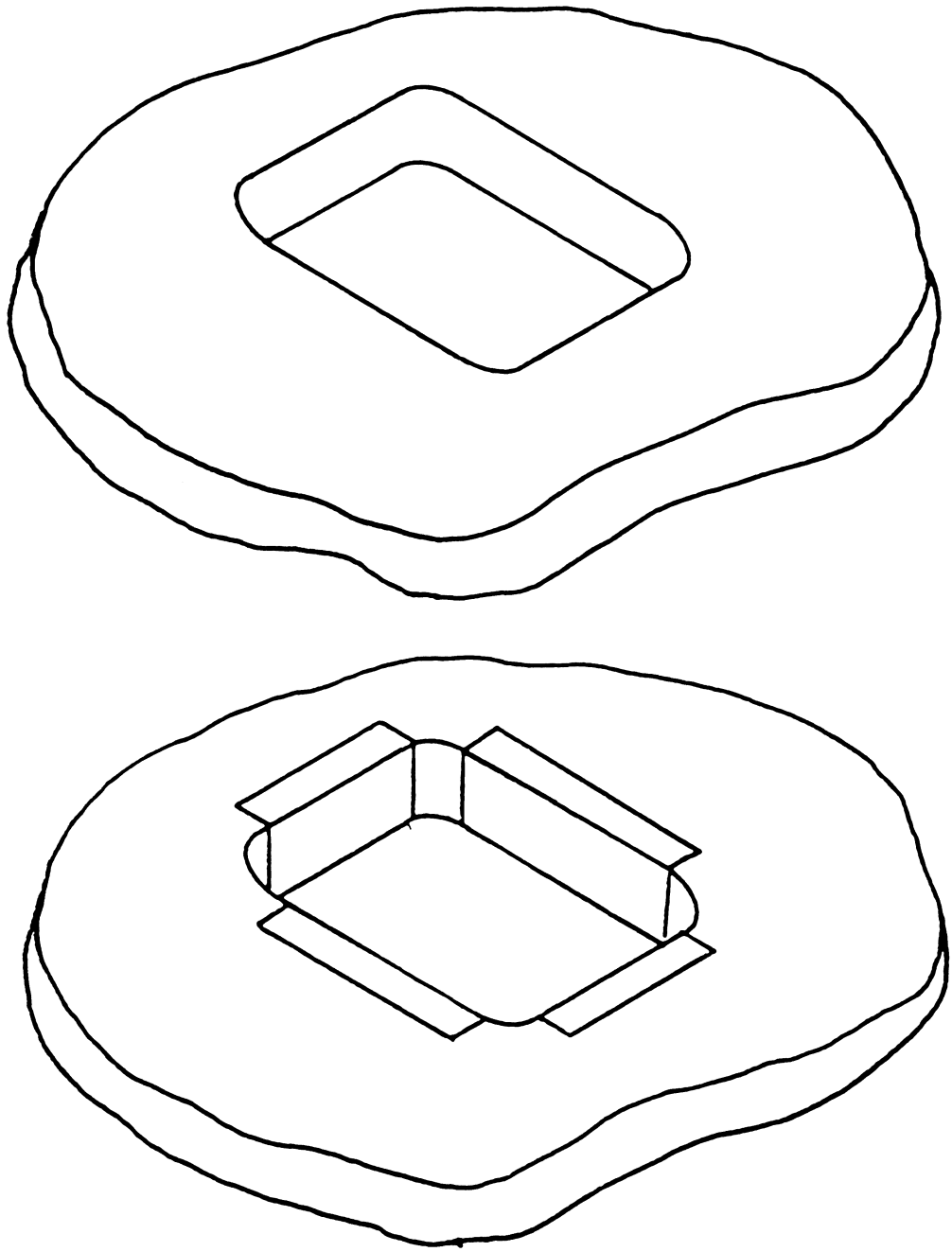

FIGURE 5-5 Reinforcement of Cutout

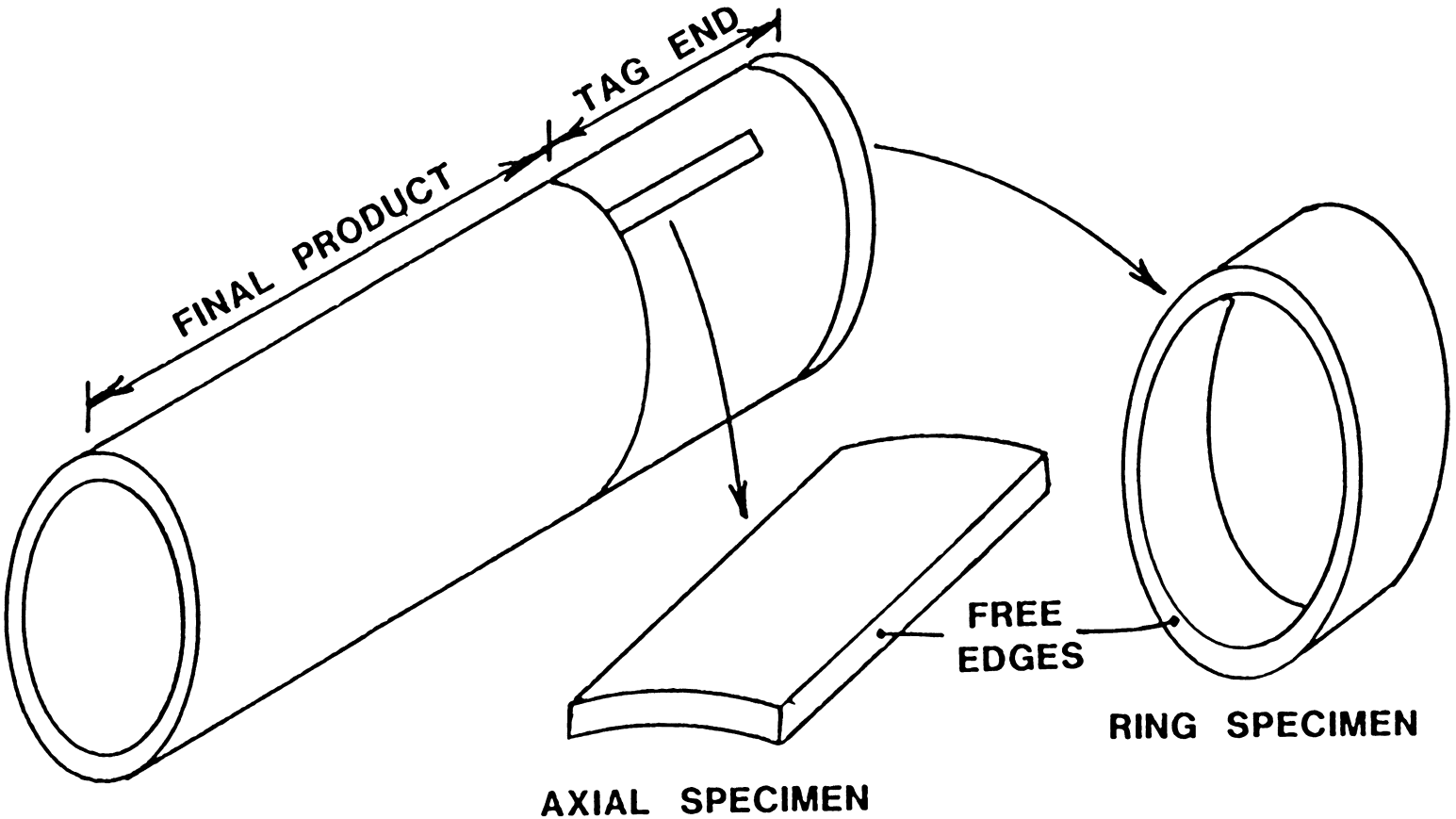

FIGURE 5-6 Tag End Test Specimens

edges would prevent edge stresses from causing the specimens to have a drastically lower strength than the final product. Therefore, a more representative strength test could be performed.

Many possible applications of the free edge reinforcement concept exist, and more will arise as the use of laminated composite materials continues to increase. Before these applications can be developed, more research, both theoretical and experimental, must be performed so that problems and potentials associated with the reinforcements can be better understood.

5.3 SUGGESTIONS FOR FUTURE WORK

Suggestions for future research work concerning the free edge reinforcement concept are presented in this section. These suggestions are classified as either theoretical or experimental, although it is recommended that any further research combine elements of both. That is, any theoretical studies should be proven via experimental verification, and any experimental studies should be extended by suitable theoretical work.

5.3.1 THEORETICAL

As Pagano and Pipes [4] noted, attempts to refine approximate solutions for the free edge problem are probably of little value. However, the development of better techniques for simulating delaminations would be beneficial. The ultimate failure of a laminate depends on the redistribution of interlaminar stresses within the laminate. Therefore, the manner in which delaminations are modelled influences the predicted failure load.

Analysis of more complex structures, such as a reinforced hole in a laminate, could show whether additional work is warranted. As in this project, an exact or highly accurate approximate solution is not necessarily needed in order to show the effects of adding reinforcement. Reinforcement concepts which appear to be effective could then be studied in an experimental program.

5.3.2 EXPERIMENTAL

This project dealt only with the NASA edge delamination tension specimen, and the experimental portion of the project was restricted to only one edge cap design. A logical followup to this work would be a more comprehensive experi-

mental program dealing with different laminates and different cap designs. In particular, thicker laminates should be studied because they can be reinforced more easily than thin laminates. Caps could be of different materials, different fiber angle orientations, and different physical dimensions (thickness, bond length, etc.). Also, different manufacturing methods could be compared. For thick laminates, the concept of placing a cured edge cap on a laminate could be compared with the concept of curing the cap in place.

In addition to further work with flat laminate free edges, more complicated reinforcement problems could be studied experimentally. Among these problems, cutouts and loaded holes in laminates under both tensile and compressive loads appear to be interesting problems which could be studied experimentally.

Any additional research on edge reinforcements should incorporate, to some degree, both theoretical and experimental work. Although conclusions about a reinforcement's ability to increase laminate strength can be reached using only experimental results, an opportunity exists with these results to use analysis to better understand the nature of interlaminar stresses near the edges. On the other hand, because of the approximate nature of the analysis, the actual strength increase brought about by the addition of reinforce-

ment can only be obtained experimentally.

Future researchers should have a greater contact with industry. It has been shown that free edge reinforcements can have a positive impact on laminate strength in some situations. The next step is to apply the reinforcement concept to structures which are used in industry.

REFERENCES

[1] R. Byron Pipes and N. J. Pagano, "Interlaminar Stresses in Composite Laminates Under Uniform Axial Extension," Journal of Composite Materials, October 1970, pp. 538-548.

[2] David B. Bogy, "Edge-Bonded Dissimilar Orthogonal Elastic Wedges Under Normal and Shear Loading," Journal of Applied Mechanics, September 1968, pp. 460-466.

[3] A. S. D. Wang and Frank W. Crossman, "Some New Results on Edge Effect in Symmetric Composite Laminates," Journal of Composite Materials, January 1977, pp. 92-106.

[4] N. J. Pagano and R. Byron Pipes, "Some Observations on the Interlaminar Strength of Composite Laminates," International Journal of Mechanical Sciences, August 1973, pp. 679-688.

[5] Ran Y. Kim, "A Technique for Prevention of Delamination," Proceedings of the Seventh Annual Mechanics of Composites Review, AFWAL-TR-82-4007, April 1982, pp. 218-230.

[6] James G. Crose and Robert M. Jones, "SAAS III Finite Element Analysis of Axisymmetric and Plane Solids with Different Orthotropic, Temperature-Dependent Material Properties in Tension and Compression," The Aerospace Corporation, San Bernardino, California, Air Force Report

No. SAMSO-TR-71-103, 22 June 1971.

[7] "ST-2: Specification for Edge Delamination Tension Test," NASA Reference Publication 1092, July 1983, pp. 7-14.

[8] Robert M. Jones, Mechanics of Composite Materials, McGraw Hill Book Company, New York, 1975.

[9] R. D. Cook, "Strain Resultants in Certain Finite Elements," AIAA Journal, March 1969, p. 535.

[10] V. D. Azzi and S. W. Tsai, "Anisotropic Strength of Composites," Experimental Mechanics, September 1965, pp. 283-288.

[11] Oscar Hoffman, "The Brittle Strength of Orthotropic Materials," Journal of Composite Materials, April 1967, pp. 200-206.

[12] Stephen W. Tsai and Edward M. Wu, "A General Theory of Strength for Anisotropic Materials," Journal of Comoosite Materials, January 1971, pp. 58-80.

[13] R. Narayanaswami and Howard M. Adelman, "Evaluation of the Tensor Polynomial and Hoffman Strength Theories for Composite Materials," Journal of Composite Materials, October 1977, pp. 366-377.

[14] Mark Shuart, Aerospace Engineer, NASA Langley Research

Center, letter to Robert M. Jones, 26 November 1984.

[15] George Lubin, Handbook of Composites, Van Nostrand Reinhold Co., New York, 1982.

[16] Carl T. Herakovich, "Composite Laminates with Negative Through-the-Thickness Poisson's Ratios," Journal of Composite Materials, September 1984, pp. 447-455.

[17] R. Hill, The Mathematical Theory of Plasticity, Oxford University Press, London, 1950.

APPENDIX A

SAAS III THEORY

The SAAS III technical report [6] contains detailed information about the workings of the SAAS III finite element computer program. The modifications which were made in order for the program to handle generalized plane strain problems are discussed here.

A.1 CONSTITUTIVE EQUATIONS

For an orthotropic material, the stress-strain relations are:

$$\begin{Bmatrix} \sigma_R \\ \sigma_Z \\ \sigma_T \\ \tau_{ZT} \\ \tau_{RT} \\ \tau_{RZ} \end{Bmatrix} = \begin{bmatrix} C_{11} & C_{12} & C_{13} & 0 & 0 & 0 \\ C_{12} & C_{22} & C_{23} & 0 & 0 & 0 \\ C_{13} & C_{23} & C_{33} & 0 & 0 & 0 \\ 0 & 0 & 0 & C_{44} & 0 & 0 \\ 0 & 0 & 0 & 0 & C_{55} & 0 \\ 0 & 0 & 0 & 0 & 0 & C_{66} \end{bmatrix} \begin{Bmatrix} \epsilon_R \\ \epsilon_Z \\ \epsilon_T \\ \gamma_{ZT} \\ \gamma_{RT} \\ \gamma_{RZ} \end{Bmatrix} \quad (A.1)$$

For an axisymmetric body with R-Z-T coordinates as in Figure A-1, the ZT and RT shear strains are zero. (The coordinate system referred to is shown in Figure A-1. The letter "T" will be used here to represent theta.) Therefore, the stress-strain relations reduce to:

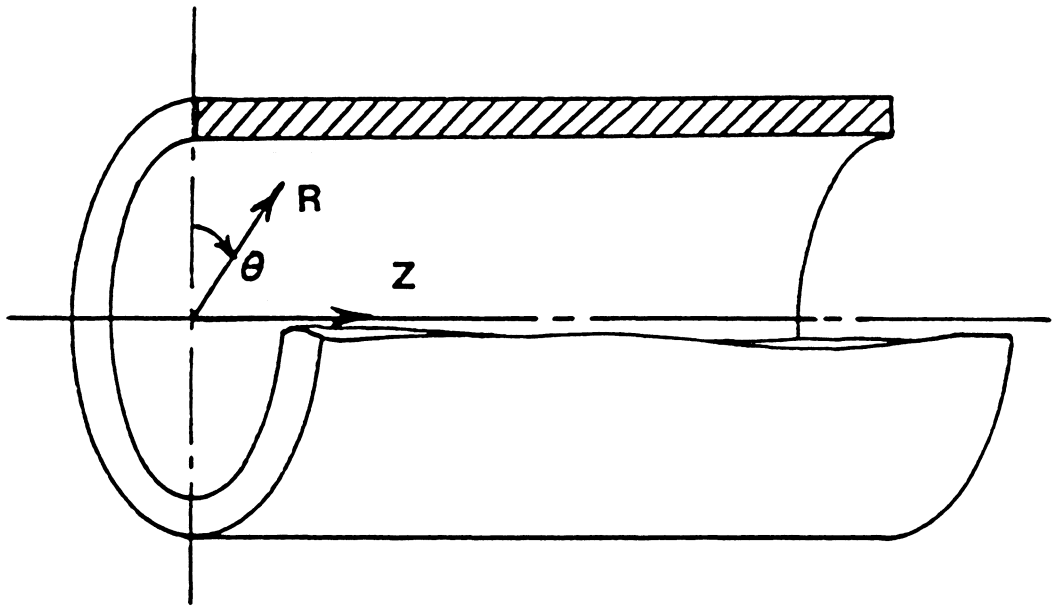

FIGURE A-1 Axisymmetric Coordinates

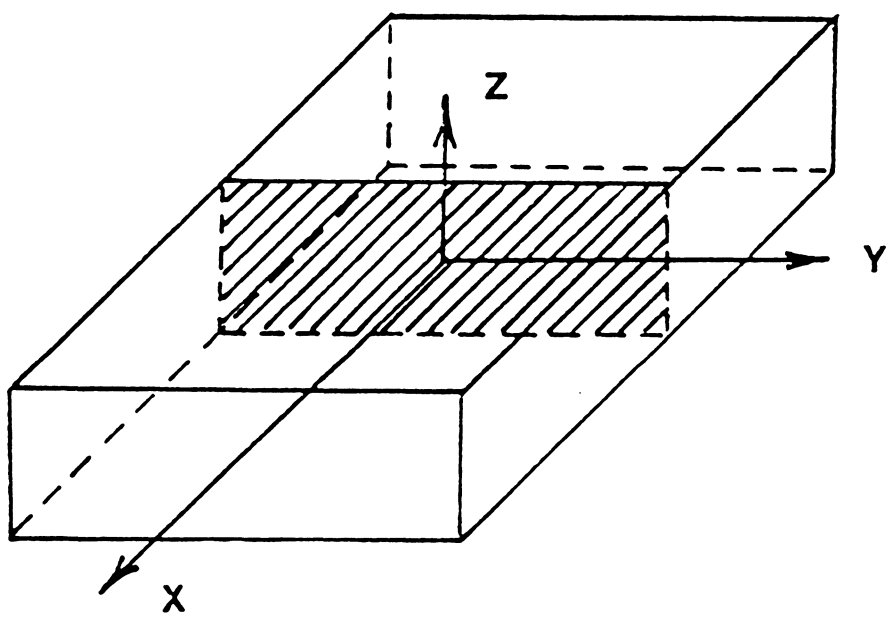

FIGURE A-2 Generalized Plane Strain Coordinates

$$\begin{Bmatrix} \sigma_R \\ \sigma_z \\ \sigma_T \\ \tau_{Rz} \end{Bmatrix} = \begin{bmatrix} C_{11} & C_{12} & C_{13} & 0 \\ C_{12} & C_{22} & C_{23} & 0 \\ C_{13} & C_{23} & C_{33} & 0 \\ 0 & 0 & 0 & C_{66} \end{bmatrix} \begin{Bmatrix} \epsilon_R \\ \epsilon_z \\ \epsilon_T \\ \gamma_{Rz} \end{Bmatrix} \qquad (A.2)$$

For generalized plane strain, the restrictions that the XY- and XZ-shear strains are zero and that the out-of-plane (X-direction) strain is a constant are consistent with the restrictions of the axisymmetric problem. Therefore, a change of subscripts is all that is necessary to form the stress-strain relations for a generalized plane strain problem. With the X-Y-Z coordinate system as shown in Figure A-2, these stress-strain relations are:

$$\begin{Bmatrix} \sigma_x \\ \sigma_y \\ \sigma_z \\ \tau_{xy} \end{Bmatrix} = \begin{bmatrix} C_{11} & C_{12} & C_{13} & 0 \\ C_{12} & C_{22} & C_{23} & 0 \\ C_{13} & C_{23} & C_{33} & 0 \\ 0 & 0 & 0 & C_{66} \end{bmatrix} \begin{Bmatrix} \epsilon_x \\ \epsilon_y \\ \epsilon_z \\ \gamma_{xy} \end{Bmatrix} \qquad (A.3)$$

These equations are valid only for orthotropic materials stressed in principal material directions. An off-axis composite lamina is clearly not orthotropic because an axial load causes the lamina to shear. Off-axis laminae may be included in SAAS III, however, if their use is restricted to balanced, symmetric laminates. Two adjacent laminae oriented at an angles of +theta and -theta to the X-axis of the laminate will be considered to be a single orthotropic unit as

described in Section 2.2.3.

Classical Lamination Theory (CLT) is used to find the properties E-X, E-Y, NU-XY, and G-XY of the combined +/-theta layer. E-Z is assumed to be the same as E-3 of the unidirectionally reinforced material. G-XZ and G-YZ are found by rotation of the 3-D compliance matrix for either the +theta or the -theta ply. (These shear moduli are independent of the sign of the lamina angle.) Poisson's ratios NU-XZ and NU-YZ are calculated by utilizing a procedure which was described by Herakovich [16]. The first step of this procedure is to use CLT to compute the A (extensional stiffness) matrix of the +/-theta layer. If the condition of having a symmetric laminate is now imposed, then the state of strain under a uniform axial load is:

$$\begin{Bmatrix} \epsilon_x \\ \epsilon_y \\ \gamma_{xy} \end{Bmatrix} = \begin{bmatrix} A_{11} & A_{12} & A_{16} \\ A_{12} & A_{22} & A_{26} \\ A_{16} & A_{26} & A_{66} \end{bmatrix} \begin{Bmatrix} N_x \\ 0 \\ 0 \end{Bmatrix} \qquad (A.4)$$

Therefore,

$$\begin{Bmatrix} \epsilon_x \\ \epsilon_y \\ \gamma_{xy} \end{Bmatrix} = \begin{Bmatrix} A_{11}^* \\ A_{12}^* \\ A_{16}^* \end{Bmatrix} N_x \qquad (A.5)$$

where: N_x = Applied load per unit width
A_{ij}^* = Component of inverted A matrix

CLT can now be used to find the stress state in each lamina:

$$\begin{Bmatrix} \epsilon_x \\ \epsilon_y \\ \gamma_{xy} \end{Bmatrix}^k = \begin{bmatrix} \bar{Q}_{11} & \bar{Q}_{12} & \bar{Q}_{16} \\ \bar{Q}_{12} & \bar{Q}_{22} & \bar{Q}_{26} \\ \bar{Q}_{16} & \bar{Q}_{26} & \bar{Q}_{66} \end{bmatrix} \begin{Bmatrix} A_{11}^* \\ A_{12}^* \\ A_{16}^* \end{Bmatrix} N_x \qquad (A.6)$$

The k superscript indicates that the corresponding quantity applies to the k-th ply. The 3-D strain-stress relations for a monoclinic (off-axis) ply are used to find the through-the-thickness strain of the ply:

$$\epsilon_z^k = S_{31}^k \sigma_x^k + S_{32}^k \sigma_y^k + S_{36}^k \sigma_z^k \qquad (A.7)$$

The S-bar terms are components of the ply's transformed 3-D compliance (strain-stress) matrix. The Z-direction strain in both the +theta and the -theta plies is the same; therefore, the Z-direction strain in the +/-theta unit is constant through the thickness.

The definition of NU-XZ is:

$$\nu_{xz} = -\frac{\epsilon_z}{\epsilon_x} \qquad (A.8)$$

under loading in the X-direction only. The expressions developed for the strains are substituted into Equation (A.8) to yield the equation for NU-XZ:

$$\nu_{xz} = -\frac{1}{A_{11}^*}\left[A_{11}^* F_1 + A_{12}^* F_2 + A_{16}^* F_6\right] \qquad (A.9)$$

where: $F_1 = S_{31} Q_{11} + S_{32} Q_{12} + S_{36} Q_{16}$

The equation for NU-YZ is developed in a similar manner:

$$\nu_{yz} = -\frac{1}{A_{22}^*}\left[A_{21}^* F_1 + A_{22}^* F_2 + A_{26}^* F_6\right] \qquad (A.10)$$

A summary of the 3-D material properties for a +/-30 degree graphite-epoxy unit, along with the source of each property, is shown in Table A-1.

A.2 EQUILIBRIUM EQUATIONS

The principle upon which the SAAS III program is based is that of stationary potential energy: for a system in equilibrium, the change in total potential energy caused by any infinitesimal displacement of the body is zero. For a system idealized with a finite number of degrees of freedom, this principle can be written as:

$$\frac{\partial V}{\partial u_i} = 0 \qquad i = 1, N \qquad (A.11)$$

where: V = potential energy

u_i = a nodal point displacement

N = number of nodal point displacements

TABLE A-1

3-D Material Properties
for a +/-30 Degree Graphite-Epoxy Unit

Material Principal Direction T-300-5209 Properties:

E-1 =	18.5 Msi
E-2 = E-3 =	1.64 Msi
NU-12 = NU-13 =	.30
NU-23 =	.36
G-12 = G-13 =	.87 Msi
G-23 =	.26 Msi

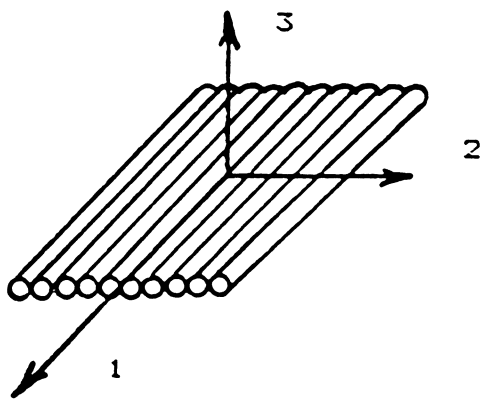

+/-30 Degree Properties:

E-X=	7.34 Msi	CLT
E-Y=	1.88 Msi	CLT
NU-XY=	1.18	CLT
G-XY=	3.83 Msi	CLT
E-Z=	1.64 Msi	E-3
G-XZ=	.55 Msi	3-D compliance matrix
G-YZ=	.31 Msi	3-D compliance matrix
NU-XZ=	-.05	Herakovich method
NU-YZ=	.26	Herakovich method

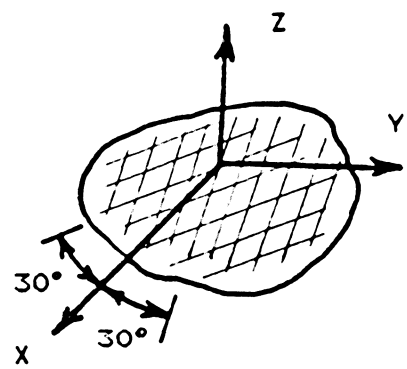

For a porous elastic body, if strain energy is defined as:

$$U = \int_{Vol} \left[\int_0^{\epsilon_i} \sigma_i \, d\epsilon_i \right] dV \qquad (A.12)$$

where: σ_i = i-th component of total stress

ϵ_i = corresponding component of strain

then the total potential energy is:

$$V = U - \int_{Vol} w_i \, F_i \, dV - \int_{Area} w_i \, P_i \, dA \qquad (A.13)$$

where: F_i = a body force

P_i = a surface traction

w_i = corresponding displacement

If the body is represented with M elements, the potential energy can be written as:

$$V = \sum_{m=1}^{M} \left[U^m - \int_{Vol} w_i^m \, F_i^m \, dV - \int_{Area} w_i^m \, P_i^m \, dA \right] \qquad (A.14)$$

If the u column vector is used to denote the unknown nodal displacements, then each element's displacement can be written as:

$$\left\{ w \right\}_m = \left[d \right]_m \left\{ u \right\} \qquad (A.15)$$

and the element's strains as:

$$\left\{ \epsilon \right\}_m = \left[\quad a \quad \right]_m \left\{ u \right\} \tag{A.16}$$

The a and d matrices are determined from the problem geometry. In transposed form, Equations (A.15) and (A.16) become:

$$\left\{ w \right\}_m^T = \left\{ u \right\}^T \left[\quad d \quad \right]_m^T \tag{A.17}$$

$$\left\{ \epsilon \right\}_m^T = \left\{ u \right\}^T \left[\quad a \quad \right]_m^T \tag{A.18}$$

The equation for the total stress of an element, as developed in Section 2.2.2, is:

$$\left\{ \overline{\sigma} \right\}_m = \left[\quad C \quad \right]_m \left\{ \epsilon \right\}_m - \left\{ \tau \right\}_m - \left\{ \sigma_G \right\}_m + \left\{ \sigma_P \right\}_m \tag{A.19}$$

The subscript G indicates modifications to accommodate generalized plane strain. This expression for stress can now be substituted into Equation (A.13) to yield:

$$U^m = \frac{1}{2} \int_{Vol} \left\{ \epsilon \right\}_m^T \left[\quad C \quad \right]_m \left\{ \epsilon \right\}_m dV - \int_{Vol} \left\{ \epsilon \right\}_m^T \left\{ \tau \right\}_m dV$$

$$- \int_{Vol} \left\{ \epsilon \right\}_m^T \left\{ \sigma_G \right\}_m dV + \int_{Vol} \left\{ \epsilon \right\}_m^T \left\{ \sigma_P \right\}_m dV \tag{A.20}$$

Equations (A.17), (A.18), and (A.20) are substituted into Equation (A.14), and the potential energy of the system can be written as a function of the nodal point displacements:

$$V = \sum_{m=1}^{M} \left[\frac{1}{2} \int_{Vol} \left\{ u \right\}^T \left[a \right]_m^T \left[C \right]_m \left[a \right]_m \left\{ u \right\} dV \right.$$

$$- \int_{Vol} \left\{ u \right\}^T \left[a \right]_m^T \left\{ \tau \right\}_m dV - \int_{Vol} \left\{ u \right\}^T \left[a \right]_m^T \left\{ \sigma_G \right\}_m dV$$

$$+ \int_{Vol} \left\{ u \right\}^T \left[a \right]_m^T \left\{ \sigma_P \right\}_m dV - \int_{Vol} \left\{ u \right\}^T \left[d \right]_m^T \left\{ F \right\}_m dV$$

$$\left. - \int_{Area} \left\{ u \right\}^T \left[d \right]_m^T \left\{ P \right\}_m dA \right] \qquad (A.21)$$

The potential energy is made stationary by applying Equation (A.11). The result is N simultaneous equations which can be written in matrix form as:

$$\sum_{m=1}^{M} \left[\int_{Vol} \left[a \right]_m^T \left[C \right]_m \left[a \right]_m dV \right] \left\{ u \right\} = \sum_{m=1}^{M} \left[\int_{Vol} \left[a \right]_m^T \left\{ \tau \right\}_m dV \right]$$

$$+ \sum_{m=1}^{M} \left[\int_{Vol} \left[a \right]_m^T \left\{ \sigma_G \right\}_m dV \right] - \sum_{m=1}^{M} \left[\int_{Vol} \left[a \right]_m^T \left\{ \sigma_P \right\}_m dV \right]$$

$$+ \sum_{m=1}^{M} \left[\int_{Vol} \left[d \right]_m^T \left\{ F \right\}_m dV \right] + \sum_{m=1}^{M} \left[\int_{Area} \left[d \right]_m^T \left\{ P \right\}_m dA \right] \qquad (A.22)$$

These equations can be simplified by introducing notation which is standard for the finite element method. The element stiffness matrix is:

$$\left[k \right]_m = \int_{Vol} \left[a \right]_m^T \left[C \right]_m \left[a \right]_m dV \qquad (A.23)$$

The system stiffness is obtained by assembling the element stiffnesses:

$$\left[K \right] = \sum_{m=1}^{M} \left[k \right]_m \qquad (A.24)$$

The body force vector for an element is:

$$\left\{ L \right\}_m = \int_{Vol} \left[\left[d \right]_m^T \left\{ F \right\}_m + \left[a \right]_m^T \left\{ \tau \right\}_m + \left[a \right]_m^T \left\{ \sigma_G \right\}_m - \left[a \right]_m^T \left\{ \sigma_P \right\}_m \right] dV \qquad (A.25)$$

The surface force vector is:

$$\left\{ R \right\}_m = \int_{Area} \left[d \right]_m^T \left\{ P \right\}_m dA \qquad (A.26)$$

The total load on the system is the summation of the element loads:

$$\left\{ Q \right\} = \sum_{m=1}^{M} \left\{ L \right\}_m + \sum_{m=1}^{M} \left\{ R \right\}_m \qquad (A.27)$$

Therefore, Equation (A.22) becomes:

$$\left[K \right] \left\{ u \right\} = \left\{ Q \right\} \qquad (A.28)$$

The N nodal point displacements are found by solving the N simultaneous equations given by Equation (A.28).

APPENDIX B

COMPOSITE FAILURE CRITERIA

There is no universally accepted criterion for predicting the strength of a composite lamina. Over the past twenty years, however, much research has been directed toward developing such a criterion. Three of the most widely known failure criteria - the Tsai-Hill, the Hoffman, and the Tsai-Wu criteria - are presented here.

B.1 THE TSAI-HILL CRITERION

In 1948, Hill proposed a criteron for the yielding of anisotropic materials [17]. Hill's work was a generalization of Von Mises' 1913 yield criterion for isotropic materials, which is widely used to predict failure in isotropic materials. Hill's criterion, which reduces to Von Mises' for isotropic materials, predicts that failure occurs when:

$$F(\sigma_y - \sigma_z)^2 + G(\sigma_z - \sigma_x)^2 + H(\sigma_x - \sigma_y)^2 + 2L\tau_{yz}^2 + 2M\tau_{xz}^2 + 2N\tau_{xy}^2 = 1 \qquad \text{(B.1)}$$

where:
$$2F = 1/Y^2 + 1/Z^2 - 1/X^2$$
$$2G = 1/X^2 + 1/Z^2 - 1/Y^2$$
$$2H = 1/X^2 + 1/Y^2 - 1/Z^2$$
$$2L = 1/R^2$$
$$2M = 1/S^2$$
$$2N = 1/T^2$$

X, Y, and Z = normal strengths along axes
R, S, and T = shear strengths for planes defined by axes

In 1965, Azzi and Tsai applied Hill's criterion to composite laminae [10]. At the time of the work of Azzi and Tsai, the most common use of laminated composites was in filament-wound pressure vessels. Because these vessels are typically very thin in comparison to their lengths and diameters, an approximate state of plane stress exists. Therefore, the Z-direction normal stress and the XZ- and YZ-shear stresses are assumed to be zero, and Equation (B.1) reduces to:

$$(G + H)\sigma_x^2 - 2H\sigma_x\sigma_y + (H + F)\sigma_y^2 + 2N\tau_{xy}^2 = 1 \qquad (B.2)$$

Azzi and Tsai simplified this expression further by noting that in most fiber-reinforced materials, the fibers are randomly dispersed in the plane which is perpendicular to the fibers. This situation implies that properties in directions transverse to the fibers are equal (i.e., the material is transversely isotropic). In particular, the Y- and Z-direction strengths are equal. This observation allows Equation (B.2) to be written as:

$$\frac{\sigma_x^2 - \sigma_x\sigma_y}{X^2} + \frac{\sigma_y^2}{Y^2} + \frac{\tau_{xy}^2}{T^2} = 1 \qquad (B.3)$$

Equation (B.3) is generally referred to as the Tsai-Hill failure criterion.

B.2 THE HOFFMAN CRITERION

In 1967, Hoffman [11] noted that Von Mises' criterion was used to predict the yielding of ductile materials. Ductile materials usually have equal yield stress in tension and compression. Fiber-reinforced materials, which are brittle, had been shown to have significantly different strengths in tension and compression. To account for this difference, Hoffman added terms which are linear functions of the normal stresses to the failure criterion. Hoffman's proposed failure condition is:

$$C_1(\sigma_y - \sigma_z)^2 + C_2(\sigma_z - \sigma_x)^2 + C_3(\sigma_x - \sigma_y)^2 + C_4\sigma_x + C_5\sigma_y + C_6\sigma_z + C_7\tau_{yz}^2 + C_8\tau_{xz}^2 + C_9\tau_{xy}^2 = 1 \quad (B.4)$$

The C values can be determined by substituting the principal material direction strengths in Equation (B.4) one at a time. For example, consider the case in which a positive value (tension) of X-direction normal stress is applied and all other stresses are zero. By definition, failure will occur when the X-direction normal stress is equal to the uniaxial tensile strength X-T. Therefore, Equation (B.4) becomes:

$$C_2X_T^2 + C_3X_T^2 + C_4X_T = 1 \quad (B.5)$$

where: X_T = tensile strength along X-axis

Similar equations can be written for each of the material's normal strengths (X-, Y-, and Z-direction tensile and compressive strengths). The resulting six equations can be solved simultaneously to yield the following:

$$\left.\begin{aligned}
C_1 &= \frac{1}{2}\left[\frac{1}{Y_T Y_C} + \frac{1}{Z_T Z_C} - \frac{1}{X_T X_C}\right] \\
C_2 &= \frac{1}{2}\left[\frac{1}{X_T X_C} + \frac{1}{Z_T Z_C} - \frac{1}{Y_T Y_C}\right] \\
C_3 &= \frac{1}{2}\left[\frac{1}{X_T X_C} + \frac{1}{Y_T Y_C} - \frac{1}{Z_T Z_C}\right] \\
C_4 &= \frac{1}{X_T} - \frac{1}{X_C} \\
C_5 &= \frac{1}{Y_T} - \frac{1}{Y_C} \\
C_6 &= \frac{1}{Z_T} - \frac{1}{Z_C}
\end{aligned}\right\} \quad \text{(B.6)}$$

where: X_T, Y_T, and Z_T = axial tensile strengths
X_C, Y_C, and Z_C = axial compressive strengths

Because the shear stress terms of Equation (B.4) are not coupled with each other or with the normal stresses, evaluation of the remaining C terms is straightforward:

$$\left.\begin{aligned}
C_7 &= \frac{1}{S_{yz}^2} \\
C_8 &= \frac{1}{S_{xz}^2} \\
C_9 &= \frac{1}{S_{yz}^2}
\end{aligned}\right\} \quad \text{(B.7)}$$

where: S_{yz}, S_{xz}, and S_{xy} = pure shear strengths

For a transversely isotropic material subjected to a state of plane stress, Equation (B.4) becomes:

$$\frac{\sigma_x^2 - \sigma_x\sigma_y}{X_T X_C} + \frac{\sigma_y^2}{Y_T Y_C} + \frac{(X_C - \sigma_T)\sigma_x}{X_T X_C} + \frac{(Y_C - Y_T)\sigma_y}{Y_T Y_C} + \frac{\tau_{xy}^2}{S_{xy}^2} = 1 \qquad (B.8)$$

Note that if the material has equal strengths in tension and compression, Equation (B.8) reduces to Equation (B.3), the Tsai-Hill criterion.

B.3 THE TSAI-WU CRITERION

In 1975, Tsai and Wu [12] proposed a strength criterion based on the assumption that there exists a failure surface in stress space of the form:

$$\sum_{i=1}^{6}\left[F_i\sigma_i + \sum_{j=1}^{6} F_{ij}\sigma_i\sigma_j\right] = 1 \qquad (B.9)$$

Equation (B.9) is the equation of an ellipsoid in 3-D stress space with the terms which are linear in stress defining a shift from the origin and a rotation of the principal axes of the ellipsoid.

Although Equation (B.9) is quite lengthy, containing six

linear terms and 27 quadratic terms, it can be simplified a great deal with the assumption that the shear stresses are not coupled with each other or with the normal stresses. This assumption allows 18 of the quadratic terms to be eliminated. If the condition of plane stress is imposed, Equation (B.9) is reduced to a polynomial of three linear and four quadratic terms:

$$F_1\sigma_1 + F_2\sigma_2 + F_6\tau_{12} + F_{12}\sigma_1\sigma_2 + F_{11}\sigma_1^2 + F_{22}\sigma_2^2 + F_{66}\tau_{12}^2 = 1 \qquad \text{(B.10)}$$

The values of the F terms can be obtained in a manner similar to that explained for the Hoffman criterion, except for F-12:

$$\left.\begin{aligned} F_{11} &= \frac{1}{X_T X_C} \\ F_1 &= \frac{1}{X_T} - \frac{1}{X_C} \\ F_{22} &= \frac{1}{Y_T Y_C} \\ F_2 &= \frac{1}{Y_T} - \frac{1}{Y_C} \\ F_{66} &= \frac{1}{S_{xy}^2} \\ F_6 &= 0 \end{aligned}\right\} \qquad \text{(B.11)}$$

Unless both the X- and Y-direction normal stresses are non-zero, the term involving F-12 in Equation (B.10) is zero. Therefore, a test in which both of these stresses are present is required to evaluate F-12. Such a combined-stress

test is difficult and expensive to perform correctly. Tsai and Wu noted, however, that the value of F-12 is bounded by a "stability condition":

$$F_{12}^2 \leq \sqrt{F_{11}F_{22}} \qquad (B.12)$$

If F-12 is not bounded by Equation (B.12), then the failure surface is no longer closed. Physically, a non-closed failure surface implies infinite strength under certain loading conditions. Narayanaswami and Adelman [13] noted that if the values obtained from Equation (B.12) are the extreme possible values of F-12, then for a wide variety of materials and loading conditions the maximum error induced by setting F-12 equal to zero is less than 10%. (For off-axis tension, off-axis compression, and biaxial tension, errors are less than 4%.) Narayanaswami and Adelman also noted that the Tsai-Wu criterion with F-12 = 0 gives almost identical results with the Hoffman criterion. In fact, the Tsai-Wu criterion reduces to the Hoffman criterion for plane stress problems if:

$$F_{12} = -\frac{1}{2X_TX_C} \qquad (B.13)$$

This value of F-12 is well within the bounds established by Equation (B.12).

The vita has been removed
from the scanned document